

CHAPTER 12

GENERIC DIAGNOSTIC ISSUES FOR A BURNING PLASMA EXPERIMENT

G. VAYAKIS* *ITER Organisation, CEN Cadarache, 13108 St. Paul lez Durance, France*

E. R. HODGSON *Euratom/CIEMAT Fusion Association*

V. VOITSENYA *Institute of Plasma Physics, NCS KIPT, Akademichna Str. 1, 61108 Kharkov, Ukraine*

C. I. WALKER *ITER Organisation, CEN Cadarache, 13108 St. Paul lez Durance, France*

Received June 6, 2007

Accepted for Publication October 5, 2007

In this chapter, we consider generic issues affecting the implementation of diagnostics in a burning plasma experiment (BPX). These are, directly or indirectly, caused by the radiation environment. In the first instance, handling nuclear radiation issues becomes a dominant factor in the choice of machine and diagnostic layout, construction, and maintenance. We discuss these integration issues first as they set the background against which more specific issues must be addressed. These include nuclear radiation effects on specific types of components and assemblies such as cables, fibers, and mirrors, and also thermal and mechanical degradation issues that must be considered in all component designs. One important consequence of the maintenance challenges brought about by the radiation environment is that degradation of front-line optical components by particle bombardment, normally handled by component replacement, also becomes far more challenging and in situ mitigation techniques must

be sought. For the same reason, recalibration techniques become more difficult. At the same time, BPX operation time is precious and extracting the optimum performance from the device may require the use of more sophisticated diagnostic techniques. Therefore, the requirements on reliability and data availability are more stringent and must be applied more widely than is common on present devices. An important goal of BPX operation is to enable the design of future power plants. We consider briefly the development needs for diagnostics for these and conclude with an assessment of the present state of readiness of the diagnostic community for the detailed design and construction of a full diagnostic set for a BPX.

KEYWORDS: *thermonuclear environment, plasma diagnostics, design guide*

Note: Some figures in this paper are in color only in the electronic version.

Contents—Chapter 12

- I. INTRODUCTION (FEATURES AND AIMS OF BURNING PLASMA EXPERIMENTS)
- II. NUCLEAR RADIATION AND ITS CONSEQUENCES ON DIAGNOSTIC LAYOUT AND CONSTRUCTION
 - II.A. The Nuclear Radiation Environment in a Working BPX
 - II.B. Relevance of Fission Technology and Experiment
 - II.C. Critical Parameters to be Controlled During Diagnostic Design
 - II.D. Optimizing the Performance of Diagnostic Equipment
 - II.D.1. Equipment Near the First Wall
 - II.D.2. Equipment on the Boundary and Outside the Vacuum Vessel
 - II.E. Shielding

- II.F. Machine Zoning and Implications on Diagnostic Design
 - II.F.1. Maintenance Zones
 - II.F.2. Radiological Zones
 - II.F.3. Confinement Zones
 - II.F.4. Implications of Crossing Boundaries
- II.G. Maintenance and Reliability Requirements
 - II.G.1. Diagnostic Components on Divertor Modules
 - II.G.2. Diagnostic Components in Port Plugs
 - II.G.3. Diagnostic Components on Vacuum Vessel Wall
- II.H. Integration of Multiple Systems into Port Plug Modules
- III. NUCLEAR RADIATION EFFECTS ON DIAGNOSTIC COMPONENTS
 - III.A. Brief Review of Radiation Effects in Insulators and Irradiation Testing Methods
 - III.B. Electrical Degradation I: RIC, RIED, and Examples (Pressure Gauges, Bolometers)
 - III.B.1. Pressure Gauges
 - III.B.2. Bolometers

*E-mail: George.Vayakis@iter.org

- III.C. Electrical Degradation II: RIEMF, TIEMF, RITES, and Examples (MI Cables and Coils)
 - III.D. Optical Degradation: RIA, RIL, and Examples (Windows, Fibers, and Mirrors)
 - III.D.1. Radiation-Induced Absorption
 - III.D.2. Laser-Induced Damage Threshold
 - III.D.3. Radiation-Induced Luminescence
 - III.D.4. Optical Fibers
 - III.D.5. Far Infrared Windows
 - III.D.6. Mirror Coatings
 - III.E. Mechanical Strength Degradation
 - III.F. Thermal Conductivity Degradation
 - III.G. Outstanding Irradiation Tasks in Preparation for a BPX
 - IV. PARTICLE BOMBARDMENT
 - IV.A. Erosion
 - IV.B. Deposition
 - IV.C. Measures to Improve the Service Life of First Mirrors
 - IV.D. ITER Examples
 - IV.E. Conclusions
 - V. MEASUREMENT STABILITY, CALIBRATION, AND RELIABILITY
 - V.A. Stability and Calibration Issues
 - V.B. Diagnostic Reliability and Data Availability
 - V.C. Specific ITER Case Studies
 - V.C.1. Plasma Shape
 - V.C.2. Core Electron Temperature
 - V.C.3. Divertor Ionization Front Position
 - VI. THE FUTURE
 - VI.A. Development of Diagnostics for Future Power Plants
 - VI.B. Readiness for a BPX
- REFERENCES

I. INTRODUCTION (FEATURES AND AIMS OF BURNING PLASMA EXPERIMENTS)

The development of diagnostics for fusion has been a long, complicated, and iterative process. Techniques have gradually been adopted, extended, and adapted to increasingly higher performance plasmas, and to yield more detailed and precise information. The transition to diagnosing plasmas with significant thermonuclear neutron production was made in TFTR (Ref. 1) and JET (Ref. 2), and considerable experience was gained in adapting diagnostic operation to a nuclear environment. Nonetheless, the campaign lengths of deuterium-tritium (D-T) machines to-date have been limited. In parallel, devices with long pulse length and significant plasma performance have come into operation,^{3,4} and simultaneously, control techniques used to attain high performance have become more sophisticated.⁵ The long pulse aspects alone are expected to change the way diagnostics are used and to allow new diagnostic opportunities to emerge.⁶

Extending present diagnostic operation to a burning plasma environment remains a demanding challenge, especially in view of the serious extrapolations required from attained flux and fluence levels⁷ but also because most designs assume routine advanced control to remain near performance limits while exploring different plasma scenarios in order to attain high-Q operation. Thus, a number of standard measurements, such as plasma shape,

have to be made with higher precision and reliability than is customary at present, and a number of measurements that are used infrequently, such as the current profile, have to be performed routinely, reliably, and, in many cases, in real-time. For these reasons, a burning plasma experiment (BPX) diagnostic set has to be more ambitious than those of present machines, at the same time coping with much harsher conditions near the front end of the diagnostic chain.

This challenge has been tackled by several design collaborations, for example, IGNITOR (Ref. 8) and FIRE (Ref. 9) but most comprehensively during the ITER design phase, starting from a preconceptual definition¹⁰ and ending in a detailed set of measurements with justified targets¹¹ and a set of diagnostic systems to attempt to meet them.¹²

It is not easy to find common features in BPX designs. However, the targets for tokamak-based reactors are more uniform. They include a thermonuclear Q of at least 20, pulse lengths of at least 1 h, maintenance intervals in excess of 1 plasma year for all in-vessel components, and first wall nuclear heat loads of at least 1 MW/m² translating to a D-T neutron flux of at least $4.5 \times 10^{17}/\text{m}^2$ (Ref. 13). Different BPXs have been designed to aim at a subset of these goals and were planned with different degrees of flexibility of operation and degrees of protection for inner diagnostic elements. Table I compares four different BPX designs with respect to key numbers that affect the diagnostic environment:

1. The pulse length is a parameter with important consequences for the diagnostics, starting from the thermal design of the front end, which can no longer rely on thermal inertia for BPX in the ITER class. It is also a determining factor in deciding whether real-time recalibration is needed and the level of reliability required of each diagnostic component. Finally, it affects the data-taking and data reduction strategy, including the application of diagnostics for real-time control.

2. The total plasma burn time is a key factor in determining diagnostic viability, design, and maintenance strategy. Maintenance of components in a BPX is always challenging. A long target burn time, such as ITER's, means that, for reasonable availability, diagnostic components have to survive for hundreds of plasma hours without interrupting the machine program for maintenance. These issues will be explored in Sec. II. In addition, a long plasma burn time at high performance brings with it, indirectly, the need to monitor a number of operational parameters, such as dust accumulation and divertor erosion, that would not be a concern in a short-life design. In this respect, ITER is much more challenging than other proposed BPXs.

3. The first wall neutron flux, by itself or combined with the plasma burn time, determines how close to the plasma particular diagnostic components can be placed.

TABLE I
Key Environmental Parameters for Four BPX Designs*

Parameter	Device			
	IGNITOR (Ref. 8)	FIRE (Ref. 9)	ITER (Ref. 12)	DEMO (Refs. 15 and 16)
Pulse length (s)	~4	~20	>400	—
Total plasma life at high performance (h)	~1	~7	4700	O(90 000)
First wall total neutron flux (n/m ² s)	3×10^{18}	1.5×10^{19}	3×10^{18}	7×10^{18}
Charge exchange wall load (kW/m ²)	~3	~20	~1	—
Neutron power/First wall area (MW/m ²)	~2	~2	~0.5	2.2

*Charge exchange wall load comparison based on the study of Budny.¹⁴

It is the driving term behind all the radiation effects on the diagnostic components, including nuclear heating, material damage, and radiation-induced voltages and currents. These will be discussed in detail in Sec. III. In this area, most BPX designs are comparable. One has to look deeper into the details of the BPX design to determine what the environment is like in the region of the diagnostic component, for example, by examining the space available for shielding, and thus to be able to work out what the real design constraints are.

4. The neutral particle flux or related charge exchange wall load is a parameter linked to first wall erosion and consequently a key factor in determining first wall lifetime and maintenance intervals. For diagnostics, it determines the lifetime of first mirrors and has other effects discussed in detail in Sec. IV. This factor is very sensitive to machine operational scenarios and to local plasma conditions so that even within one BPX design there is considerable span in the expected lifetime. There is also considerably more interest in predicting it than on today's devices because of the difficulty of component maintenance in a BPX.

In general, a BPX design with technological, reactor-validation goals, such as ITER, brings with it heavier constraints than a burning plasma physics demonstration experiment. These arise by the combination of prompt issues due to the high fluxes in a BPX with long pulse and long-life issues, including an increased emphasis on reliability and maintainability. These issues are discussed further in Sec. V.

Section VI starts by assessing the need to develop diagnostics for future demonstration and prototype reactors. It goes on to examine the overall state of readiness of diagnostic development for a BPX.

Throughout this paper, generic problems that affect any BPX and will likely exist in any reactor design are illustrated by examples drawn from the ITER design and

research and development (R&D) effort. As the detailed design of most of the ITER diagnostics still lies in the future, these illustrations should be taken for what they are: a snapshot of design solutions, mitigation strategies, and open questions that must be resolved on the way to a functioning magnetic confinement reactor prototype.

II. NUCLEAR RADIATION AND ITS CONSEQUENCES ON DIAGNOSTIC LAYOUT AND CONSTRUCTION

II.A. The Nuclear Radiation Environment in a Working BPX

In a BPX such as ITER the average first wall neutron flux level is of the order of 1.5×10^{18} n/m²s, equivalent to 0.5 MW/m²s, 5 to 10 times higher than experienced in the high fusion yield TFTR and JET D-T shots.¹⁷ Long pulse lengths produce in addition a neutron fluence many orders of magnitude greater than experienced so far in fusion devices. Because of the radiation environment, the design and integration of diagnostics within BPXs must incorporate, from the outset, all aspects relevant to burning plasma operation and subsequent maintenance.^{18,19} Special requirements for radiation compatibility and remote handling in such a reactor-class machine become primary design drivers of diagnostic components. The basic BPX technological design requirements for permanent machine systems significantly affect the neutron environment and maintenance strategy for diagnostics, and as a consequence, the reliability required of diagnostic equipment. Overall, system reliability in burning plasma devices will be required to be significantly higher than in earlier generation devices as the length of remote operations significantly affects machine availability. At the same time, the number and complexity of diagnostic systems in a BPX is comparable to today's machines^{20,21} and their implementation poses considerable challenges as a result.^{19,22,23}

II.B. Relevance of Fission Technology and Experiment

Diagnostic equipment within the primary vacuum of a BPX is similar to that in existing plasma physics experiments adapted to a reactor-like environment and provided to characterize underlying physical parameters that determine the burn process. Relatively few of these diagnostics directly measure the burn process. In contrast, fission reactor diagnosis is predominantly intended for process control. Detailed measurement of the local parameters is not required; mechanical and thermal measurements, along with neutron diagnostics, suffice. Even in experimental fission plant, the reaction process is generally fixed; the experimental measurements are from specimens within extractable rigs and loops placed in the reactor, not of the reaction process itself. Therefore, there is little direct relevance of diagnostic use in fission to a BPX. There is large technological overlap, however, as the environments are similarly hostile: fission plant instrumentation, electrical sensor, and cabling technology is directly applicable to BPX sensors, thermocouples, bolometers, soft X-ray photoelectric detectors, and engineering instrumentation. The use of mineral insulated (MI) cabling, widespread in fission, has found good applicability in BPX designs, generally for the two requirements of installation robustness and good thermal contact of the nuclear heated conductor to a thermally grounded sheath. However, whilst in fission reactors instrumentation wiring can generally be extracted directly, reducing the concerns about nuclear effects on the transmission lines and their maintenance, in BPXs this is not often the case: many cables are permanent and follow complex paths for several metres at the same neutron flux as the measuring element.

Many BPX neutron diagnostic techniques benefit from the long history of R&D for fission reactors. In the control and surveillance of fast breeder reactors, durable fission chambers are able to operate in extremes of temperature and gamma dose. The neutron diagnostics in a BPX are an extrapolation of these to fusion neutron energies. Rhodium self-powered neutron detectors (SPND) are used in fission reactors for core power and spatial fission reactivity measurement and control and can be adapted for BPXs. Neutron Activation (rabbit) transfer systems are used in virtually all fission plants, and their technology can be transferred to BPXs. Optical and microwave diagnostic systems, on the other hand, are rare in fission reactors and the technology of their implementation is a speciality of BPXs. All the intrinsic design features of these are therefore unique to BPXs.

Finally, the testing and full qualification of prototypes and materials for the front-ends of BPX diagnostics is realistically only achievable in present-day fission plants. The differences in spectrum between fission and fusion devices make it challenging to design appropriate experiments as the heating rate, fast and slow neutron flux environment cannot simultaneously be matched (see

Sec. III.A). With care, however, extrapolation to BPX conditions is possible and key prototype testing of front-end components in fission plants is an essential element of BPX diagnostic development.

II.C. Critical Parameters to be Controlled During Diagnostic Design

BPX nuclear design requirements at the first wall are determined by the machine operational program and vary considerably (Table I). For ITER, the entire operational phase will last about 20 years, with a few thousand hours of D-T operation. Operation and details of the nuclear parameters for ITER are given in Table II. A set of critical parameters arises from these requirements that must be simultaneously controlled during each component or sub-system design and thereby influence diagnostic designs:

1. local and integrated nuclear effects on the superconducting magnets
 - a. The peak fast neutron fluence (> 0.1 MeV) to the closest coil insulator [Toroidal Field Coils (TFC) in ITER] is limited to 5×10^{21} n/m².
 - b. For the ITER TFC, 50 W of nuclear heating is acceptable from each port due to cryopant limitations. Achieving this turns out to be a primary function of the port shielding (see Sec. II.E).
2. damage and gas production rates in nearby structural and pressure boundary components
 - a. For ITER special low-boron stainless steel,²⁴ material should be limited to ~ 0.1 (dpa) to allow rewelding. Thus, diagnostic penetrations must not increase exposure of structural components beyond this level.
3. neutron fluxes and residual radiation doses at maintenance locations
 - a. For ITER, neutron reactions with the alloying elements of stainless steel and impurities generate radioactive isotopes (⁵⁴Mn, ⁵⁶Mn, ⁵⁵Fe, ⁵⁷Co, ⁵⁸Co, ⁶⁰Co, ⁵⁷Ni, ⁵¹Cr, and ⁹⁴Nb dominate the activation levels^{25,26}). Activated corrosion by-products are generated within the first wall and blanket cooling circuit. Diagnostic design must not significantly increase activation and corrosion by-product levels.
4. radiation conditions at personnel access locations
 - a. For any personnel access, the residual dose rate should be as low as reasonably achievable (ALARA). In the port cell, the ITER ALARA target at the end of D-T operation is < 100 μ Sv/h, 10^6 s (~ 12 days) after shutdown. This is a key driver of the shielding design and, indirectly, can limit diagnostic first wall aperture size (Sec. II.E). Outside the ITER

TABLE II
ITER Operation and Nuclear Parameters

Parameter	DT Phase Nominal Design Value	Value for Assessment ^a
Maximum fusion power (MW)	500	700
Average FW neutron fluence ($\text{MW} \cdot \text{yr} \cdot \text{m}^{-2}$)	0.3	0.5
FW neutron flux ($\text{MW} \cdot \text{m}^{-2}$) ^b		
Average	0.56	0.79
Mid-plane outboard	0.78	1.09
FW 14 MeV neutron flux (peak at outboard, $\text{n} \cdot \text{m}^{-2} \cdot \text{s}^{-1}$)	4.4×10^{17}	6.1×10^{17}
FW scattered neutron flux ≥ 0.1 MeV (peak at outboard, $\text{n} \cdot \text{m}^{-2} \cdot \text{s}^{-1}$)	2.4×10^{18}	3.4×10^{18}
Pulse burn length (s)	400–3000	
Integrated full power operation time (h)	4700	7600
Total heat from plasma to in-vessel components ^c (MW)	812	1090
Maximum radiated power to FW (MW)	136	136

^aValue whose consequences on the design need to be assessed by the designers in view of possible machine operation with or without upgrades.

^bPower excursions of up to $\sim 20\%$ for several seconds must be foreseen.

^cIncludes a neutron energy multiplication factor of 1.5.

bioshield, the ITER target is $10 \mu\text{Sv/h}$ (24 h after shutdown). This is a key driver of the biological shield design.

- b. Appropriate safeguards and monitoring are required as described in the Zoning section, Sec. II.F.
5. radiation effects on the diagnostic components (see Sec. III)
6. performance of diagnostic equipment (see Sec. II.D)

II.D. Optimizing the Performance of Diagnostic Equipment

The first wall neutron flux and/or fluence determine how close to the plasma particular diagnostic components can be placed. Local values of the flux and fluence drive all the radiation effects on the diagnostic components, including nuclear heating, material damage, and radiation-induced voltages and currents (see Sec. III). Even at the first wall, there is already significant variation between BPX designs (Table I). Since, furthermore, shielding can influence these numbers by orders of magnitude, one has to look deeper into the details of the BPX design to determine what the environment is like in the region of the diagnostic component and thus to be able to work out what the real design constraints are.

Diagnostic equipment at a number of locations is shown in Fig 1. The environment for these typical diagnostic component locations has been given in detail elsewhere.²⁷ The approximate neutron and gamma fluxes at typical locations for diagnostic components during operation are shown in Fig. 2. Detailed analysis including

the effect of local penetrations is required if the errors on these estimates are to be reduced to below an order of magnitude.

II.D.1. Equipment Near the First Wall

Design of diagnostic sensors near the first wall must consider the effect of nuclear heating and material effects (Sec. III). Components are either water cooled (front-end mirrors) or are small and light, using high-temperature materials and relying on conductive and radiative cooling to obtain acceptable operating temperatures (e.g., pickup coils, bolometers, small moving parts).

Many diagnostics on the plasma side of the vacuum vessel wall are essential for basic BPX operation (e.g., magnetic diagnostics). They are distributed over hundreds of diagnostic locations over the complete inner surface of the vessel. The topology of tokamaks makes the approach of using removable modules spanning the whole region from the sensor to a less challenging environment, as used in the ITER ports and in fission environments, unsuitable for providing this full coverage. Thus, redundancy is required. Replacement is required for some sensors. Where replacement is possible, diagnostic structures must be designed to make remote handling (RH) installation as easy and reliable as possible. Wiring between the sensors and the outside world has to follow a complex path to a suitable exit from the vacuum vessel or the cryostat and is typically not replaceable. Thus, redundancy is even more important, and where some aspect of the design cannot be fully qualified, this redundancy must extend to the types of wiring and connections installed.

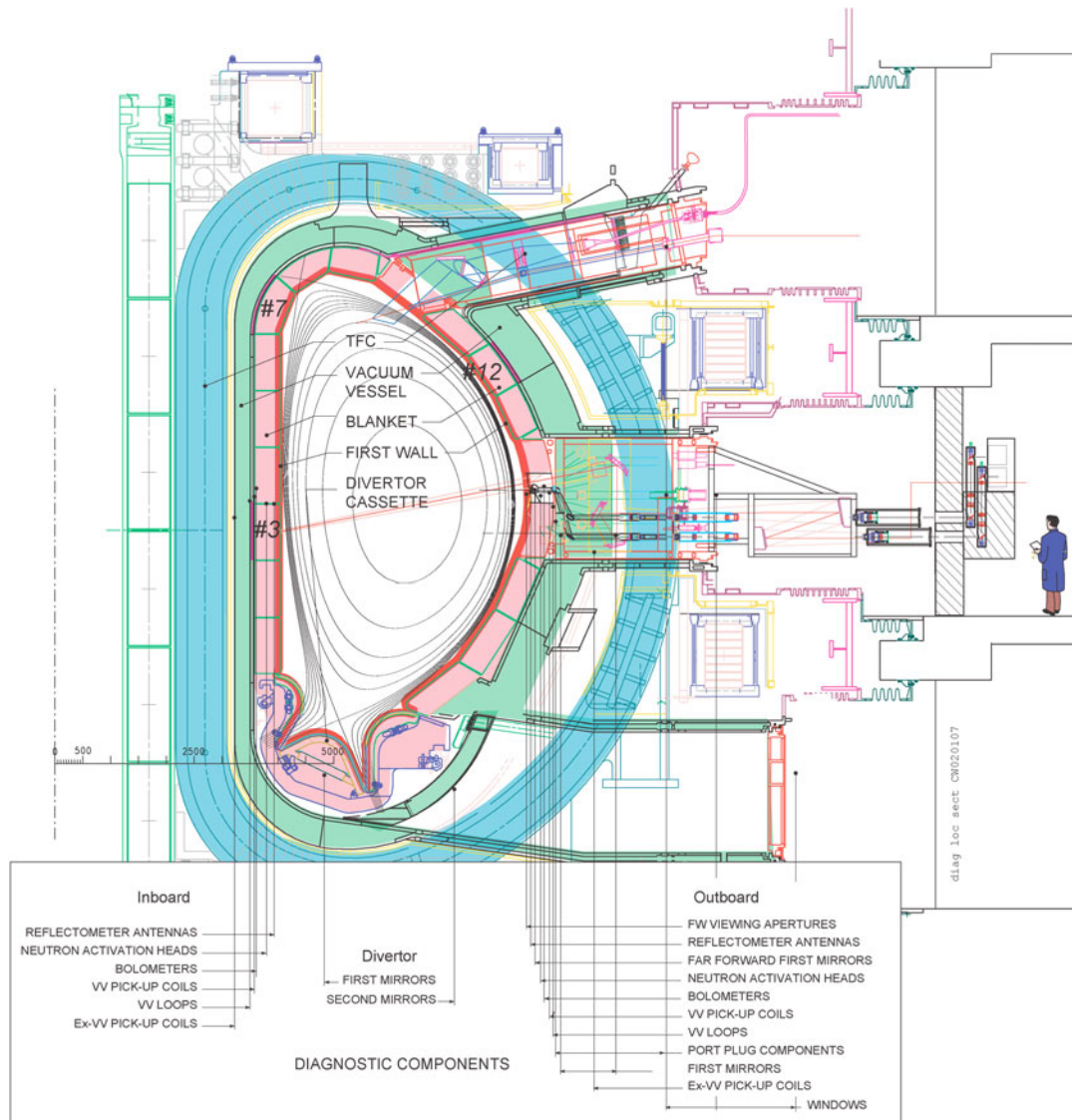


Fig. 1. Cross section of ITER showing location of diagnostic components and major basic machine elements.

The segmented nature of the first wall, and the need for efficient maintenance, naturally generate gaps between the shielding. These can be used to view the plasma. Because of the gaps, there is wide variation of radiation levels: For example, on the vessel wall at the blanket gap the fast neutron flux (>0.1 MeV) for ITER is 0.2 to $1 \times 10^{17} \text{ n} \cdot \text{m}^{-2} \text{ s}^{-1}$ (0.8 to $4 \times 10^{16} \text{ n} \cdot \text{m}^{-2} \text{ s}^{-1}$ for 14 MeV neutrons) giving a fluence of 0.4 to $2.0 \times 10^{24} \text{ n} \cdot \text{m}^{-2}$ over the ITER lifetime. This is reduced by a factor of about 4 at the center of the blanket module.

For ITER, equipment with a direct view of the plasma from local sites includes bolometers, soft X-ray photoelectric detectors, lost alpha particle detectors, interferometry and polarimetry retroreflecting mirrors, calibration black bodies, and waveguide antennas (Fig. 3 for bolometry and magnetics; see also Ref. 28). This

equipment generally relies on the blanket modules or divertor structure for shielding, but requires viewing apertures, sometimes enlarged natural gaps existing for machine engineering purposes—assembly tolerances, remote handling, thermal expansion, etc.—for sufficient signal. The shielding afforded by this layout is relatively weak ($\frac{1}{10}$ to $\frac{1}{50}$ of first wall levels).

Equipment that does not require a direct view of the plasma includes magnetic pickup coils and loops, halo current detectors, neutron activation irradiation stations, pressure gauges, gas analyzers, dust collectors and monitors, as well as necessary signal cabling and connectors. The intrinsic shielding of the blanket is usually reduced because of the need to remove material to accommodate these diagnostics, and this is usually a constraint on sensor size.

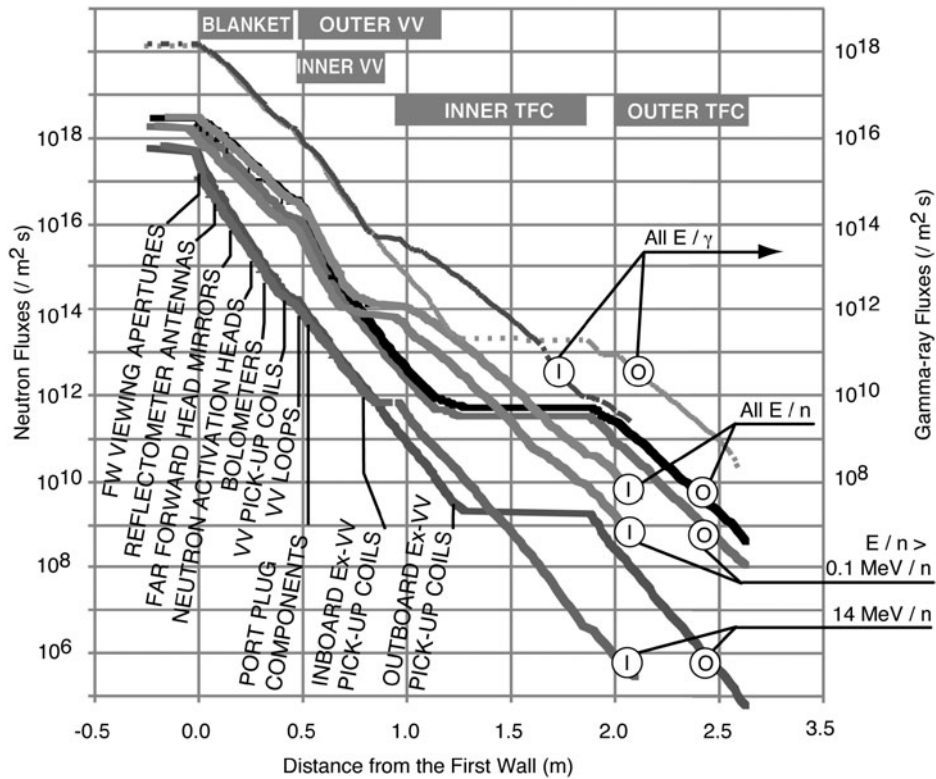


Fig. 2. Neutron and gamma fluxes on diagnostic components during operation for 500 MW. The solid curves are from a simplified 1D equivalent (cylindrical) model of the machine. This averages out the effect of gaps and does not include diagnostic penetrations.

Port plugs and divertor diagnostic modules are convenient means of packaging a number of diagnostic components. These include more elements with a direct view of the plasma as described earlier and, particularly, first mirrors with protection shutters, in-vessel neutron detectors, neutron flux monitors, microfission chambers, and X-ray spectrometer crystals. For equipment in port plugs, there are more choices on the layout, but the integration of multiple diagnostics in any one port plug poses special challenges (see Sec. II.H).

II.D.2. Equipment on the Boundary and Outside the Vacuum Vessel

On the boundary of the port plug there will be a number of vacuum feedthroughs for electrical, optical, microwave signals as well as mechanical feedthroughs for motion control, e.g., of shutters, and for coolant loops. These are generally well enough protected from the radiation that their performance is little affected and there is insignificant nuclear heating, although particular design attention is paid to them because of their function as containment boundaries.

It is often convenient to place diagnostic detectors in the region close to the rear of the port plug. The radiation

levels here, generally controlled for minimizing activation and maintenance doses, often need to be further reduced during operation for these detectors. Again, some equipment here will have a direct view of the plasma, albeit highly collimated.

A little further away, outside the bioshield, the port cell is able to accommodate significant volumes of equipment as long as it can be readily removed for port plug maintenance. Although the port cell is accessible for personnel access 24 h after operation, there will be a significant gamma activity in the area during operation. A certain amount of local gamma shielding may be required for diagnostic equipment.

II.E. Shielding

The need for shielding arises from the reasons discussed in Sec. II.C:

1. protection of the cryogenic coils from neutron damage and excess heat
2. minimization of the material damage to components that must be rewelded
3. minimization of activation of removable components

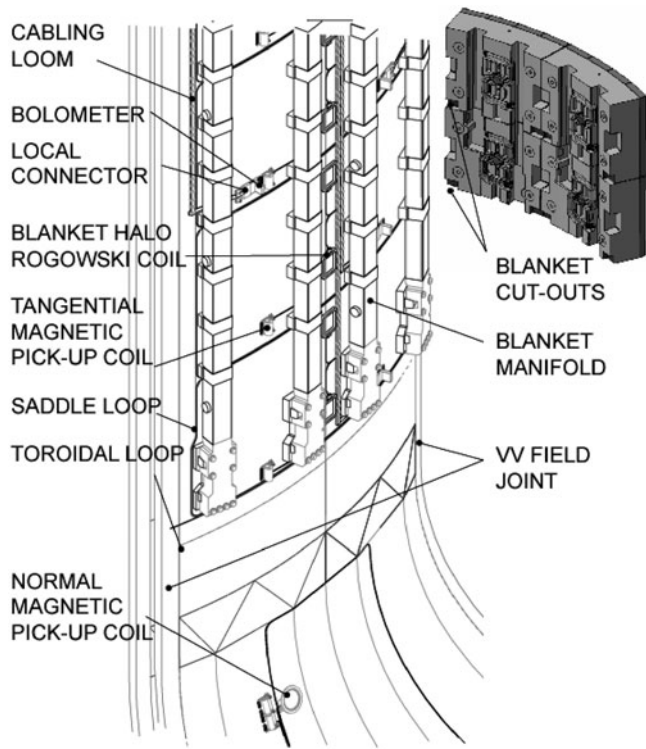


Fig. 3. Part of the ITER inboard vacuum vessel with blanket and divertor removed, showing installed diagnostic sensors and cabling looms.

4. reduction of dose rates to areas where personnel access must be allowed.

But it also arises because of the need to provide

1. reduction of fluxes for some diagnostic components
2. collimation of neutrons for measurements.

The shielding immediately behind the first wall reduces the flux of fusion and scattered neutrons by approximately two orders of magnitude to lower the damage level of the vessel welded joints. The shielding purpose here is therefore for high-energy neutron moderation and capture.

The port plug assemblies must also be shielded (Table III). For plugs with no apertures, the thickness of the shield should be similar to that of the blanket modules plus vacuum vessel, but the presence of apertures requires special measures to maintain similar levels of neutron leakage. Paths through the basic steel/water layers for transmission of system elements, diagnostic signals, heating power, test blanket coolant, etc., must be designed to minimize the additional neutron leakage to the vessel, coils, and maintenance access points, such as flanges. Labyrinths and doglegs are effective, but additional shielding can be required. There are several diagnostic systems requiring straight line of sight access to the plasma, such as neutron, neutral particle, and X-ray diagnostics. Here the shielding can only

TABLE III

Description of Types of Shielding Proposed for ITER Along a Path Through an ITER Port Plug to the Port Cell*

Location	Component	Shielding Type	Typical Size (m)	Role and Properties of Shielding
In primary vacuum	First wall	80% steel, 20% water	0.06	Structural and thermal support to high heat flux components and shielding.
	Blanket shield	60% steel, 20% water	0.40	Most effective location for coil protection and reduction of vacuum vessel damage. Ratio of steel to water chosen for minimum thickness.
	Structural components	80 to 95% steel, balance water	0.1 to 0.3	Cooled structural components that must also shield.
	Port plug front	30 to 70% steel, balance water	1.5 (Equatorial) 4.5 (Upper)	Surrounds diagnostic components and labyrinths. Ratio of steel to water chosen to match vessel shielding for minimum weight.
	Port plug back	Stainless steel with boronated steel and water	0.5	Allows the remaining neutrons to be captured, increases local activation at a controlled location.
Behind port plugs	Local diagnostic instrumentation protection	Steel, polyethylene, lead	0.1 to 0.5	Neutron shielding where water difficult to provide. Gamma shielding during port access.
		Concrete	0.3 to 1.0	Economical neutron and gamma shield with potential for structural use
	Biological shield	Boronated concrete		Absorb remaining thermalized neutrons.
		Lead	0.1 to 0.3	Disposable. Gamma protection of diagnostic sensors.

*Percentages are by volume.

be affected by thick walls and neutron beam dumps after the detector.

Behind the port plug is a region (interspace region in ITER) where more shielding may be required to make up any shortfalls in the effectiveness of the port plug shielding as regards flux levels on diagnostic equipment and the activation of material in the accessible port interspace region. A design guideline adopted for ITER is that the contribution of the diagnostic penetrations to the activation dose in the port interspace be limited to less than ~10% of the total background dose from all other sources including the primary gap (20 mm) between the plug and the port.

The biological shield is, as its name implies, the final nuclear shielding system that represents the limit of routine personnel access. At regions such as the ports the bioshield must be removable to allow access for maintenance. There will be more activation on the plasma side so consideration must be given to replaceable faces and hot spots. The amount of human intervention required to clear access to the ports is an important factor in determining the real accessibility for diagnostic maintenance in this region due to occupational exposure limits.

Behind the bioshield (the Port Cell region of ITER) is a region where diagnostic systems would require frequent personnel and equipment access during maintenance periods. There are likely to be other limitations due to nonradiation effects, such as magnetic fields, confinement safety, fire prevention, ventilation zoning, etc.

During periods of port plug maintenance there will be high gamma levels when a port plug is removed and parked in its contamination control cask, both from the port plug itself and from the open port. This can have implications for local shielding requirements to protect sensitive equipment and for the transport path of diagnostic signals to the diagnostic hall to allow unfettered

access to the bulk of the diagnostic instrumentation during these periods.

II.F. Machine Zoning and Implications on Diagnostic Design

Diagnostics in a BPX have components in multiple zones defined by maintenance, radiological, and confinement boundaries. These are examined in turn below. Additional zonings that are not BPX-specific (such as beryllium and electromagnetic zones) can also exist in a BPX but will not be discussed further.

II.F.1. Maintenance Zones

All components inside the bioshield must ideally be designed to last the lifetime of a BPX. However, even when this succeeds, the experimental nature of the device and its operating scenarios also mean that some form of replacement should be possible if at all practicable. In practice, certain measurements can only be performed by devices of finite or uncertain lifetime, and provision for their replacement is required. The configuration of the BPX and the replacement or lifetime specifications of key machine components determine the type and complexity of RH maintenance operations that are planned. The RH classification of ITER components will be typical for all BPXs and is shown in Table IV.

The location of vulnerable diagnostic components is decided based on useable lifetime and accessibility for replacement. The design generally includes maintenance features that allow scheduled maintenance operations to be performed reliably and quickly, in order to maximize machine availability.

Maintenance of in-vessel components will generally consist of the replacement of components. The removed,

TABLE IV
ITER Remote Handling (RH) Maintenance Classification

RH (Maintenance) Class	Components	Requirements Prior to ITER Construction
Class 1	that require scheduled remote maintenance or replacement.	All RH equipment will be designed in detail. Feasibility of tasks will be verified and may involve the use of mock-ups.
Class 2	that are likely to require unscheduled or very infrequent remote maintenance.	All RH equipment will be designed in detail. Feasibility of tasks will be verified where deemed practical and necessary and may involve the use of mock-ups.
Class 3	not expected to require remote maintenance. The projected maintenance time in case of failure may be long.	The procedure of maintenance will be defined prior to ITER construction.

activated, and contaminated components will be transported to a hot cell for eventual repair and refurbishment, or alternatively, for preparations for disposal as waste.

Table V shows typical diagnostic components with their maintenance class and the direction of the access. From this, the generic and dedicated tooling can be determined and a zoning of the machine from a maintenance standpoint is effectively defined.

II.F.2. Radiological Zones

Radiological zoning is a very important consideration for the protection of workers against ionizing radiation. The dose limits for zoning apply to irradiation doses and to internal doses, the equivalence being derived from inhalation dose factors, breathing rate and so on. It affects directly the design of the shielding and the maintenance strategy for each diagnostic assembly.

For ITER, as an example, three types of zones are defined, designated by a color code as shown in Table VI. In a supervised zone personnel could be exposed to a total dose <math><1 \text{ mSv/yr}</math>, $\frac{1}{10}$ of the annual limits set for equivalent dose to skin, hands, feet, and eye lens. In a controlled zone exposure could be to a total dose of 6 mSv/yr (or $\frac{3}{10}$ of the annual limits for equivalent dose to hands, feet, and eye lens). The zoning is usually demarcated by fixed walls.

II.F.3. Confinement Zones

Confinement of radioactive and hazardous materials limits the mobilization and dispersion of tritium and activation products in the event of an accident. Radioactive and hazardous inventories are identified and an appropriate level of confinement is provided based on the level of risk. On ITER, two confinement systems are designed so that sequential barriers are provided with appropriate treatment of penetrations through the confinement.

The first confinement system is provided for normal facility conditions of operation, testing, and maintenance. The port plug, with feedthroughs for diagnostic signals, windows, etc., that provides the primary vacuum boundary, is designated the first confinement boundary for diagnostics. The second confinement system envelops the first and includes components, vaults, cells, and rooms with appropriate depressurization, filtration, and detritiation (Fig. 4).

Each confinement system includes one or more static or dynamic barriers. Examples are elements of the vacuum vessel (port plug flange, windows), process piping, port cell walls, and building walls, as seen in Fig. 4. Dynamic barriers, such as burst disks, relief valves, vacuum valves, shutters, and detritiation systems, require moving parts in order to fulfil their confinement function. The confinement barriers must be reliable and

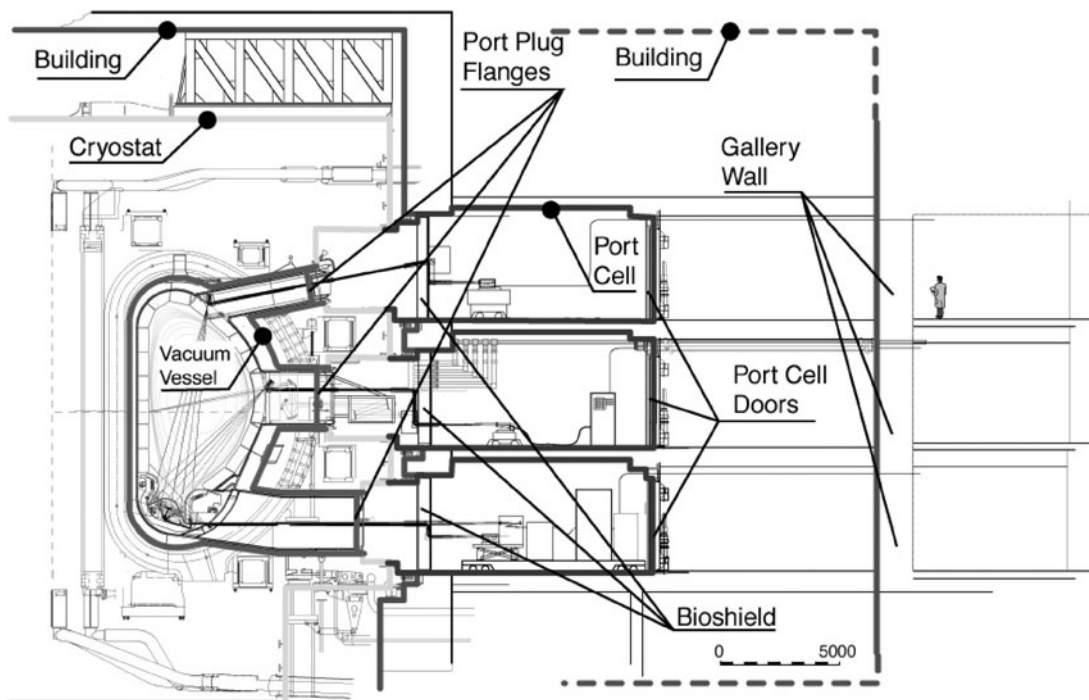


Fig. 4. General arrangement of the ITER buildings showing the main confinement boundaries (vacuum vessel, cryostat, port cells and building, marked by •), as well as key elements of radiological protection (port plug flanges, bioshield, port cell doors and building walls).

TABLE V
Maintenance Zones for Diagnostic Components in ITER

Zone	Typical Component	Class	Type	Access	Generic Tooling	Dedicated Tooling	To Gain Access	Intervention required	Special Considerations
Near first wall	Polarimeter retroreflectors	2	In-vessel RH	From inside of vessel	Robot mounted on IVT*	Yes	IVT* required	Cleaning or replacement	Alignment
	Reflectometry antennae							Replacement	
	Far forward mirror assembly					Cooling cut and reweld shutter reconnection			
Vacuum vessel-near blanket gap	Some magnetic coils, bolometers, vacuum photodiodes, interferometry retroreflectors	2			Robot mounted on IVT*	Yes	Blanket module removed	Substitution replacement	Recalibration Location definition Intervention time
Diagnostic port	Blanket shield module	2 or 3	Port RH	Hot cell	RH handling and contamination control cask	Hot cell tooling	Port plug to hot cell	Substitution replacement in hot cell	Retest port plug
	Far-forward assembly, first mirrors, shutters, second mirrors, sensors						Port plug dismantled	Cleaning, rectification or substitution replacement in hot cell	
	Port plug		Port interspace	Manual assisted handling	Special grippers	Removed port interspace structure	Refurbishment in hot cell		
On port plug boundary	Windows, sensors, detectors, interspace pipes	2	Port RH with limited manual assistance	Port interspace	Yes	Yes	Remove interspace equipment	Cleaning, rectification, or substitution	Contamination control, ORE, reseal vacuum
	Interspace structure mirrors, waveguides, cables, connectors, detectors	Manual		Bioshield opening	Yes	Yes	Remove bioshield plug and equipment	Adjustment, replacement, repair	
	Interspace-side bio-shield plug structures, mirrors, cables, detectors		At port	Port cell	Yes	No	Through bioshield plug		
In port cell	Mirrors, waveguides, cables, connectors, detector shield blocks, supports, etc.		In port cell	Port cell opening	Yes	Yes	Personnel access to port cell	Refurbish, replace, adjust, calibrate, align	Access space, ORE, alignment
Divertor cassette	First mirrors, shutters, sensors, cables, connectors, antennas, waveguides	2	Cassette RH	Removed cassette	Robot mounted on divertor rail	Hot cell tooling	Cassette removed	Substitution replacement in hot cell	All in hot cell. Retest cassette and rack assembly
Divertor port	Shielding, cooling pipes second mirrors, cables, connectors, waveguides		In port RH	Port interspace	Robot mounted on port rail	Yes	Removed primary closure	Substitution, replacement and repair in hot cell	Contamination control

*IVT = in-vessel transporter. Two or more equatorial ports have to be removed for its deployment.

TABLE VI
Proposed ITER Radiological Zoning According to Total Doses

Radioprotection Zoning		External Exposure		Internal Exposure	
				Atmospheric Contamination	
Type	Color	Dose	Dose Rate	Total Dose in 1 h	VDO*
Nonregulated area		$<80 \mu\text{Sv}$ in 1 month		—	None
Supervised	Blue	$<7.5 \mu\text{Sv}$ in 1 h		$<7.5 \mu\text{Sv}$	<0.3
Controlled	Green	$<25 \mu\text{Sv}$ in 1 h		$<25 \mu\text{Sv}$	<1
Specially regulated	Yellow	$<2 \text{ mSv}$ in 1 h	$<2 \text{ mSv/h}$	$<2 \text{ mSv}$	<80
	Orange	$<100 \text{ mSv}$ in 1 h	$<100 \text{ mSv/h}$	$<100 \text{ mSv}$	<4000
Restricted	Red	$>100 \text{ mSv}$ in 1 h	$>100 \text{ mSv/h}$	$>100 \text{ mSv}$	>4000

*1 VDO (derived operational value) leads to an internal dose rate of $25 \mu\text{Sv/h}$.

independent, with no common parts and physically separated to avoid common mode failure.

II.F.4. Implications of Crossing Boundaries

It is necessary that the diagnostic systems, signals, and transmission lines cross all these boundaries (maintenance, radiological, and confinement). This naturally segments the diagnostic. The diagnostic components must be broken down into elements corresponding to the type of maintenance, activation, contamination, etc., of the zones and different procedures adopted for access, alignment, and calibration (see Table VII). To access the elements within the first containment boundary these are handled in a modular way as for the port plugs. An example of such an implementation is shown in Fig. 5.

On ITER at last count there were 118 diagnostic nonmetallic windows, representing $\sim 3 \text{ m}^2$ of first boundary area. Compared with the vacuum vessel structure, these have a brittle and sometimes weak transparent element, and generally, designs (type, materials, and quantities) cannot be defined early in the BPX design. To mitigate the inherent weakness of windows a number of precautions can be taken:

1. A maximum diameter can be set (160 mm for ITER).
2. Windows can be mounted on a removable component (port plug flange in ITER).
3. Windows can be replaceable in situ.
4. Windows can be protected from off-axis impact.

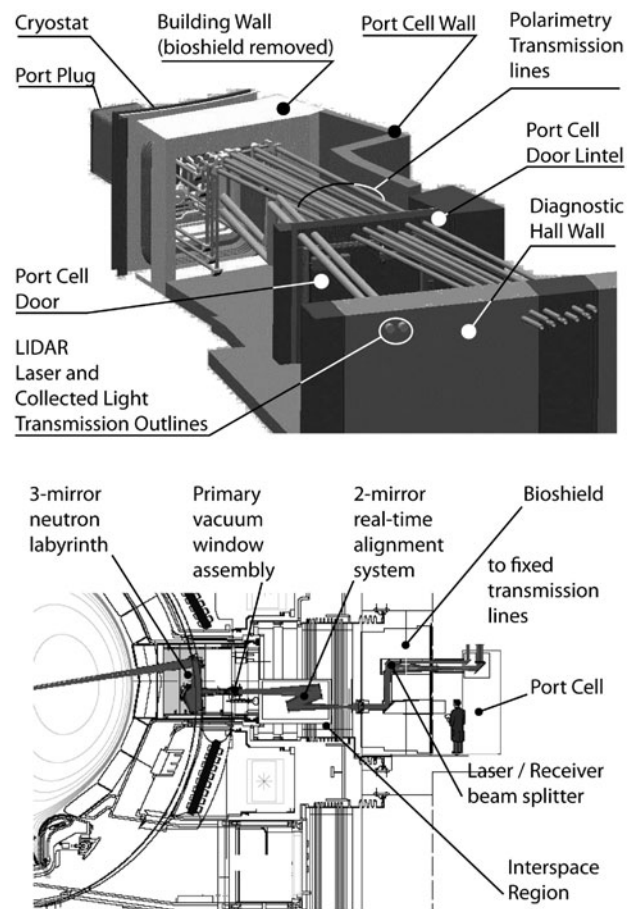


Fig. 5. Top: Transmission line paths for the ITER LIDAR and polarimetry diagnostics from the back of the port plug (in the interspace through to the tokamak/diagnostic hall wall). Bottom: Detail of the LIDAR lines up to the port cell.

TABLE VII
ITER Diagnostics Crossing Functional Boundaries*

Zone or Boundary	Features of Diagnostic Equipment	Access	Differential Pressure Rating	Neutron (Gamma) Attenuation Requirement
Plasma to first wall	Apertures and occasionally hardware such as waveguides	No human intervention	200 kPa	1E4 (1E6)
First wall to blanket shielding	Apertures and occasionally hardware such as waveguides			
Blanket to port plug shielding	Removable diagnostic modules			
Port plug	Labyrinths/doglegs			
Port plug flange	Vacuum feedthroughs/windows/contamination barriers during maintenance	Very restricted human intervention during shutdown	0 kPa	100
Port plug interspace	Conventional transmission with radiation hard elements and movement compensation			
Bioshield within port cell	Tunnels/labyrinths	Limited human intervention during pause in operation	160 kPa	(100)
Bioshield to port cell	Conventional transmission			
Port cell	Removable diagnostic equipment			
Port cell to port cell door and lintel	Conventional transmission	Controlled human access possible during operation Restricted during port plug transport	O(500 Pa)	100
Port cell door and lintel	Ventilation controlled feedthroughs/windows/access doors			
Gallery	Transmission lines that can accommodate large equipment transport	Unrestricted access		
Gallery wall	Ventilation controlled feedthroughs/windows			
Diagnostic building				

*Refer to Fig. 4 for the locations of the boundaries.

5. Windows can be type-tested, batch-tested to destruction, and proof-tested before and after installation.

6. First windows can be backed by a partially pumped interspace.

This last precaution provides an interspace that can be monitored. The operator is not left long-term in ignorance of a developing failure state, failure is evident, and planned repair is possible. The interspace can be provided either as shown in Fig. 6, by a sealed window or lens near and outside the first window, or by using the natural interspace of the second confinement system (window or valve).

Despite all precautions, a BPX must anticipate window failure in normal operation. The designs aim to min-

imize likelihood, by as much design analysis as is practical, implementation, manufacturing, and testing rules, and the mitigating measures listed earlier.

II.G. Maintenance and Reliability Requirements

The diagnostic system is a necessary tool for the operation of the BPX. It must be reliable to permit the operational aims of the machine to be reached efficiently. The implications of this are explored further in Sec. IV.B. Additionally, it must not weaken the fundamental device and it must not be a cause of unwanted events, such as laser power on windows breaking the vacuum containment, or multiple failure of magnetic sensors leading to major disruptions. At the same time, the BPX is an experimental, first-of-a-type device. Survival through

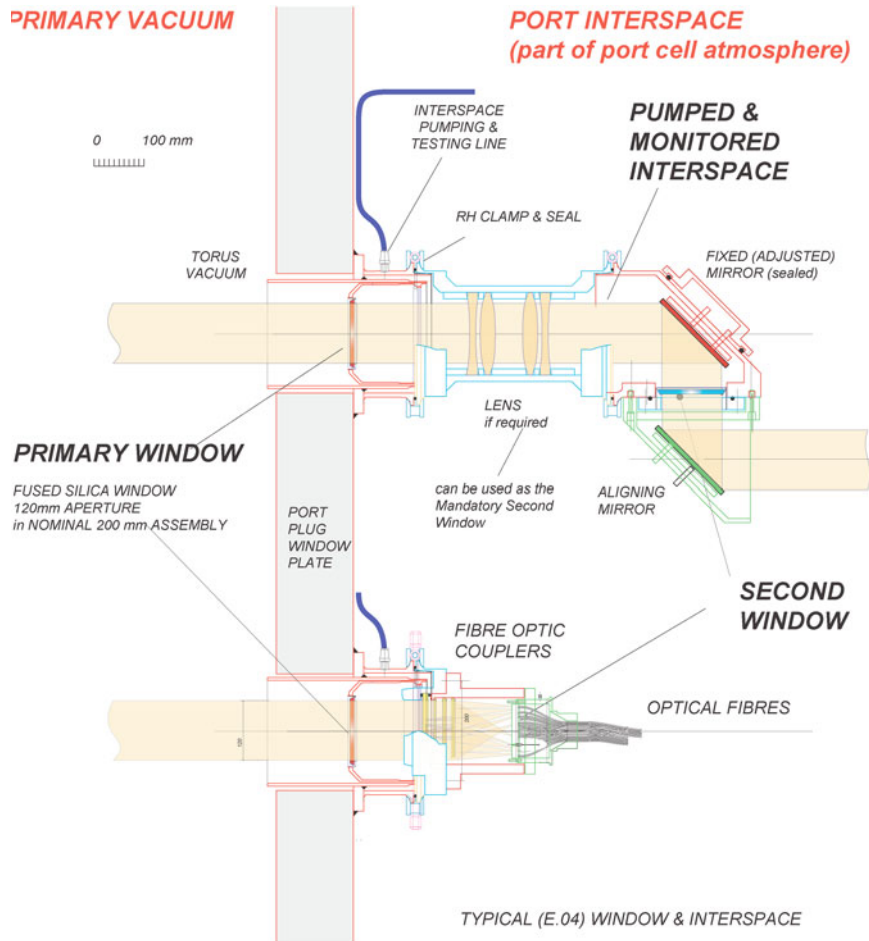


Fig. 6. Example ITER diagnostic window arrangement.

off-normal events in the context of diagnostics equipment must be considered in detail. For example, components of diagnostic systems will be required to survive plasma disruptions and, in some more difficult cases, to measure reliably during disruptions. Surviving the failure of interfacing systems is also important. If the BPX design anticipates surviving a water leak, then so must the diagnostic; hydrosopic window material would be at risk. Similarly the diagnostic components must be robust enough to survive system and control errors that the BPX survives. An example of this is the need to withstand thermal shocks from water cooling operational errors.

It will be necessary to anticipate failures and breakdowns of many systems and to mitigate their consequences, primarily of the required safety elements on confinement boundaries, for the protection of public and personnel. Obviously from a machine investment standpoint it is also desirable to be able to recover from these upsets.

The majority of the in-vessel diagnostic sensors are essential for BPX operation and must therefore survive for the expected life of the supporting system: vacuum

vessel, divertor, or port plug blanket. Survivability cannot be guaranteed, however, so they must also be repairable. Where this is not possible a degree of redundancy must be planned. We consider the implications of this for systems mounted in different regions of the machine as follows.

II.G.1. Diagnostic Components on Divertor Modules

Diagnostic components in the divertor are mainly mounted on the cassette bodies (see Fig. 7). They are generally too small to be considered for independent maintenance and so are not handled in-vessel. They include

1. detectors, including bolometer cameras, magnetic pickup coils, pressure gauges, and neutron flux monitors, with their associated cables and connectors. Only thermocouples and Langmuir probes with their cables and connectors are likely to be incorporated in the high heat flux components (HFC).

2. optical systems, including first mirror arrangements for visible impurity influx monitor, dust monitor,

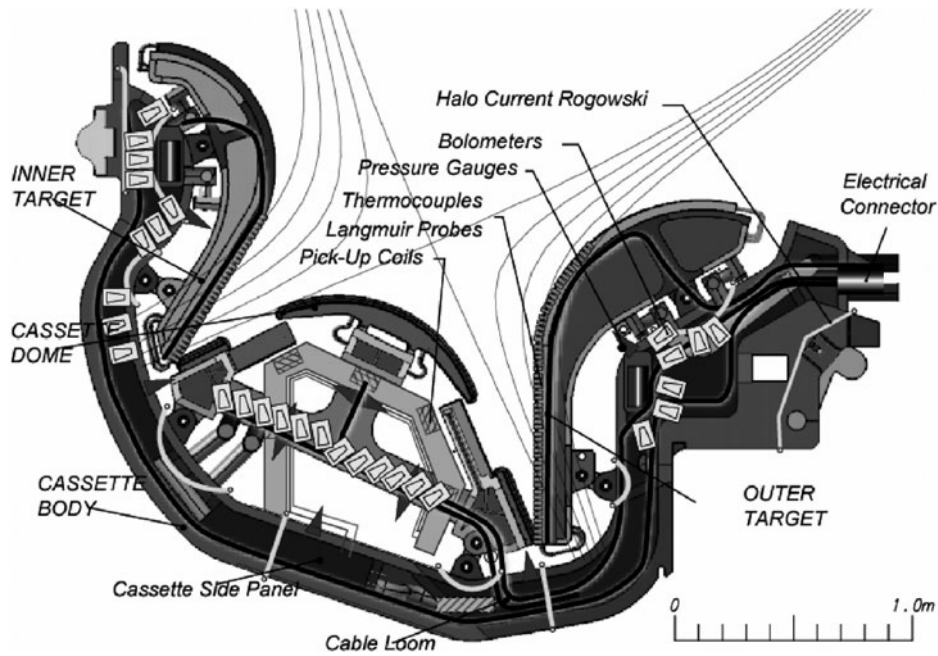


Fig. 7. Multiple diagnostic sensors installed in the divertor. A number of sectors have been folded into one to generate this layout.

laser induced fluorescence, and IR thermography. These will incorporate cooling features, static baffle elements, and moving shutter elements with the appropriate drive connections.

3. microwave systems, including antennas, waveguides, mirrors, and waveguide connections for reflectometry and interferometry.

The diagnostic components on the divertor must be particularly robust because of their proximity to the plasma, the power deposition onto the divertor, and the potential for contamination with deposits and dust. Their required life will be established against the replacement lifetime of the divertor targets, consumable components that must be replaced periodically (for ITER, RH Class 1 in Table IV, up to 5 times in the machine life). Nevertheless, components must survive more than 1000 h of plasma burn. Intervention time has to be minimal, and replacement components or subassemblies must be on hand for the predicted maintenance intervals.

II.G.2. Diagnostic Components in Port Plugs

The port plug concept adopted in ITER gives a good example platform for the implementation of diagnostics in modules. These modules also provide some flexibility for upgrades. Diagnostic port plugs (see Figs. 8 and 9) are likely to require unscheduled or very infrequent maintenance (RH Class 2 in Table IV; see Ref. 29 for a de-

scription of the ITER port plug maintenance approach). This is driven by the maintenance requirement of the first wall armour, which is the most exposed water-cooled element. There must be the capability to replace or repair these because of the technological risk from erosion, water leakage, etc. It is impractical from the point of view of machine operation time to anticipate routine

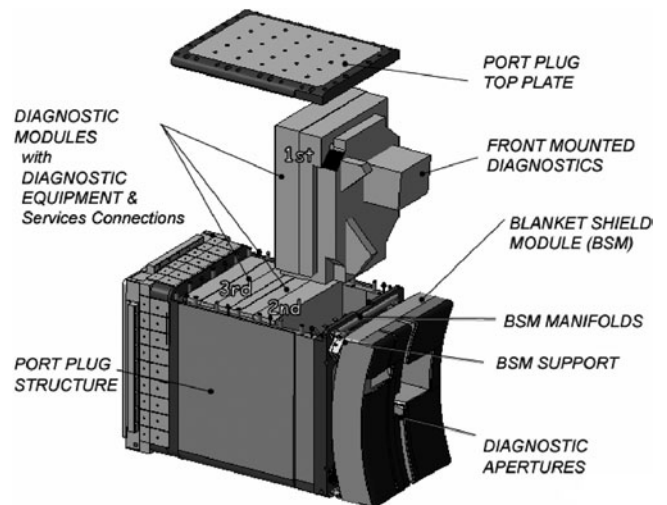


Fig. 8. Schematic of port plugs for diagnostic installations in ITER equatorial ports.

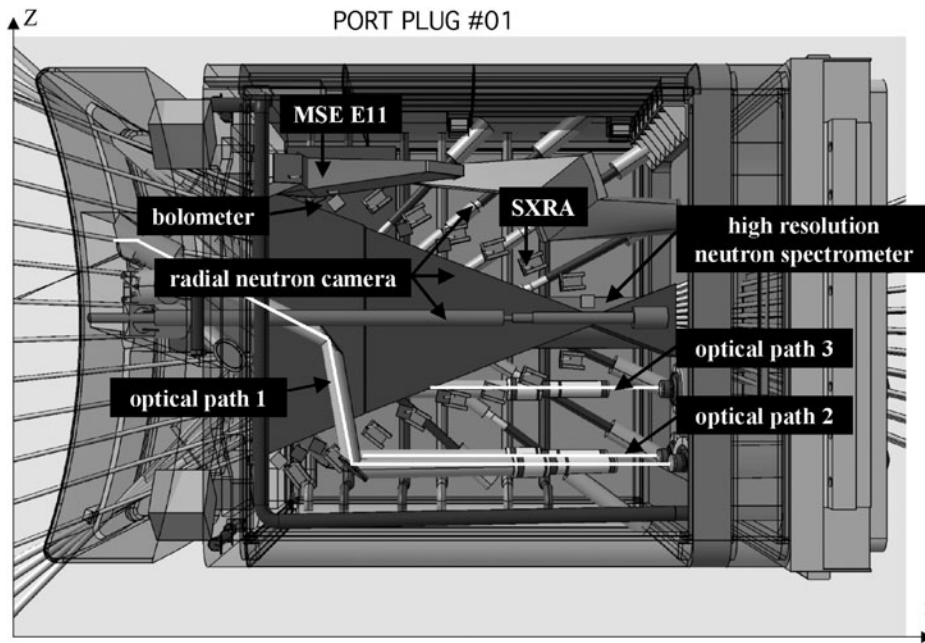


Fig. 9. Semi-transparent side view of ITER equatorial port 01, showing the implementation of six separate diagnostics (one, the visible/IR monitor, with three optical paths) within a single ITER equatorial port plug.

maintenance access. Replacement or refurbishment is unlikely to be more than a few times in the whole machine life cycle.

Mirrors within port plugs should be designed to survive for the full burn time (4700 h in ITER) and conditioning time, although control of erosion and contamination is still a major concern for BPX diagnostic design (see Sec. III) and this may not be possible for all cases. It is therefore desirable to allow window replacement without necessarily dismantling a complete port plug. To enable this refurbishment, diagnostic components will be installed within discrete modules that can be replaced in a hot cell with a minimum of operations.

Diagnostic windows and feedthroughs are in principle vulnerable components (see above). For this reason they should be placed where they are accessible for in situ maintenance. On ITER generally this means near the port plug flange. There, radiation effects are modest (total neutron flux of order 10^{14} n/m²s) and the window can have a long nominal lifetime. At this rate, more than 28 000 h of burn time are required to reach 5% transmission loss for an 8 mm KU-1 window (10^{22} n/m²) at 400 nm (Ref. 30). Similarly, the ITER LIDAR system window can tolerate more than 13 000 h of burn before UV degradation reaches 0.1% at 600 nm and is not at all affected by radioluminescence³¹ (RIL; see Sec. III). It is more likely that the actual in-service lifetime will be dominated by the more difficult to predict events, such as weld leaks within the assembly, and flaw-induced cracking within the window. These elements can be designed to be replaced either in a hot cell facility or in situ; the

latter choice was made for ITER as the activation levels near the port flange are low enough for local maintenance for a large part of ITER life.

II.G.3. Diagnostic Components on Vacuum Vessel Wall

The principal diagnostic components mounted in the vacuum vessel wall (Fig. 3 for the ITER implementation) are sensors for the magnetic diagnostics, bolometers, micro-fission chambers, soft X-ray and UV detectors, and waveguides for reflectometry. Replaceable components are not likely to have active cooling in the exchangeable part and will not be expected to require remote maintenance (they are RH Class 3 in Table IV). Sensors are mounted at sites where the maximum protection possible is offered by the blanket modules. Sensors and cabling are cooled by conduction to the vacuum vessel and thermal radiation to the blanket, and typically are designed to operate in the range 50 to 200 K above ambient temperature during operation, with some exceptions. For ITER, the operating ambient temperature is in the range of 378 K (well-shielded inner part of the vacuum vessel) to 473 K. Component design targets range from 10 K above ambient (for magnetic coils, where thermoelectric currents can be an issue; see Sec. III.C) to 200 K or more above ambient (for waveguide antennas that must come close to the plasma, can be cooled only by low-area contact, and are tolerant of temperature-induced deformation).

All components will have to be designed for the full machine life, with substantial margin. Bolometer

cameras viewing the plasma between blanket modules may require replacement because of the dimensional stability of substrate and thin film under irradiation after ~ 1400 h (see Sec. III.B). The temperature excursions mentioned earlier are proportional to the fusion power, and therefore, a large number of cycles ($>10^4$) must be accommodated over the machine life. Baking conditions (100 to 140 K excursion) for a smaller number of cycles must also be survived by all components.

II.H. Integration of Multiple Systems into Port Plug Modules

Usually, several diagnostic systems must be packed within the port plug. Care must be taken that the labyrinth in the shielding for one system is not made ineffective by another system. Neutronic analysis of the complete arrangement is required. This analysis must also include the surrounding machine geometry giving an intrinsic neutron leakage, such as gaps round removable components (for example, the port plug itself).

The vacuum or containment boundaries of port plugs are particularly congested areas. The size of components is mainly determined by handling requirements and a desire to use standard sizes of similar components. As a result, it is sometimes advantageous to share components at the boundary, such as vacuum extensions, between systems.

Systems mounted on the back of port plugs may be well protected from their own radiation leakage, but the shine-through from neighbouring systems is an important factor in their design. There is little space in the ITER port interspace, and it is likely that the various diagnostic components will share a common support structure.

Systems mounted on the back of port plugs may be well protected from their own radiation leakage, but the shine-through from neighbouring systems is an important factor in their design. There is little space in the ITER port interspace, and it is likely that the various diagnostic components will share a common support structure.

The design of the ITER equatorial port #01 is shown here (Fig. 9) as an example to illustrate many of these points. The Radial Neutron Camera requires a long vertical slot in the first wall to accommodate the fan array of sight lines. Diagnostic sensors such as bolometers and soft X-ray detectors are located in the neutron camera aperture and have a substantial view of the plasma using the same slot. Similarly the channel for the high-resolution neutron spectrometer uses the same first wall aperture.

An example of the neutronic effect of combining diagnostics is given by the ITER equatorial port plug #10 with LIDAR, Polarimetry and Divertor Thomson scattering.^{32–34} The model of the port plug used for this calculation is as shown in Fig. 10. The port plug is modelled as a steel frame with 150 mm base, 100 mm sides, and 160 mm flange, filled with shielding (60% stainless steel–40% water) with a 20 mm gap to the port. The LIDAR system in one half of the model has a 180 mm aperture at the first wall. It includes five 300 to 500 mm diameter mirrors and two ~ 150 mm quartz windows in the seal flange. The polarimetry system, in the second part of the model, has ten 140 mm diameter

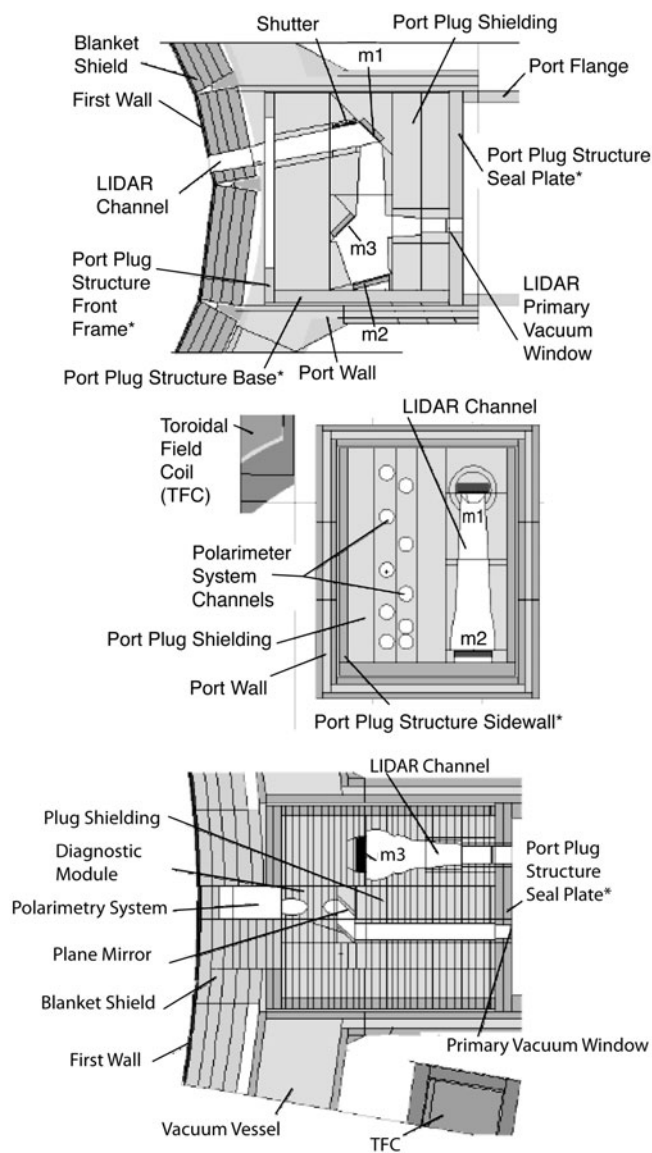


Fig. 10. Sections through the Monte Carlo model used to analyze the effect of cross talk between the ITER LIDAR and polarimetry systems on the same port.^{33,34} Top: Vertical section along a major radius through the LIDAR system. The plasma is on the left. Middle: Vertical section facing toward the plasma showing the LIDAR system on the right and the 10 polarimetry channel exits on the left. Bottom: Horizontal section at the level of LIDAR mirror m3, showing the proximity between the LIDAR and polarimetry neutron labyrinths for a representative channel. Mirror m3 is 500 mm. Other key dimensions and compositions may be found in the text.

cylindrical channels and 115 mm quartz windows in every channel. There is a 230×140 mm rectangular slot at the entrance of the channels.

When the MCNP results are analyzed, it is found that the polarimetry system increases the neutron flux and

nuclear heating at the neighbouring LIDAR elements. The flux in the last (3rd) LIDAR mirror is increased by about 4 times (7×10^{12} to $2.9 \times 10^{13} \text{ m}^{-2}\text{s}^{-1}$) and the nuclear heat deposition by about 8 times (12 to 100 W/m^3). At the LIDAR window, the increases in flux ($\sim 4.5\times$, or from 2.1×10^{11} to $9.5 \times 10^{11} \text{ m}^{-2}\text{s}^{-1}$) and in nuclear heat deposition ($\sim 14\times$, or from 0.14 to $\sim 2 \text{ W/m}^3$) are much larger although absolute levels are low. The fast neutron flux at the Polarimetry system mirrors is 1 to $2 \times 10^{16} \text{ m}^{-2}\text{s}^{-1}$, total flux is $\sim 2\times$ higher. Volumetric nuclear heat deposition at the mirrors is 50 to 150 kW/m^3 . These are unaffected by the presence of LIDAR. Window neutron fluxes are less than $3 \times 10^{12} \text{ m}^{-2}\text{s}^{-1}$ (fast) and $6 \times 10^{12} \text{ m}^{-2}\text{s}^{-1}$ (total) and the volumetric nuclear heat deposition is 1 to 7 W/m^3 , similar to the LIDAR values.

For the plug structure, the plug Be-first wall receives nuclear heating at 4.6 MW/m^3 , the remainder of the blanket heat sink layer 6.4 MW/m^3 . This is attenuated to 1 W/m^3 by the port plug flange. The total nuclear heat in the plug is 3.0 MW, typical for the heating of two normal blanket modules. Overall, the residual dose rate between the plug flange and bioshield due to neutron streaming through the integrated diagnostic port structure is below $80 \mu\text{Sv/h}$ two weeks after shutdown and $<1 \text{ W}$ is contributed to the neighbouring PF and TF coils at 4 K. These values are within allowable levels.

It can be seen that, with care, the elements of many diagnostics can be integrated into one location. There is competition for space and neutron shine-through inventory, although some savings can be made using plasma access elements, such as blanket slots, of one system to provide access for another.

III. NUCLEAR RADIATION EFFECTS ON DIAGNOSTIC COMPONENTS

The BPX plasma will give rise to high-energy neutron and gamma fluxes, penetrating well beyond the first wall, implying a need to use, or if necessary develop materials and components whose properties are resistant to radiation damage. In most cases, components in the primary vacuum will have to survive for the full machine life so that both prompt ionizing radiation flux (dose rate) and neutron and gamma fluence will play important roles. An additional complication is that, as dose-dependent radiation effects build up in the materials, the response to prompt flux changes can also change. For structural metallic materials the problem of radiation damage is expected to be severe, although tolerable, only near to the first wall. However, the problem facing the numerous insulating components required for diagnostic systems is far more serious due to the necessity to maintain not only the mechanical, but also their extremely sensitive physical properties intact. Nearly all diagnostics systems^{7,35} require insulating ma-

terials, from electrical insulation in coils and probes, cables, bolometer substrates, insulating breaks and feed-throughs, to transmission components for optical and electromagnetic diagnostics, allowing sensitive instrumentation to be located remotely. Windows have to transmit signals over a broad spectrum ranging from radio frequency dielectric windows, through to the infrared, visible, and ultraviolet. The use of optical fibers is a particular case with specific constraints. For all these uses, in addition to mechanical strength and volume stability to satisfy their structural role (e.g., windows, where embrittlement and tritium retention must be considered), the physical properties of concern will be electrical conductivity, dielectric loss and permittivity, thermal conductivity, and optical properties (transmission and luminescence). After a short review of radiation effect mechanisms in insulators, the radiation effects on these properties will be discussed, illustrated by representative examples of work on the radiation testing of actual diagnostic components.

III.A. Brief Review of Radiation Effects in Insulators and Irradiation Testing Methods

In a BPX, insulating materials will be required to operate under a radiation field in a number of key systems. The radiation flux and fluence levels will depend, as discussed in Sec. II.A, on location in, and design of, a given device. The radiation intensity will depend not only on the distance from the plasma, but also in a complex way on the actual position within the machine due to streaming along the numerous penetrations required for cooling systems, blanket structures, heating systems, and diagnostic and inspection channels, as well as the radiation coming from the water in the outgoing cooling channels due to the $^{16}\text{O}(n,p)^{16}\text{N}$ nuclear reaction. However, one-, two-, and even three-dimensional models are now available that enable the neutron and gamma fluxes to be calculated with confidence at most, if not all, machine positions.^{32,36,37} Due to the marked variation in radiation levels, most studies of radiation effects have taken this into account by providing, where possible, materials data as a function of dose rate (flux), dose (fluence), and irradiation temperature.

Radiation damage may be divided into three main components: displacement damage, ionization effects, and transmutation. In a fusion environment displacement damage, which affects both metals and insulators, results from the direct knock-on of atoms/ions from their lattice sites by the neutrons, giving rise to vacancies and interstitials. Those primary knock-on atoms (PKAs) with sufficient energy may go on to produce further displacements, so-called cascades. The numerous point defects thus produced may either recombine, in which case no net damage results, or they may stabilize and even aggregate producing more stable extended defects. These secondary processes that determine the fate of the vacancies and

interstitials are governed by their mobilities. These mobilities are highly temperature dependent, and in the case of insulators even depend on the ionizing radiation level (radiation enhanced diffusion). Displacement damage is measured in dpa (displacements per atom) where 1 dpa means that each atom in the material has been displaced from its structural lattice site an average of one time. At the first wall of ITER the displacement damage rate will be of the order of 3×10^{-7} dpa/s. (As a “rule of thumb,” 10^{25} n/m² \equiv 1 dpa on the oxygen/nitrogen sublattice of ceramic insulators.) In contrast, ionizing radiation, although absorbed by both metals and insulators, in general only produces heating in metals. However, certain aspects of radiation damage in metals, such as radiation enhanced corrosion and grain boundary modification, are related to ionization. The effects of ionization on insulators are in comparison quite marked due to the excitation of electrons from the valence to the conduction band, giving rise to charge transfer effects. Ionizing radiation is measured in absorbed dose Gy (Gray) where 1 Gy = 1 J/kg. At the first wall of ITER the dose rate will be of the order of 10^3 Gy/s. For the envisaged operational life, this results in the accumulation of about 3 dpa and 10^{10} Gy in the first wall region. These levels quickly decrease when moving away from the plasma, and by the vessel inner wall two orders of magnitudes are lost in neutrons and three in γ (Fig. 2). Some electrical components (coils, bolometers) will be situated in the harshest locations, but windows will be at the back of labyrinths under lower fluxes (e.g., 10^{14} n/m²s⁻¹ for LIDAR windows).

The response of insulators to both displacement and ionizing radiation is more complex than in the case of metals. Apart from a few specific cases (diamond, for example), insulating materials are polyatomic in nature. This leads to the following:

1. There are, in general, two or more sublattices that may not tolerate mixing. This gives rise to more types of defects than can exist in metals.
2. Because of the electrically insulating nature, the defects may have different charge states, and hence different mobilities.
3. The displacement rates and thresholds, as well as the mobilities, may be different on each sublattice.
4. There may be interaction between the defects on different sublattices.
5. Displacement damage can be caused in some cases by ionization alone (radiolysis).

As a consequence of these factors, although radiation damage affects all materials, the insulators are far more sensitive to radiation damage than metals. While stainless steel, for example, can withstand several dpa and GGy with no problem, some properties of insulating materials can be noticeably modified by as little as 10^{-5} dpa

or a few kGy. In addition to displacement damage and ionization, the high-energy neutrons will produce nuclear reactions, in particular (n, γ) , (n, α) , and (n, p) in all the materials, giving rise to transmutation products.³⁸ These will build up with time and correspond to impurities in the materials that may modify their properties, in particular for insulators that are particularly sensitive to impurities. Furthermore, some of these transmutation products may be radioactive and give rise to the need for remote handling and hot cell manipulation in the case of component removal, repair, or replacement. However, with careful choice of materials for a next-step machine such as ITER, transmutation products, with the possible exception of hydrogen and helium, are not expected to present a serious problem.

The result of these radiation damage processes are flux and fluence dependent changes in the physical and mechanical properties of the materials, which may be particularly severe for the insulators. The properties of concern that suffer modification are the electrical and thermal conductivity, dielectric loss and permittivity, optical properties, and to a lesser extent the mechanical strength and volume stability. The effects of such changes are that the insulators may suffer Joule heating leading to breakdown due to the increased electrical conductivity and/or lower thermal conductivity, windows and fibers become opaque from the microwave to the optical region and emit strong luminescence (radioluminescence), and in addition the materials may become more brittle and may suffer swelling. Clearly some materials are better than others. The organic insulators that are widely used in multiple applications in general degrade under purely ionizing radiation and are not suitable for use at temperatures above $\sim 200^\circ\text{C}$; as a result their use will be limited to remote handling applications during reactor shutdown. The alkali halide class of inorganic insulators have been extensively studied and are widely used as UV optical windows and mirror coatings (MgF₂) and scintillators (NaI); however, they are susceptible to radiolysis (displacement damage induced by electronic excitation) and degrade at low radiation fluences. Of the numerous insulating materials it is the refractory oxides and nitrides that in general show the highest radiation resistance. Of these the ones that have received specific attention within the fusion program include MgO, Al₂O₃, MgAl₂O₄, BeO, AlN, and Si₃N₄. In addition different forms of SiO₂ and materials such as diamond and silicon have been examined for various window and optical transmission applications.

In recent years, because of the acute lack of data for insulators and the recognition of their high sensitivity to radiation, most work has concentrated on the immediate needs for ITER. At the present time no entirely suitable irradiation testing facility exists, and as a consequence experiments are being performed in nuclear fission reactors and particle accelerators, as well as gamma and X-ray sources, in an attempt to simulate the real operating

conditions of the insulating materials and components. The experiments required must simulate the neutron and gamma radiation field, i.e., the displacement and ionization damage rates, the radiation environment, i.e., vacuum and temperature, and also the operating conditions such as applied voltage, or mechanical stress. It is furthermore essential that in situ testing is carried out to determine whether or not the required physical properties of the material or component are maintained during irradiation.

Experimental fission reactors have the advantage of producing a radiation field consisting of both neutrons and gammas, although in most cases the actual neutron energy spectrum and the displacement to ionization ratio are not those that will be experienced in a fusion reactor. To date, experimental fission reactors have in the main been used for irradiations in the metals programs, where the emphasis is on the neutron flux and little consideration is given to the gamma field. As a result, the irradiation channels have in general been optimized with this criterion. It is possible to select positions within the reactors that, together with suitable neutron absorber materials and neutron to gamma converters, provide acceptable radiation fields, though this is not generally done and results must therefore be interpreted with care for fusion applications. Additional difficulties with in-reactor experiments come from the inaccessibility of the radiation volume, which makes it difficult to carry out in situ measurements and to monitor the local process parameters. Nevertheless, in situ measurement of electrical conductivity, optical absorption and emission and even radio frequency dielectric loss have been made. The problem of irradiating in vacuum still remains, with most experiments using a controlled He environment. Many experiments rely on nuclear and gamma heating balanced by He conduction to reach the required temperature and hence have difficulty with temperature control, due in part to the changes in the reactor power, but also to the problem of calculating the final sample or component temperature from sparse measurements. Furthermore, the temperature distribution reached in this way may bear little resemblance to the same sample in the fusion environment where, in vacuum, cooling relies on nonuniform conduction and radiative transfer, rather than quasi-uniform conduction through He. One additional difficulty comes from the nuclear activation of the sample or component, which generally means that post irradiation examination (PIE) has either to be carried out in a hot cell, or postponed until the material can be safely handled and, in some facilities, may be impossible.

Particle accelerators are ideal for carrying out in situ experiments in vacuum and at well-controlled temperatures due to the easy access and the very localized radiation field. High levels of displacement damage and ionization can be achieved with little or no nuclear activation. It is, however, in the nonnuclear aspect of the

radiation field where their disadvantage is evident, and great care has to be taken to ensure that appropriate displacement rates are deduced to enable reliable comparison with the expected fusion damage. A further serious disadvantage is due to the limited irradiation volume and particle penetration depth. This in general means that only small thin material samples or components can be tested.

Radiation testing for diagnostic systems takes full advantage not only of fission reactors and particle accelerators, but also ^{60}Co gamma irradiation facilities and even X-ray sources. The use of such widely different radiation sources can be justified as long as the influence of the type of radiation on the physical parameter of interest is known. This in certain cases is true for radiation-induced electrical conductivity and radioluminescence, for example, where for low total fluence it is the ionizing component of the radiation field that is important. In certain cases, for example, when testing fusion yield detectors, or changes in properties for materials very near the first wall, sample irradiation using 14 MeV sources can also be appropriate.

In situ measurements can now be made during irradiation of the important electrical, dielectric, and optical properties. In addition other aspects such as mechanical strength and tritium diffusion are being assessed during irradiation. There has been considerable progress on the understanding of the pertinent effects of radiation on in-vessel components and materials, in particular for diagnostic applications.¹¹ Problems that have been addressed and irradiation testing performed include RIEMF and TIEMF (radiation- and temperature-induced electromotive force) for MI cables and coils, bolometers, hot filament pressure gauges, a comparison of absorption and luminescence for different optical fibers and window materials, and dielectric protective coatings for second mirrors. Many papers have been published discussing general aspects of radiation damage in insulating materials for fusion applications, and recent reviews contain the most pertinent references.³⁹⁻⁴⁵ Comprehensive details and additional references for much of the work discussed later are to be found in several papers and reports.^{30,46-54} In the following the radiation effects are presented in detail together with examples of their influence on specific diagnostic components arising out of recent R&D (Ref. 11).

III.B. Electrical Degradation I: RIC, RIED, and Examples (Pressure Gauges, Bolometers)

Electrical resistance, more generally discussed in terms of the electrical conductivity (the inverse of the resistance), is an important basic parameter for numerous systems and components including MI cables and magnetic coils, feedthroughs and stand-offs, and wire insulation. Any reduction in the electrical resistance of the insulator material in these components may give rise

to problems such as increased Joule heating, signal loss, or impedance change. The main candidate material for these applications is Al_2O_3 , and is also the one that has been most extensively studied, both in the polycrystalline alumina form and as single crystal sapphire. At the present time three types of electrical degradation in a radiation environment are recognized and being investigated; these are radiation-induced conductivity (RIC), radiation-induced electrical degradation (RIED), and surface degradation. Of these types of degradation, RIC was the first to be addressed in a fusion context, as this enhancement of the electrical conductivity is ionizing flux dependent and hence a possible cause for concern from the onset of operation of any fusion device. RIC has been studied for many years, and a sound experimental and theoretical understanding exists.⁵⁵⁻⁵⁹ The mechanism involves excitation of electrons from the valence to the conduction band, and trapping in shallow defect levels within the band gap, and its magnitude depends in a complex way on ionizing radiation dose rate, temperature, and material impurity content, making it difficult to predict in a specific material grade without detailed experimental characterization.^{57,58} With neutron dose the number and type of defects in the material increases and modifies the RIC; however, RIC is sufficiently "well understood" to be accommodated by current designs. It is important to remember that RIC is a flux dependent effect and will be present from the onset of operation of any BPX machine. Hence devices that are sensitive to impedance changes, and employ, for example, MI cables, must take RIC into account. The extent to which that is difficult depends on the details of the machine. For example (Fig. 11), the effect of prompt RIC at the first wall of ITER, FIRE, and IGNITOR differs by a factor of 5.

In contrast to RIC, RIED is a permanent enhancement of the volume electrical conductivity caused by radiation-induced defects in the presence of an electric field. After a certain period of exposure, it comes to dominate over RIC (see Fig. 12). It is a more serious problem, not only from the point of increasing the electrical conductivity beyond that of RIC, but also because this type of degradation is still not fully understood. There is even no general agreement as to whether RIED exists as a real volume degradation, due to the inherent experimental difficulty of separating surface and volume conductivities. Many relevant references can be found in Refs. 39 and 60, where the importance of electrical field, temperature, total dose, dose rate, radiation source and spectrum, material type, and irradiation environment (vacuum, air, He) is discussed. Available in-reactor results support earlier indications that RIED is a complex phenomenon depending on material type.⁶¹ Recent reports on aluminium colloid identification for degraded alumina⁶² help to confirm earlier results and modelling, where colloid production was suggested as being the cause of RIED, and was related to observed gamma alumina formation and material embrittlement.^{60,63} Available data

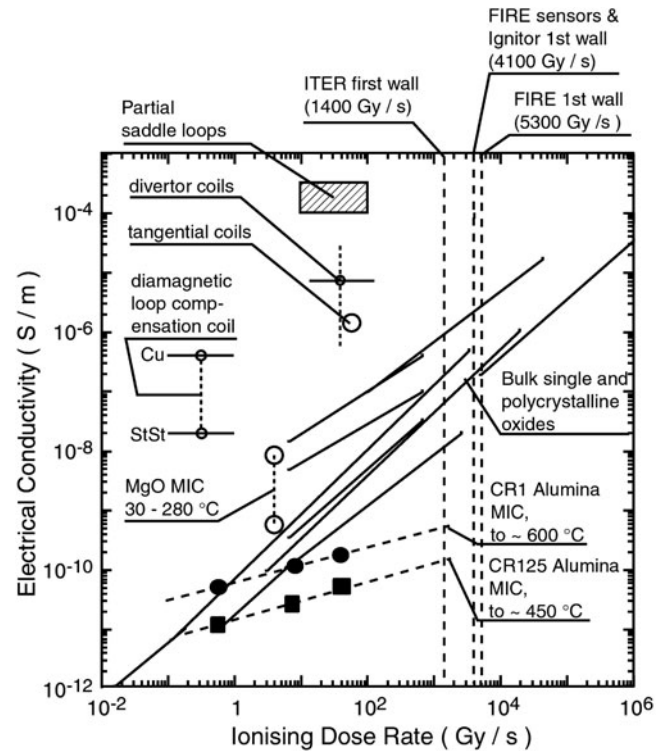


Fig. 11. Critical conductivity that can be tolerated by various ITER sensors against the ionizing dose rate at their location (points and ranges on upper left corner of figure) compared to experimental data on RIC observed in typical insulators [bulk and in mineral insulated cable (MIC) form], plotted against ionizing dose rate. Typical BPX first wall values of ionizing dose rate are also shown. After Ref. 85.

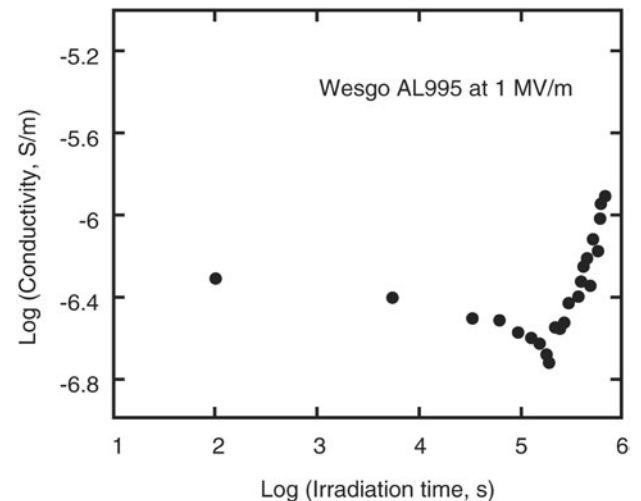


Fig. 12. Electrical conductivity for 995 alumina irradiated at 450°C , 700 Gy/s , $1\text{E}-10\text{ dpa/s}$, with an applied electric field of 1 MV/m . Data from Ref. 66. The onset of RIED is indicated by the sharp rise in conductivity at around $2 \times 10^5\text{ s}$.

has enabled moderately safe operating conditions to be recommended for ceramic insulator use (typically <100 Gy/s, <473 K and <0.15 MV/m), but further work is clearly required to ensure reliability of selected insulators in ITER and beyond.

For insulating components, surface degradation may prove to be even more serious than RIC and RIED volume effects. Two types of surface degradation have been examined, a contamination caused by poor vacuum, sputtering, or evaporation⁶⁴ and a real surface degradation related to radiation-enhanced surface vacuum reduction and possibly impurity segregation.^{65,66} Both forms are affected by the irradiation environment and ionizing radiation. However, the real surface degradation effect is strongly material dependent. It is important to note that this type of degradation occurs in vacuum but not in air or helium. This stresses the extreme importance of a representative irradiation environment for material testing. Most insulating materials in ITER must indeed operate in high vacuum, whereas to date many in-reactor experiments have been performed in helium. To address this an active vacuum general purpose radiation test facility for assessment of ceramic insulators and diagnostic components has been prepared and used to investigate electrical degradation.⁶⁷

III.B.1. Pressure Gauges

Pressure gauges are used to monitor neutral gases, and specific sensor design work was conducted for ASDEX, using a hot filament and electrode assembly with insulated feedthroughs.⁶⁸ Several of these pressure gauge mock-ups have been irradiated to investigate the impact of neutron, gamma, and electron irradiation on the electrical feedthroughs, the most critical component of the pressure gauge that may degrade due to RIC, RIED, and surface effects.^{49,53,69–70} Following initial screening under electron irradiation, an in-reactor irradiation up to 0.1 dpa, 1.5 GGy, at 673 K in static vacuum was performed. It was found that the insulation resistance of the feedthroughs remained sufficiently high, >2 M Ω compared with the required 100 k Ω , to guarantee correct operation of an operational hot filament pressure gauge. Furthermore, other possible causes of degradation (ionization of residual gas, RIEMF effects) were insignificant.

III.B.2. Bolometers

Bolometers will be placed inside the vacuum vessel in very demanding locations, where in ITER they will accumulate at least 0.1 dpa, and in recent years significant steps have been taken toward developing and testing radiation-hard bolometer sensors. The reference resistive bolometer type envisaged for ITER (Ref. 11) is based on the high-temperature gold on mica miniature bolometer developed for JET (Ref. 71), based on a bolometer first used on other machines.⁷² These bolometers employ a

thin mica substrate as support for a delicate gold meander electrical resistance bridge network. Neutron irradiation tests performed on one such bolometer, however, have shown several problems related to irradiation damage, including a weakening of the gold grids due to partial transmutation of gold to mercury, detachment of the meander from the substrate possibly related to this alloy change and/or substrate swelling, as well as basic electrical contact problems following high-temperature neutron irradiation even below 0.01 dpa (Refs. 42, 48, and 73). Using platinum on alumina, aluminium nitride or silicon nitride should allow higher temperature operation, reduced metal transmutation and substrate swelling, as well as better metal to ceramic adhesion. Sheets of alumina and AlN with platinum resistance tracks have been prepared and irradiated with electrons and neutrons at high temperature in vacuum to assess the behavior and compatibility of the materials.^{53,74–77} While no degradation of the platinum or the substrates was observed by 0.013 dpa, electrical contact with the thin film again proved problematic. Bolometers using silicon nitride are also being developed, have been successfully tested during electron irradiation, and are now ready for in-reactor testing.⁷⁸ Anticipated radiation effects (RIC, RIED, surface degradation) on the electrical insulation of the mica, alumina, aluminium nitride, and silicon nitride substrates have so far proved to be negligible compared with the swelling, transmutation, and simple electrical contact problems.

To reduce the number of cables, a capacitive bolometer based on ferroelectric materials with potentially high performance has been proposed⁷⁹ and is being developed further as a radiation-hard alternative to the resistive bolometers.^{80–83} The dielectric properties as a function of temperature (293 to 673 K) and frequency (1 to 250 kHz) before and after neutron irradiation have been measured for different types of ferroelectric films. Irradiation and annealing measurements on PbZrO₃ films, a highly oriented perovskite antiferroelectric material, to a neutron fluence of 10^{22} n/m² show only moderate radiation damage, and thus, these films are most promising for further investigations. However, in situ measurements during ionizing radiation show marked degradation of the low frequency dielectric (capacity) properties.⁵² Further development is underway to improve both the material radiation response and the delicate electrical contacts present in these prototype devices.

III.C. Electrical Degradation II: RIEMF, TIEMF, RITES, and Examples (MI Cables and Coils)

It is convenient at this stage to introduce also RIEMF, although strictly speaking it is not a materials degradation, but an induced voltage or current that “degrades” the signal quality carried by MI coaxial cables in a radiation field. RIEMF effects, already observed decades ago on fission reactor cables, are caused by radiation-induced

currents flowing across the cable insulator triggered by charged particles (e.g., energetic electrons by Compton interactions, recoil protons, β -emitting isotopes) created by gamma or neutron reactions with sufficient energy to enter the cable insulating material and inducing a current between core and sheath. RIEMF can produce several volts between the inner and outer conductors, or supply tens of microamps of current. Many diagnostic systems requiring the detection of nA currents or μV DC voltages, using long sections of such cables, or even using the cables themselves as sensors in magnetic probes, will be particularly vulnerable.^{84,85} Early systematic studies on RIEMF (Ref. 86) were followed by in-reactor tests using different materials for the core wires: stainless steel, copper, or nickel.^{84,87-91} The results showed a complex pattern, with strong dependence on cable geometry and material. In addition the induced currents vary with time, and in some cases change polarity without remaining proportional to reactor power. In order to better understand the RIEMF, recent theoretical⁹² and experimental⁹³ work has concentrated on the prediction of induced currents. Validation irradiations of coiled and straight MI cables under gamma and neutron environments showed that neutron effects are well modelled, while the strong dependence on the cable environment and its orientation, observed under gamma irradiation, requires a larger model basis, involving the cable surroundings and a fine tuning of the energy spectrum. From all the work on RIEMF one may conclude that at the onset of irradiation (operation of ITER) gamma-induced RIEMF will dominate. With irradiation time, nuclear reaction effects, in particular beta emission, can also become important giving rise to a time-varying RIEMF. These latter effects can be minimized by choosing materials with low neutron capture cross sections. From this point of view, steels or Inconel are preferable to copper for the central conductor. The importance of the insulation, alumina or magnesia, has not been ascertained due to the lack of available MI cables identical in all but insulation material. However, its role appears to be minor, with no clear differences being reported. Dependence on MI cable size (inner conductor diameter, insulation thickness, outer sheath diameter and thickness) can now be modelled, but again has not been experimentally validated due to the lack of availability of suitable cables.

An additional complication has recently been highlighted,¹¹ the generation of significant voltages in the microvolt range along the central conductor itself due to temperature differences of order 100 K. In-reactor tests of MI coils coupled to integrators^{48,94} indicated that phenomena additional to RIEMF must be considered, such as thermoelectric effects for the central conductor due to transmutation or defect generation [radiation-induced thermoelectric sensitivity⁹⁵ (RITES)]. Moreover, strong thermal effects [temperature-induced EMF (TIEMF)] on the differential voltage for MI cable coils were reported even without radiation.⁹⁶ It is becoming clear that voltages

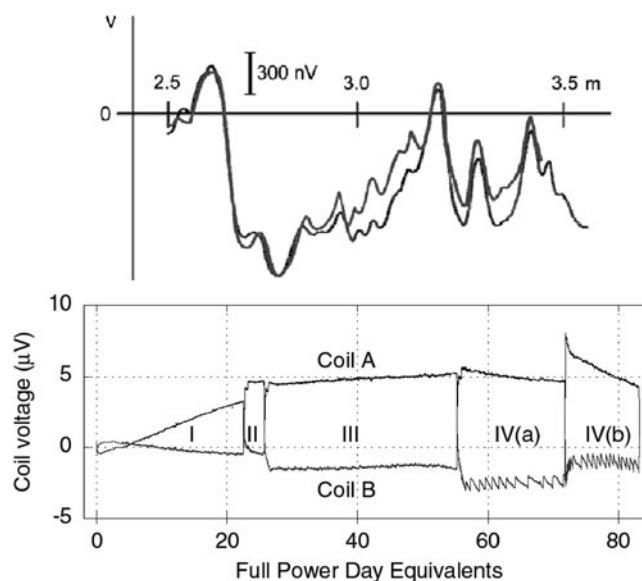


Fig. 13. Top: Direct measurements of TIEMF in virgin MI Cable heated to ~ 73 K above room temperature over a ~ 80 mm width with an air gun travelling at ~ 25 mm/s; two successive runs are shown. After Ref. 98. Bottom: Voltage attributed primarily to RITES measured in situ in a fission reactor across two test coils wound from MI Cable over four reactor cycles obtained over a period of about a year. After Ref. 95.

along the central conductor of MI cables due to TIEMF and RITES exceed that possibly induced by any asymmetric RIEMF current appearing along the conductor.^{54,97} Examples of such voltages are shown in Fig. 13.

Recently, specific in-reactor experiments⁹⁹ have confirmed that transmutation is almost certainly a major contributing cause to RITES in copper cables, while defect generation is the most likely contributor in stainless steel. Extrapolation of these results to ITER-like spectra suggests that both copper and steel-core cables will be affected, but the effect is more manageable for copper within the expected ITER lifetime.

Further work is also underway on TIEMF, which is particularly large for Cu-cored MI cables. It has been confirmed that these positive and negative voltages are generated at localized points of the cable, suggesting that some inhomogeneity is present, but no geometric variations have been observed by X-ray imaging of the cable core and sheath. Furthermore, no annealing or modification of the sensitive regions has been observed for heating up to 823 K, indicating that the problem was not related to work hardening effects in the copper.¹⁰⁰ Detailed examination of the sensitive regions of the Cu cored MI cables show severe surface damage (grooves and cavities) for the Cu wire extracted from the MI cable, compared with the highly polished surface of normal

single strand Cu wire. In addition microscopic regions of recrystallized Cu grains and inclusions of SiO₂ have been observed.¹⁰¹ It is suggested that these features may modify the local Seebeck coefficient and give rise to TIEMF.

The combined effects of TIEMF and RITES make cable selection difficult. TIEMF results suggest the use of hard metals (steel, for example) or, possibly, alloys for the MI center conductor, to avoid the insulator grains damaging the conductor during drawing. RITES results favor copper. An option is to move away from MI cable altogether. This allows to combine the use of copper with better control of manufacturing micro-damage. Another, very effective, mitigation measure is to improve the thermal conductivity of the coils. Such a coil design is already under investigation for the ITER tangential sensor coils. The total effective temperature difference in a coil winding can be reduced below 10 K using a winding potted in ceramic compound.¹⁰² Other coil methods, for example, sintered coils¹⁰³ or, where possible, embedding MI-wound coils in coolant loops,¹⁰⁴ are under consideration. Reducing the temperature differentials may also be the only option for the in-vessel wiring conduits, where use of MI cable may be difficult to avoid.

For magnetic coils, RIEMF, TIEMF, and RITES far outweigh other radiation effects. For RIC and RIED the choice of insulator type and thickness, and placing the MI cables and coils in a shielded area (≤ 100 Gy/s) and sizing the insulation for low electric fields (< 0.15 MV/m), one can ensure that they will not affect reliability or the measurement. For ITER, the highest temperature of the inner vessel tangential coils during the bulk of the irradiation can be as high as 513 K and could be an issue, but the improvement of coil cooling required to mitigate TIEMF and RITES will likely bring the coil temperature into the acceptable range (< 473 K). The large number of effects and the complexity of the components involved (coil assembly, joints and feeder cables and conduits), combined with the difficulties of maintaining the coils imply that, as for the bolometers, systematic irradiation tests of prototypes will be required for all the elements in the magnetics signal chain.

III.D. Optical Degradation: RIA, RIL, and Examples (Windows, Fibers, and Mirrors)

Another area of concern is related to the effects of radiation on the optical properties of materials to be used as transmission components (windows, lenses, optical fibers, mirror coatings) for the UV, visible, and IR wavelengths. Radiation-induced optical absorption (RIA) and light emission (RIL) (radioluminescence) impose severe limitations on the use of any optical material within a radiation field. RIA is a function of dose: both ionization and displacement damage produce a buildup of defects (impurity and vacancy related) in the transparent insulator materials that generally result in transmission loss due to broad absorption bands in the UV

to IR range. RIL in contrast is a function of dose rate and is caused by excitation of impurity and vacancy defects through electron and hole ionization production. Like RIC this radioluminescence will be a problem from the onset of operation of any BPX. Both RIA and RIL depend strongly on irradiation temperature, and with few exceptions both effects are less severe at higher temperatures due to reduced defect stability and quenching. For diagnostic applications the optical components are expected to maintain their transmission properties under high levels of ionizing radiation (to > 10 Gy/s) and atomic displacements (to $> 10^{-10}$ dpa/s), at elevated temperatures (373 to 473 K), during many hundreds of hours. Of the two initial candidate materials sapphire and SiO₂, although sapphire is considerably more radiation hard in terms of RIA than SiO₂, the intense RIL compared to the better SiO₂ grades was shown to be one of the main limitations for sapphire to fulfil the role of transmission component, making it extremely difficult to separate out the plasma emission from the window emission and absorption in the UV to NIR range.¹⁰⁵ Further work has concentrated almost exclusively on silica-based materials, and in particular two radiation hard Russian fused silicas, KU1 (high OH) and KS-4V (low OH) materials, considered as suitable for general window applications and lenses.¹⁰⁶⁻¹⁰⁸

III.D.1. Radiation-Induced Absorption

Results on the gamma radiation-induced absorption for bulk KU1 and KS-4V are in general agreement for irradiations up to 100 MGy and temperatures up to 300°C. Under these conditions the induced absorption bands are below 350 nm. In the case of KU1 these bands markedly reduce with increasing temperature, allowing usable transmission down to 250 nm (Ref. 107). KS-4V, on the other hand, is anomalous, the absorption increasing with temperature up to a maximum at about 100°C. However, it may be safely used above 350 nm (Refs. 108 and 109). Because of the difficulty of irradiating optical fibers at different controlled temperatures such behavior has not been reported, but should equally occur for fibers made from KS-4V. Low dose fast and 14 MeV neutron irradiations also produce very similar defect damage with the induced absorption bands being below 350 nm for damage levels $\leq 10^{-5}$ dpa. However, for higher doses the intense UV absorption bands begin to extend well into the visible range.^{110,111}

An important aspect of RIA, which has so far received little attention, is that of recovery effects, noted already in TFTR (Ref. 112). One of the typical features of a BPX is the pulsed operation. Although the aim is to reach a quasi-continuous regime, ITER, for instance, will certainly experience repetitive plasma burn interruptions. This aspect is not always easy to simulate in the usual irradiation experiments and is seldom considered in gamma tests. Recovery phenomena are, however,

nonlinear and the actual evolution of RIA can depend on the radiation history.¹¹³

III.D.2. Laser-Induced Damage Threshold

Recently completed work on laser-induced damage in KU1 and KS-4V for LIDAR applications has confirmed the limited influence of radiation-induced absorption and electrical conductivity on the damage threshold for high-power laser transmission. This is not expected to be a problem, as the expected ionization levels (<100 Gy/s) do not increase the electron density in the conduction band enough to enhance significantly any dielectric breakdown mechanism, and thermal effects are not of concern due to the low RIA for KU1 and KS-4V at typical LIDAR laser wavelengths. On the other hand, metallic deposition due to sputtering or evaporation can seriously reduce the damage threshold even for deposited layers only a few nm thick. The effect is strongly material dependent and requires further examination. Furthermore, self-cleaning with subthreshold laser pulses is not effective for all deposited materials.^{114–116} More recently, severe degradation of the optical and electrical properties of KS-4V due to surface bombardment by hydrogen ions has been reported.¹¹⁷ This potential problem is being further examined to quantify the risk.

III.D.3. Radiation-Induced Luminescence

Radioluminescence effects are a major concern in the optical materials for fusion diagnostics. The light comes from two sources: Cerenkov emission due to the passage of relativistic electrons through the material and ionization-induced excitation of electronic levels of defects and impurities. The former is common to all the different materials, while the latter is material specific. The Cerenkov emission is essentially temperature independent, but the defect-related emission in general shows strong thermal quenching and for irradiation temperatures above ~ 423 K may be significantly reduced in intensity. Materials with high radiation tolerance, such as sapphire, have been excluded due to their intense RIL (Refs. 105 and 118). In contrast, silica, and in particular KU1 and KS-4V, show far less intense RIL. In these materials in addition to the unavoidable Cerenkov emission, which decreases from the UV as the inverse square of the wavelength, small RIL peaks due to electronic excitation effects appear in the visible region. The 450 nm peak observed in many silicas has an intensity proportional to dose rate¹¹⁹ but fortunately is thermally quenched above 423 K (Ref. 120).

III.D.4. Optical Fibers

Several different optical fibers have been examined¹¹ to assess radiation-induced absorption and light emission, the viability of high-temperature operation and annealing, jacketing material, and the influence of hy-

drogen loading. In addition, parallel work is being carried out on the possibility of photo-bleaching using high-intensity lasers to recover transmission, “holey” fibers for improved transmission and radiation resistance, and fibers with extended blue-UV transmission.^{110,121–128}

The fibers that have been examined were provided by the EU (STU and SSU polymer jacketed from Heraeus), Japan (MF and FF polymer jacketed, fluorine doped from Mitsubishi and Fujikura), and the Russian Federation (KU1 and KS-4V aluminium jacketed and hydrogen loaded from FORC/IOFAN). Irradiations have been carried out to total doses in excess of 10 MGy and 10^{22} n/m², and for temperatures from about 303 to 573 K. An example of the results of such an irradiation is shown in Fig. 14. Under these conditions the most promising fibers are the hydrogen loaded KU1 and KS-4V. Above 400 nm these fibers show the lowest RIA. Although the KU1 is the slightly better material up to about 700 nm, the intrinsic OH band and its harmonics notably affect transmission above 800 nm. So for a fiber required transmitting in the visible and IR regions the hydrogen loaded KS-4V may be a better choice. There is no doubt that hydrogen loading for any of the other materials would also show marked improvements in their radiation tolerance. Above about 5 MGy, however, the beneficial effect of hydrogen loading in suppressing absorption is lost as the conversion to OH centers saturates.¹²² Up to 10 MGy, the main mechanisms in the radiation damage process are electronic, involving electron and hole trapping. Hence the wide differences observed in induced absorption of the fibers tested due to variations in intrinsic trapping

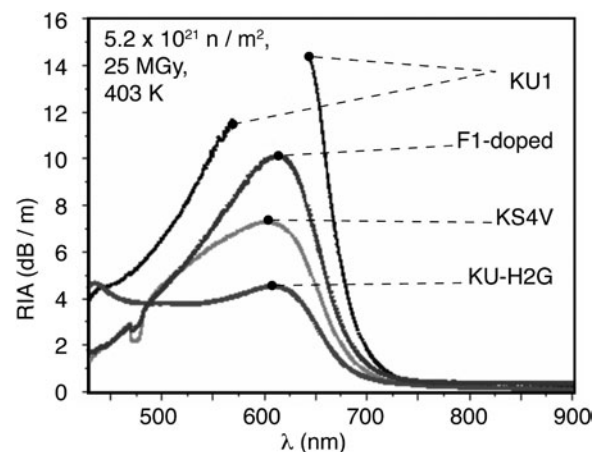


Fig. 14. Example of the results of an in situ RIA measurement under reactor irradiation of four fiber types, in the region where moderate absorption is expected (above 400 nm). The hydrogen-loaded fiber sample, KU-H2G, exhibits the lowest absorption at conditions representative of default ITER service near a first window or toward the rear end of a port plug and for ITER end-of-life fluence. After Ref. 121.

centers (defects and impurities). These trapping centers are thermally unstable, which explains the observation of effective thermal annealing for irradiation at higher temperature, or post-irradiation thermal annealing. Above this dose, displacement damage leading to extensive structural damage begins to dominate. As these levels are reached, all the fibers show similar degradation of the optical properties. However, by this time the fibers are of little use for diagnostic applications. Furthermore, as the extended defects are highly stable, thermal annealing is no longer possible.

All the fibers show intense RIL (radioluminescence). For small samples, windows, for example, the different components of RIL, together with the absorption, can be readily observed. However, in the case of fibers this is not so: the observed light emission at the end of the fiber is dominated by the self-absorption and non-uniform irradiation conditions. A broad emission band is generally observed for the fibers peaking at about 500 nm (see Fig. 15). Below 400 nm self-absorption reduces the emission to zero. Furthermore, the better hydrogen loaded fibers exhibit more intense RIL simply due to their lower RIA.

The successful application of metal (aluminium) jacketing to the KU1 and KS-4V fibers, with similar plans to coat SSU and STU is a necessary step toward reliable operation in the harsh radiation environment and at elevated temperatures. The commonly used polymer coating (Acrylate) degrades rapidly at high temperatures, but more so in an ionizing radiation field. As mentioned earlier, irradiation at high temperature ($>150^{\circ}\text{C}$) generally

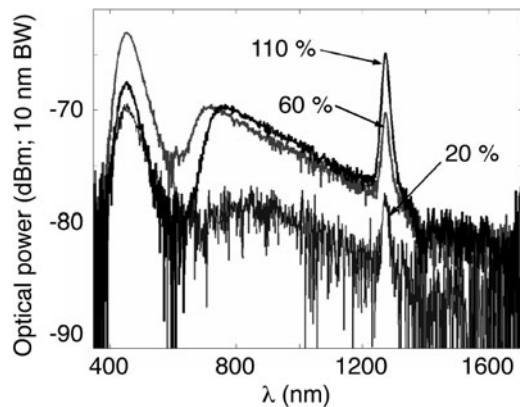


Fig. 15. Raw RIL spectra measured for a KS4V class fiber sample of ~ 1.2 m effective length near the beginning of the irradiation of Fig. 14 as a function of nominal reactor power (%) (Ref. 121). Superimposed on the Cherenkov background is a strong intrinsic absorption + RIA edge below 400 nm, an RIA dip near 600 nm due to Non-Bridging Oxygen-hole Centers and a peak around 1240 nm, also associated with the presence of oxygen. Other details of the experiment can be found in Ref. 121.

reduces RIA as well as quenching RIL. These effects were clearly demonstrated on TFTR and JET some years ago.¹²⁹ Hence metal jacketed fibers will allow operation at higher temperatures, as well as the possibility of post-irradiation annealing of the radiation-induced defects. Limited work is now underway to examine the possibility of in situ photo-bleaching of the radiation-induced damage using high-intensity UV lasers,¹³⁰ in situ hydrogen loading, the potential of so-called “holey” fibers (fibers containing an array of vacuum, air, or liquid filled holes) to improve radiation resistance,¹²³ as well as fibers to extend transmission into the blue-UV region.

III.D.5. Far Infrared Windows

Although little work has been done so far, for applications beyond 3000 nm into the far infrared (FIR) both sapphire and chemical vapor deposition (CVD) diamond show excellent radiation resistance with little or no RIA and RIL. For CVD diamond the degradation of the transmission was negligible at $10.6 \mu\text{m}$ up to 10^{21} n/m^2 (Ref. 46).

III.D.6. Mirror Coatings

For many diagnostics high-quality second mirrors for the optical UV-visible-NIR range will be required, and will be subjected to high ionization and neutron fluxes ($\leq 100 \text{ Gy/s}$, $\leq 10^{17} \text{ n/m}^2\text{s}$) and temperatures of the order of 200°C . For these applications commercially available high-quality mirrors are being examined.^{131–133} These mirrors consist of a thin evaporated aluminium layer on a solid glass substrate, usually Pyrex, protected (overcoated) with a controlled layer of transparent SiO or MgF_2 . Several problems have been encountered with the overcoating dielectric layer. It has been observed that the SiO converts to SiO_2 in the presence of ionizing radiation. This causes swelling of the dielectric layer, which together with the refractive index change affects the reflectivity. Furthermore, in some cases the swelling has been observed to crack the layer and render the aluminium surface of the mirror susceptible to corrosion in the presence of water vapor, a problem in the case of loss-of-coolant accident (LOCA). Work is underway to find more stable protective coatings such as SiO_2 and Al_2O_3 .

III.E. Mechanical Strength Degradation

Some insulating components such as windows, stand-offs, supports, or feedthroughs, will be under or suffer mechanical stress. For these it is important to assess possible radiation-induced changes in the mechanical properties. During the early work on ceramic materials for fusion applications, considerable attention was paid to the mechanical properties of refractory oxides and nitrides. Post-irradiation examination of the mechanical properties of aluminas indicated that significant degradation of the mechanical strength would only occur

for radiation damage levels of the order of 1 dpa or above.^{134–136} However, evidence was found for two types of radiation enhanced degradation of the mechanical strength, enhanced implying degradation for damage levels $\ll 1$ dpa. The first of these is RIED associated. Sapphire and aluminas were observed to become fragile, apparently due to internal stress following RIED degradation, at damage levels of the order of 10^{-4} dpa (Ref. 63). This internal stress is most probably due to the formation of small regions of γ -alumina within the α -alumina matrix, observed in TEM studies for RIED degraded sapphire, and explained in one of the RIED models.⁶⁰ The other type of enhanced mechanical degradation is related to subcritical crack growth (SCCG). Although SCCG is a well-known phenomenon in load-bearing ceramics, leading to a deterioration in fracture strength with time, the fracture behaviour of a ceramic material subjected to irradiation or applied electric fields while under stress had not previously been investigated. In view of the importance of radiation enhanced effects this has now been examined. A series of tests to determine the time-to-fracture of two types of aluminas (Deranox 975 and 995) held under different constant loads below the critical stress have shown quite clearly that the time-to-fracture is markedly changed when the ceramics are tested during irradiation at 1.5 Gy/s with ^{60}Co gammas.¹³⁷ In the case of the 975 alumina a tenfold increase in the time-to-fracture was observed, while for the more pure 995 alumina a decrease by a factor of 2 was recorded. The authors note that in the case of the 975 alumina the gamma irradiation inhibits the crack growth and conclude that the effect is dependent on microstructural details of the silica glass phase at the alumina grain boundary. This was followed by experiments on high purity silica glass, where a similar increase in time-to-failure was recorded, in support of the glass phase hypothesis.¹³⁸ Additional work on the effect of concurrent stress and electric fields on mechanical strength during irradiation is necessary to fully assess this potential problem. In contrast in the absence of concurrent stress, no significant neutron-induced effects were observed on the mechanical strength of silica material up to 10^{-4} dpa (Ref. 139). The strength was actually more dependent on the surface quality of the windows.

In the case of actual components one must consider the assembly as a whole, as, for example, windows. Windows act as vacuum and tritium barriers, and must not only ensure good optical transmission, but must maintain their mechanical strength and low tritium permeability. These relate to the whole window assembly, and in particular to the ceramics-metal joint. Microcracking, for instance, caused by radiation-induced segregation and subcritical crack growth may lead to enhanced tritium diffusion and leaks.¹⁴⁰ Studies are ongoing on the thermal and mechanical resistance of different window materials and assembly methods (e.g., gold-bonded quartz, bronze-brazed sapphire, welded borosilicate).¹⁴¹ They need to be validated under radiation and high temperature.

III.F. Thermal Conductivity Degradation

As in the aforementioned case for mechanical properties, very little work has been done in recent years on thermal conductivity. Thermal conductivity in ceramics is reduced by the presence of point defects, and to a lesser extent by extended defects or aggregates. Hence one expects a reduction in thermal conductivity on irradiation, together with a notable influence of the irradiation temperature; i.e., irradiation above temperatures at which the radiation-induced defects become mobile and can aggregate should lead to a lower degradation of the thermal conductivity. Available early data confirm this.^{142,143} The thermal conductivity of a typical alumina is of the order of 30 W/m/K. This is sufficiently high to ensure adequate cooling in most cases, particularly if we compare with stainless steel, the most probable structural and support material, which has a thermal conductivity of only 16 W/m/K. However, in the case of SiO_2 the conductivity is only about 1.4 W/m/K, hence extreme care must be taken to ensure adequate cooling for windows made from this material to avoid excessive nuclear heating. The case of CVD diamond, with a thermal conductivity of ~ 1900 W/m K, is a special case. This high conductivity, essential for successful operation of the ECRH windows, begins to degrade by about 10^{-5} dpa (1800 W/m K), and by 10^{-3} dpa is reduced to 200 W/m K. However, the expected dose for these windows will be $\leq 10^{-5}$ dpa (Ref. 144). Theoretical and experimental work to enable a better understanding of the thermal conductivity degradation is ongoing (Ref. 145).

III.G. Outstanding Irradiation Tasks in Preparation for a BPX

From the foregoing, it is clear that, in preparing a diagnostic front end, a number of irradiation R&D steps are required, spanning materials, critical interfaces between materials, subassemblies, and complete functional units. For the case of ITER, a long period of generic tests focusing on materials has generated the knowledge base necessary to prepare diagnostic-specific tests concentrating on specific materials formed into subassemblies, or batch tests. Thus, for magnetics, the planned tests are for cables, wound coils, and complete coil/joint/cable assemblies. For neutron diagnostics, entire in-vessel sensors (microfission chambers) will require testing. For optical and spectroscopic systems, research is planned on specific fibers, window assemblies, and coated mirrors, with some tests of radiation-hardened detectors. Entire bolometer and vacuum photodiode prototypes will have to be tested to assess such properties as electrical joint reliability under irradiation. During ITER construction, a number of new diagnostics will have to be developed, in particular for the in situ measurement of dust, and it is expected that these, too, will require specific pre-installation irradiation R&D programs.

IV. PARTICLE BOMBARDMENT

In ITER, just under half of all measurements of plasma parameters have to be based on analysis of electromagnetic radiation in different spectral regions, from a few nm (VUV) up to 118 μm (FIR). The type of information varies considerably by diagnostic, and ranges from simple light collection from a predefined path to fine-scale imaging. It can require, in addition, the preservation of polarization through multiple reflections.

Because of the high levels of ionizing radiation from the burning plasma the first few elements of the instruments providing these measurements have been designed to use reflective optics in a labyrinth configuration. In most cases these are metal mirrors fabricated with bulk metals. One mirror in each arrangement must face the plasma. These first mirrors will be subject to all types of radiation emanating from hot plasmas (neutrons, gammas, photons, and energetic particles), but the strongest modification of the mirror properties will come from charge exchange atoms (CXA). These will modify the mirror surface by sputtering.

CXA sputtering is not the only mechanism of mirror degradation. The reference design of the ITER divertor targets uses carbon-carbon composites. Volatile hydrocarbon molecules, formed when hydrogen isotopes strike the divertor plates, can move freely inside the reactor and deposit on remote surfaces, including first mirror surfaces.

Other diagnostics can suffer from particle bombardment and deposition: for example, contamination films or erosion of the meanders can change the sensitivity of bolometers. Deposited heat load from the neutrals, which is not part of the radiative power measurement, can also generate a spurious signal. Diagnostics relying on electrical insulators, such as Langmuir probes and pressure gauges, can be disabled by electrically conducting deposited films.

Most of these effects exist in today's plasma devices. One exception is the steady presence of superthermal (up to ~ 4 MeV) alpha particles in certain regions within one Larmor radius of the first wall. For metal mirrors in particular, the direct effects of gammas and neutrons on the reflectivity are low; therefore, knowledge obtained in today's fusion experiments and particle bombardment rigs should enable accurate estimates to be made of the changes that will occur to diagnostic mirrors in a BPX, although it is necessary to rely on modeling to predict the CXA flux spectrum and to extrapolate to BPX conditions. Alpha particle bombardment can also be simulated in test rigs (see, e.g., Ref. 146). There is also some evidence that low-energy He bombardment can affect the properties of metals,^{147,148} including their reflectivity.¹⁴⁹

In a BPX aimed at reactor-like performance, the main challenge comes from the large number of plasma hours required to reach technologically relevant levels of neutron fluence. For ITER at end of life, with a total of 4700 h of burn time and $\sim 5 \times 10^{25}$ n/m² fluence at first

wall level, the corresponding fuel atom bombardment exceeds 1.5×10^{27} particles/m²; that is over 10^7 potential interactions per initial first wall atom. Carbon and other contaminant flows, such as beryllium, are at a few percent of this level, but are still significant: 0.1% of the fuel atom fluence translated to a net carbon deposit would leave a ~ 100 μm thick film. A small part of these flows reaching key components can be enough to degrade diagnostic performance: net erosion or deposition on mirrors at the nm/h level has the potential to translate to lifetimes much smaller than those of the key in vessel components.

Additional contamination can arise during wall conditioning and, in present devices, this effect often dominates or at least complicates the interpretation of experimental results in mirror experiments. For a BPX, the time spent in conditioning is required to be a lower fraction of the total plasma time; nevertheless, significant contamination can occur. For this reason, BPX optical diagnostics must incorporate shutters to eliminate this source of contamination.

IV.A. Erosion

During normal plasma operation, CXAs have a very broad energy distribution. In the main chamber of ITER, the mean energy and flux are expected to vary considerably by position. The details are rather sensitive to the plasma conditions.^{150,151} An indicative range of values around the main chamber periphery is shown in Table VIII.

A comprehensive attempt to document gross erosion rates for one ITER regime was made by Behrish et al.¹⁵⁰ In the regime considered there, for the outer midplane position the gross surface erosion for 4700 h was ~ 850 μm —Be and Cu, 500 μm —Fe, 250 μm —Mo, and 100 μm —W (earlier estimates¹⁵² were 2 to 3 times lower). This level of sputtering-induced erosion would lead to unacceptably short lifetime for mirrors fabricated from polycrystalline metals because of development of large-scale step structure micro-relief and small-scale structure in-grain micro-relief (see, e.g., Refs. 153, 154, and 155). These modifications decrease the specular component of the reflectivity and hence the resolving power.

To reduce the effect of CXA bombardment, the solid angle of plasma exposure of many first mirrors can be reduced by a front aperture constraint (stop)^{156,157} or by placing the mirror near the end of a long duct.¹⁵⁸ These strategies can be very effective, but not with systems combining large étendue and wide field of view, for example, CXRS and MSE (Refs. 159 and 160). There, first mirrors have to be quite open to the plasma to meet the measurement requirements and the level of reduction of the CXA flux at the mirror location is only about one order of magnitude less than the first wall. In addition, for these diagnostics, there is the requirement to preserve polarization. Other systems where there may be erosion

issues are those needing a reflector embedded in the ITER first wall [for example, the Interferometer/Polarimeter and Polarimeter systems, where, however, the long wavelengths used (5 to 10 and 57 to 118 μm , respectively)] mean that the systems should be able to tolerate a moderate amount of roughness. Nonetheless, a special study is required for these systems because of (a) the triple reflection at off-normal incidence near the plasma within the retroreflector and (b) the strong requirement for the preservation of polarization information. Some results of long-term ion sputtering on operation of a retroreflector can be found in Ref. 161.

IV.B. Deposition

To date, a considerable amount of data has been accumulated in numerous experiments on the structure and composition of C-based films deposited on different parts of modern medium- and large-scale fusion devices. In several experiments with in-vessel mirrors it was found that the structure and composition of deposited films depends strongly on the mirror location relative to carbon-based wall protection structures and on the regime of device operation (see, e.g., Ref. 162). Carbon-based films strongly modify reflectance. Figure 16 shows the calculated dependence of reflectivity at 632.8 nm for a Cu mirror as a function of the thickness of contaminating films of differing composition: a pure carbon film and the type of hydrocarbon film found on windows of the JT-60U tokamak.¹⁶³ The effect on reflectivity depends strongly on film characteristics, and for carbon film a thickness of only 10 nm causes a noticeable drop of reflectivity.

The deposition film on mirror surfaces also influences the polarization angle of reflected light. This effect depends on the film thickness and on the angle of incidence of the light. Figure 17 shows the calculated and

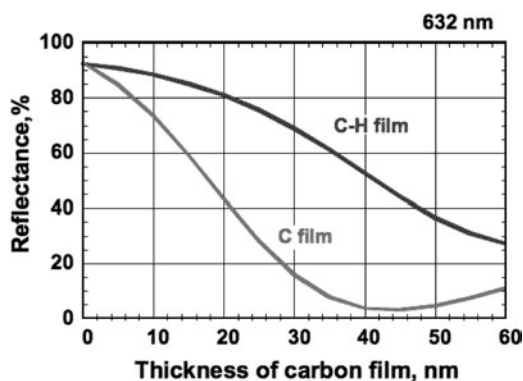


Fig. 16. Normal incidence reflectance of Cu mirror at the wavelength 632.8 nm depending on the thickness of deposited carbon and hydrocarbon films.

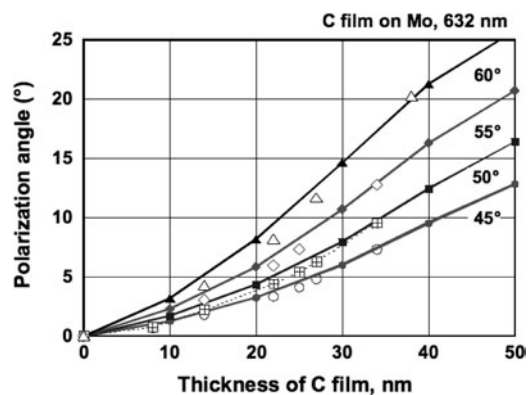


Fig. 17. Rotation of the polarization angle of reflected light as a function of the thickness of carbon film at 632.8 nm. Shown as measured by ellipsometry on a Mo mirror at the indicated incidence angles (open points) and as calculated (solid points and lines).

measured values of polarization rotation for the wavelength 632.8 nm as a function of the film thickness for four different angles of incidence.

In experiments where the rate of carbon deposition exceeds the rate of erosion by CXA, the thickness of contaminating layer gradually increases, changing both the absolute value and spectral dependence of the reflectivity. Recent experiments exposing mirrors inside several fusion devices (LHD, T-10, Tore Supra, TEXTOR) have shown that, for the locations investigated, deposition is a more severe cause of mirror degradation than sputtering-induced erosion.¹⁶² Pure surface erosion was observed only for one mirror in LHD, fixed directly on the wall and in closest proximity to the confined plasma. After exposure in qualitatively similar positions in the Tore Supra tokamak, evidence of both competing processes was observed. All mirrors (monocrystalline Mo, polycrystalline SS, and polycrystalline Cu) were eroded (as was measured by a profilometer), but at the same time were covered by a thin contaminating film. In T-10, during two experimental campaigns, erosion was not observed, most likely due to the close proximity of the mirror samples to a graphite limiter. In these experiments a thin deposit was found, even on mirrors shutter-protected during vessel wall conditioning (when some small deposition would be expected). A common result for all four devices was the appearance of a complex contaminating film of unknown composition on all mirrors recessed with respect to the nearby plasma-facing components. This includes samples in the diagnostic ports of LHD and T-10, the inner part of a corner cube retroreflector in Tore Supra and a "periscope-like" system in TEXTOR. The film could be surface deposited hydrocarbons, but may also include the formation of metal carbides on the surface and contain other impurities from the plasma, such as first wall metals.

IV.C. Measures to Improve the Service Life of First Mirrors

It has been suggested¹⁶⁴ that a possible way to prevent the roughening of the first mirror micro-relief, when the CXA fluence cannot be reduced sufficiently by other means, is to fabricate mirrors from monocrystalline metal or as a metal film on a metal substrate rather than the usual polycrystalline metals. The benefits have been verified by results of comparative tests.¹⁵³ In these, mirrors of various metals with different structure were bombarded by ions of deuterium plasma with a broad energy distribution. As can be seen from Fig. 18, monocrystalline and thin-film mirrors retain their optical properties even after more than 6 μm has been eroded by sputtering. Given, then, an attenuation of the direct CXA flux on the mirror by more than an order of magnitude compared to the first wall, all the aforementioned materials except stainless steel can in principle be used in ITER. Monocrystalline W, in particular, can be used at CXA flux levels only a few times smaller than those at the first wall. Amorphous alloys and metals in a nanocrystalline state also hold promise as suitable first mirror materials, because it is expected that their sputtering behaviour will be similar to that of thin films or well-prepared monocrystalline mirrors.

It was found when experimenting with monocrystalline mirrors that they can be highly resistant to long-term sputtering, but only provided that the mechanical treatment during mirror fabrication does not give rise to a significant increase of defects in the material. To avoid multiplication of defects, special precautions have to be undertaken at every step of the process, for example, by

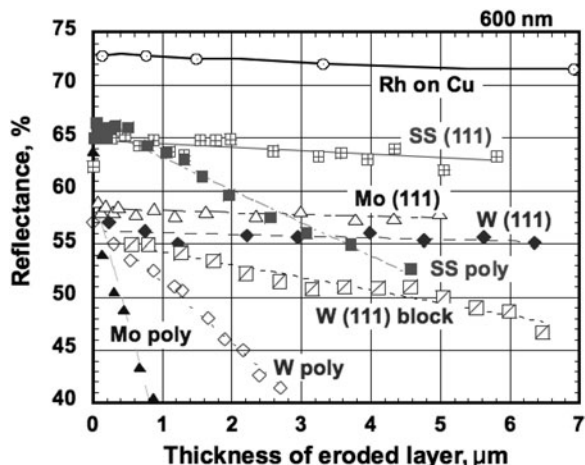


Fig. 18. Reflectance at a wavelength of 600 nm and normal incidence of mirrors fabricated from single- and polycrystalline SS, Mo, W, and Rh-on-Cu as a function of the thickness of the layer eroded by ion bombardment. “W(111) block” means a polycrystalline mirror with the majority of grains oriented in the same direction.

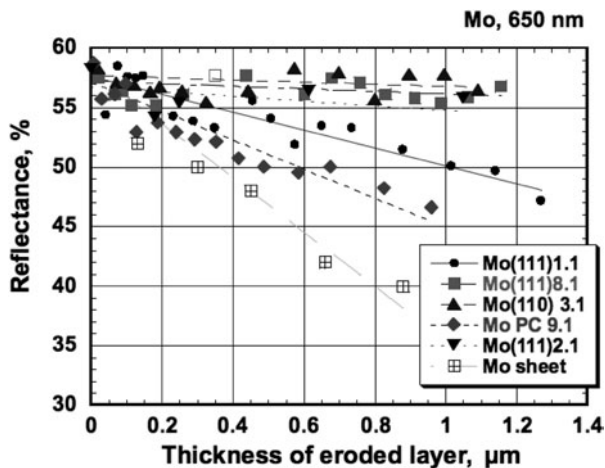


Fig. 19. Reflectance, at 650 nm and normal incidence, of mirrors made from single- and poly-crystalline Mo, as a function of the layer eroded due to ion bombardment. The “Mo(111)1.1” sample was prepared without special precautions, in contrast to the other monocrystalline samples.

using spark erosion cutting instead of a lathe, etc. As an example, in a comparative experiment of Mo mirrors subject to bombardment by D plasma ions, the optical properties of an imperfectly made monocrystalline Mo mirror degraded almost as fast as the optical properties of a polycrystalline Mo mirror (Fig. 19).

The foregoing discussion makes it clear that, while it is possible in principle to find ways of dealing with large amounts of CXA-induced erosion, principally by selecting the mirror material, it is more difficult to deal with deposition. In practice, therefore, every design for a long-life BPX first mirror has to incorporate a strategy for (a) the reduction of the net deposition rate, (b) the protection of the first mirror from unnecessary exposure to contaminant flux, (c) the mitigation of the effects of deposition on the measurement, and (d) a maintenance strategy to restore the performance of the diagnostic on demand and at reasonable intervals.

Reducing the net deposition rate can involve

1. reorienting or repositioning the first mirrors
2. using baffles to reduce the solid angle of exposure to the plasma to the minimum consistent with the measurement requirements¹⁵⁷
3. choosing the mirror material to prevent the formation of carbides, for example, copper¹⁶⁵
4. shaping or patterning the sides of the duct that houses the mirror to reduce the flux of sputtered material directed toward the mirror¹⁶⁶
5. keeping the mirrors at an elevated temperature as demonstrated in experiments^{167,168}

6. using a controlled flow of neutral particles to change the deposition conditions locally.

The first two methods may well involve some compromise in the throughput of the system.

The obvious example of protection is the use of shutters. They can shield the mirror whenever the diagnostic information is not needed (for example, during routine startup, during wall conditioning) or the risk of unacceptable deposition rates is very high (a high erosion ELM regime that the control system is in the process of avoiding, for example). Of course this assumes that the diagnostic is not in active use for plasma control at this time.

Mitigation of the effect of deposition means designing a system that is tolerant of thin deposited films. In practice this can be achieved by a combination of

1. appropriate recalibration techniques
2. in situ methods of cleaning in-vessel mirrors without interruption of the experimental program.

Recalibration can take place continuously, between plasma pulses or at longer intervals. For the typical deposition rates in regions outside the divertor in ITER, it is expected that recalibration will be needed infrequently (after many pulses), so there are probably no long-pulse issues. For the divertor region, however, it is conceivable that cleaning may have to be arranged between every pulse and that data recovery will then require online recalibration.

For cleaning, two different approaches are under investigation: using a local discharge in deuterium close to the mirror¹⁶⁹ and using a pulsed laser for ablation of the C film by scanning the laser spot along the mirror surface.^{170,171} In the first case, the C film is being removed

mainly by chemical erosion.¹⁵³ While the results are promising, significant development is needed before a practical implementation is ready for routine use.

A maintenance strategy could include intervention to provide in situ cleaning, local replacement of key components or as a last resort, removal of the supporting structure (plug, cassette, etc.) for maintenance. It should be in place for all cases as there is no guarantee that the reduction, protection, and mitigation measures will be successful. For diagnostic components in the divertor in particular, it is clear that even a solution incorporating all these elements cannot be reliably proven to be workable (i.e., that the final maintenance interval will be reasonable) without further dedicated appropriate experiments in today's test stands and devices, incorporating similar strategies as the intended final application in a BPX.

IV.D. ITER Examples

Charge Exchange Recombination Spectroscopy (CXRS) for the edge. In order to achieve the necessary wide angle of view, the first mirror of the CXRS diagnostic must be quite open to the plasma [solid angle about 0.5 sr (Ref. 160)], and the main CXA flux will bombard the mirror surface at an angle of incidence close to 45 deg. The CXA flux to the first mirror has not yet been estimated but will probably be close to that of the first wall flux (Table VIII, "top of upper port" location). The 45-deg angle of impact of the CXA to the surface will enhance sputtering effects: both the sputtering rate and the rate of relief development will be higher than for the case of predominantly normal incidence at the same CXA flux. Therefore, sputtering

TABLE VIII
Charge Exchange Flux and Energy for the Fuel Species for a Typical ITER Pulse
for Various First Wall and Mirror Locations^a

Location and Exposure Angle	Total D Flux (Neutrals and Ions Over 5 eV/m ² s)	Mean Energy of D Neutrals (eV)
Top of upper port	7×10^{20}	15
Bottom of upper port	8×10^{20}	39
Mirror in upper port (recessed 500 mm/0.1 sr)	6×10^{18}	53
Equatorial port	6×10^{19}	225
Mirror in equatorial port (recessed 500 mm/0.1 sr)	2×10^{18}	330
Inner upper region	4×10^{20}	8
Inner midplane region	3×10^{20}	25
Retroreflector in inner midplane region (recessed 300 mm/0.15 sr)	2×10^{19}	31
Outer baffle	3×10^{19}	200
Mirror under dome (recessed ~400 mm/0.02 sr)	$\sim 0^b$	0.1

^aSee Ref. 151.

^bTotal flux of D and D₂ down to 0 eV is $8 \times 10^{20}/\text{m}^2 \text{ s}$.

effects are potentially important for this mirror. Nonetheless, on the basis of the results summarized in Sec. IV.A, a monocrystalline tungsten mirror is likely to be unaffected by CXA at this location. Recent calculations¹⁵¹ show that, near this location, in addition to the D-T flux, there will be a C flux at a level of $\sim 1\%$ of the total CXA flux, and a He flux at a level of 0.1%. Such a mixture could lead to the appearance of C deposits,^{172,173} and therefore, deposition mitigation and cleaning measures could also be needed.

For the ITER LIDAR system,¹⁵⁸ the first mirror is recessed enough that CXA sputtering effects are unlikely to be important. This allows more freedom for material selection of the very large first mirror. Deposition will dominate, and therefore, appropriate shuttering and/or cleaning techniques are required. The size of the first mirror makes in situ replacement difficult, but the mirror can be exchanged by removing the port plug to a special area (the ITER hot cell). A similar situation applies to the Edge Thomson scattering system,¹⁵⁸ whose two mirrors (one for the primary laser beam and another for scattered light) will be located inside the upper port.

The behaviour of the first mirrors of the main plasma H_α monitor and visible/IR TV systems is difficult to predict. The sputtering effect can be estimated from the geometry of the front end: both diagnostics observe plasma through small (axes of a few mm) elliptical holes (Fig. 20). A simple geometrical calculation suggests that the sputtering rate on the first mirror will be more than two orders of magnitude below first wall levels and could be handled by normal metallic mirrors. However, because of the camera-like geometry of this diagnostic, in reality the CXA flux could well be nonhomogeneous along the first mirror surface, with a maximum near the central

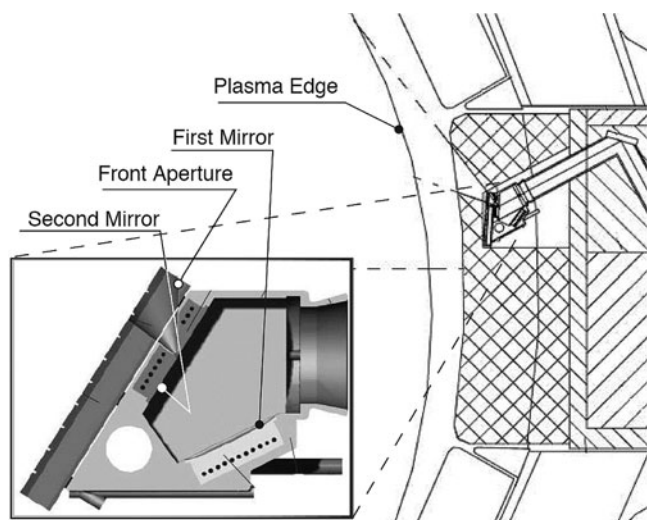


Fig. 20. Typical geometry of an H_α line within an ITER port. The solid angle at the aperture is of order 0.3 sr; the solid angle at the first mirror is 0.01 sr.

part of the first mirror and decreasing toward the edge. For this reason, monocrystalline molybdenum has been chosen for the H_α mirrors.^{156,157} At the same time, there could be significant amounts of material sputtered off the front aperture edge, which is exposed to near-first wall levels of CXA flux, and some of this could redeposit on the first mirror.

For the polarimetry diagnostic, the first mirror takes the form of a retroreflector. However, the wavelength used (57 or 118 μm) is long enough that erosion or deposition are not expected to be a problem.¹⁶¹ In contrast, the characteristics of retroreflectors for the toroidal interferometry/polarimetry can be significantly modified, as the planned wavelength is shorter (5 to 10 μm). Furthermore, these retroreflectors are planned to be located in long (relative to the cross section size) channels.¹⁷⁴ Thus, the CXA flux will be strongly weakened and the deposition of contaminants will probably play the main role in modification of the retroreflector optical properties. In the case of uniform deposit, its appearance will lead to the rotation of the polarization angle of the reflected beam.¹⁶¹

For optical systems under the divertor dome, deposition of contaminants on the first mirror, and probably other mirrors, will be the main reason of deterioration of optical properties and, in this case, the rate of deposit growth can be very high (see e.g., Ref. 175). It is also particularly hard to estimate accurately, as the transport of carbon can be dominated by transient events such as ELMs and disruptions. Some indication could be given by the fact that the ITER divertor design allows 8 mm of local erosion before replacement of the divertor is necessary. This amount of CFC material removed over a footprint on the target of 20 mm poloidal extent and redeposited over the entire divertor surface would result in a uniform coating of order 100 μm . Less than 1% of this amount on the first mirror is enough to disable all but FIR transmission. Neglecting transients, the CXA flux at typical mirror locations under the dome (0.02 sr solid angle) has been estimated to be of order $10^{21}/\text{m}^2$, 99.5% of this D_2 with a mean energy of 0.1 eV (Ref. 151). This flux is much higher than for typical main chamber locations, and the energy much lower (there is no significant component above 5 eV).

In practice, the redeposition is highly nonuniform and hard to predict with any accuracy. Thus, protection, mitigation, and cleaning methods are essential in planning a divertor optical diagnostic. Examples of these can be found in the systems proposed for the divertor Thomson Scattering systems.¹⁷⁶

IV.E. Conclusions

The rate of in-vessel mirror modification under plasma impact strongly depends on the mirror location. The experimental data indicate that the erosion can prevail over deposition for mirrors located near the plasma but far

from limiters and the divertor. In contrast, deposition is more probable for mirrors located in ducts and near graphite limiters, and definitely must be expected for the divertor.

For the regions where the CXA flux is high, the best mirror materials are monocrystalline tungsten or molybdenum. In locations where the CXA flux is strongly attenuated with respect to first wall levels, but sputtering is still expected to be the dominant degradation mechanism, it should be possible to use mirrors from polycrystalline metal with low sputtering yield (W, Mo) or fabricated as thin film on a polycrystalline metal substrate.

In locations where deposition dominates, the mirror surface material can be chosen from a wide variety of options. However, for these mirrors, special provisions must be made to reduce the deposition rate, including protection of the mirror from known high-deposition regimes, to measure and compensate for its effect and to allow for periodic maintenance.

V. MEASUREMENT STABILITY, CALIBRATION, AND RELIABILITY

V.A. Stability and Calibration Issues

Many diagnostic systems rely on periodic recalibration to maintain accuracy and detect systematic drifts. On present devices, this process is often rare and, when it does happen, relatively intrusive. For example, special equipment may be required within the vacuum chamber such as radiation sources, retroreflectors, or electromagnetic sources and choppers. Whether diagnostic measurement stability is an issue or not depends primarily on the environment surrounding the more vulnerable elements of each system and the two key factors of pulse length and total plasma burn time (Table I). An additional factor that must be taken into account is that a BPX is a mechanically stressed device. The various machine components, such as port plugs, that support diagnostic elements, are subject to large forces and excursions, particularly during disruptions. It is thus conceivable that transmission line elements may become misaligned and introduce calibration errors, and these must be detected and compensated for.

It is possible to compile a diagnostic-specific table with the potential stability issue and corresponding possible design, calibration, or maintenance solution(s), where these are available. A compilation like this is by necessity machine-specific, and ITER, as the most developed design, is the most concrete example that can be discussed. Table IX shows this list for ITER, and what follows is a brief discussion of the issues appropriate to each generic group.

Magnetics have good long-term stability. They can be designed so that their sensitivity is unchanged at fluence levels that are well in excess of ITER's, for

example.¹⁷⁷ They can also be well shielded from radiation and particle fluxes without sacrificing sensitivity. One stability issue is drift within long pulses due to direct and indirect radiation-induced voltages (see Sec. II). This can be mitigated using a sensor set of poorer time resolution or by recalibration against other diagnostics.⁸⁵ Sensors mounted on substructures are subject to mechanical decalibration, as the structure can shift due to thermal expansion, or irreversibly after a major disruption. This can be reduced by careful design. For the case of the ITER divertor cassette, for example, movement is limited to a few mm and can be corrected by survey at campaign intervals (1 to 3 yr). The long-term high-frequency performance of the magnetics will change slightly as the insulator resistivity and permittivity change due to radiation damage. This can be corrected using ex-vessel measurements of the insulation characteristics.

Optical systems in port plugs are vulnerable to erosion/deposition and mechanical misalignment as well as machine movement. They will require recalibration at intervals ranging from a few pulses to one campaign (1 to 3 yr). Optical systems in the divertor are vulnerable to deposition and mechanical misalignment as well as machine movement. They will require recalibration at intervals ranging from within a pulse (continuous recalibration) to several pulses. In addition, several spectroscopic systems can decalibrate due to radiation damage of the (mostly ex-vessel) sensors. These will need periodic (few pulses to campaign length) ex-vessel recalibration.

Neutron systems are vulnerable to sensor sensitivity changes and also to mechanical misalignments in many cases. They will probably require recalibration at campaign intervals for individual sensors and, occasionally, for the whole system using in-vessel sources. They are also vulnerable to changes in both the local configuration and the global configuration. For example, change of any port plug will require at least a Monte Carlo simulation of its effects on all the neutron diagnostics and may also require recalibration.

Bolometers are vulnerable to erosion/deposition as well as radiation damage. They will need in situ recalibration on a per pulse basis, but this is in any case a feature of modern bolometers.¹⁷⁸

Microwave systems are very robust with the exception of mechanical movement, and for this reason need to incorporate recalibration features that can be used at least on a campaign interval (see, e.g., Ref. 179). In fact, for the case of reflectometry such recalibration is normally included in real time as part of the basic operation of the system. Therefore, all that is required in addition is the ability to detect new faults in the transmission line as part of a more infrequent system survey recalibration procedure.

Systems electrically interacting with the plasma (Langmuir probes, pressure gauges, faraday cups) are subject to the effects of erosion/deposition and prompt

TABLE IX

List Diagnostic Proposals for ITER (Including a Number Not Presently Included in the ITER Reference), Their Potential Stability Issues and Possible Recalibration or Other Techniques to Mitigate Their Effect

Group	ITER WBS 5.5. . .	Diagnostic	Stability Issue	Recalibration Technique
Magnetics	A.01	Outer vessel sensors (coils and hall probes)	None expected for coils	NA
			Sensitivity and offset drift due to radiation (Hall probes)	Built-in offset correction; sensitivity cross check against coils at each pulse startup
	A.02	Inner vessel sensors (coils and loops)	Radiation, thermoelectric and combined currents, integrator drift	Against A.01 and F.03 within a pulse
	A.03	Divertor magnetics (coils)		
	A.04	External Rogowski (coils and fibers)	Integrator drift	Against A.01 and optical fiber measurement within a pulse
	A.05	Diamagnetic loop system (coils and loops)	Radiation, thermoelectric and combined currents, integrator drift	Cross check using outer loop within a pulse
			Mechanical shifts in TF/PF structures	Reperform initial cross-talk calibration between campaigns
A.06	Halo current sensors	None expected	NA	
Neutron	B.01 B.02	Radial neutron camera Vertical neutron camera	Detector aging due to radiation	Remove, recalibrate and reinsert detectors between campaigns
			Mechanical shifts in port or in-vessel structures	Reperform initial calibration
			Machine structural changes due to maintenance or upgrades	
	B.03	Microfission chambers	Detector burnup	Reperform initial calibration
	B.04	Neutron flux monitors	None known at present	NA
	B.07	Gamma-ray spectrometers	None known at present	NA
	B.08	Activation system	None	NA
	B.09	Lost alpha detectors	For scintillator-based technique, sensitivity change due to irradiation	None known
	B.10	Knock-on-tail spectrometer	None known at present	NA
	B.11	High resolution neutron spectrometer	None known at present	NA

(Continued)

TABLE IX (Continued)

Group	ITER WBS 5.5...	Diagnostic	Stability Issue	Recalibration Technique
Optical	C.01 C.02 C.03 C.04 and C.08	Thomson scattering (core) Thomson scattering (edge) Thomson scattering (X point) Thomson scattering (divertor)	Sensitivity change due to first mirror (FM) or window coating or optics misalignment	Repeat initial calibration between campaigns
			Chromatic sensitivity change for the same reasons	Use second laser at different wavelength in real time
	C.05	Toroidal Interferometer/ Polarimeter	Polarization change due to erosion/deposition	Recalibration between pulses
	C.06	Polarimeter		
C.07	Collective scattering	None	NA	
Bolometric	D.01	Bolometers (All)	Sensitivity change due to erosion, deposition or radiation effects	Perform in situ recalibration between pulses
Spectroscopic and NPA	E.01 and E.12 E.02 E.06 E.04	CXRS based on DNB (core) H-Alpha Visible continuum array Impurity/influx mon (divertor)	Sensitivity change due to FM coating	In situ light source or shutter retroreflector to recalibrate between pulses
	E.03	VUV (main plasma)		
	E.07	Soft X-ray array (vacuum photodiode)	None known at present	NA
	E.08	Neutral particle analyzer	None known at present	NA
	E.10	Laser induced fluorescence	Sensitivity change due to FM coating	Recalibration using known gas pressure between campaigns
	E.11	MSE based on heating beam	Polarization change due to FM coating	Use calibration light beam brought into FM view by shutter between pulses
Microwave	F.01	ECE (main plasma)	Mechanical misalignment of in-port structures	Use in-port calibration source
	F.02 F.03 F.04 F.09	Reflectometer (main plasma, LFS)	Mechanical movement of in-vessel antenna structures	Use known leaks and reflections as reference
		Reflectometer (plasma posn) Reflectometer (divertor) Reflectometer (main plasma, HFS)		
	F.07	Fast wave reflectometry	None known at present	NA
	F.10	Interferometer (divertor)	None known at present	NA

(Continued)

TABLE IX (Continued)

Group	ITER WBS 5.5...	Diagnostic	Stability Issue	Recalibration Technique
Plasma facing and operational	G.01 & G.10	IR cameras, Vis/IR TV	Sensitivity change due to FM coating	In situ shutter hot source or shutter retroreflector to recalibrate between pulses
	G.02	Thermocouples	Small sensitivity changes due to irradiation	Cross calibrate against coolant calorimetry
	G.03	Pressure gauges	Sensitivity change	Reference gas injection between pulses
	G.04	Residual gas analyzers	None known at present	NA
	G.06	IR thermography (divertor)	Chromatic or other coating on FM	Cross check with coolant calorimetry and G.01/10
	G.07	Langmuir probes	Area changes due to erosion	None
	G.08	Erosion monitor based on time delay reflectometry	Coating on FM	Measurements against fixed reflectors not facing the plasma
	G.09	Dust monitor	None known at present	NA

RIC, so that they will have to incorporate in situ recalibration features.

V.B. Diagnostic Reliability and Data Availability

One feature that is common to BPX designs is that the cost of any volume within the toroidal field magnet system is very high. Therefore, there is a lot of pressure to miniaturize and minimize any diagnostic presence that would have an impact on the volume available to the plasma. At the same time, in a high-performance D-T device, the vacuum vessel is also part of the primary radioactive material confinement system. The indirect consequence of this is that, often, access for diagnostic maintenance is reduced, especially for systems with components distributed behind the first wall. This comes about because multiple penetrations for wiring and diagnostic withdrawal are not desirable. This means that such systems, which include magnetic diagnostics and can be quite complex, have to be designed to a very high level of reliability and with some redundancy.

Diagnostic reliability is also an issue that is directly linked to the use of the diagnostic operationally and also to contribute to the BPX programmatic aims. In this respect, the nomenclature established by ITER for specific measurements, that is, measurements for Machine Protection and Basic Control (1a), Advanced Control (1b), and for Physics Understanding (2) (Ref. 11) is very helpful. The corresponding measurement list is shown in

Table X, with the measurements suggested for machine protection¹⁸⁰ in Table XI. The machine cannot be operated unless every group 1a parameter is available. The machine cannot be operated in specific advanced scenarios unless certain 1b measurements are available. (Control for such scenarios may require optimization and monitoring of the ion or electron temperature profile, certain aspects of the q profile, etc.) The machine can be operated with a group 2 parameter missing. A particular physics program, however, may require specific group 2 parameters and therefore the operation of specific diagnostics. Depending on the plasma regime, therefore, different measurements enter the control category. This has been explored in Ref. 11, and the full table of measurements for the most demanding mode of operation appears in Table XII.

Depending, therefore, on the available diagnostic set and the degree of redundancy, certain diagnostics can be classified as "Basic Control," etc., for that regime. The issue can rapidly become very complicated as there are diagnostics that appear in different roles in separate control loops at different times or regimes of operation.^{11,181}

In order to establish targets for diagnostic reliability then, it is useful first of all to establish a target for the reliability and availability for each measurement. Table XIII summarizes a possible set of reliability and availability targets for each type of measurement. The reasoning behind it is necessarily somewhat arbitrary,

TABLE X

Classification of ITER Measurements According to Their Importance for Control Purposes*

Group 1a	Group 1b	Group 2
Measurements for Machine Protection and Basic Control	Measurements for Advanced Control	Additional Measurements for Performance Evaluation and Physics
<ul style="list-style-type: none"> ⇒ Plasma shape and position, separatrix—wall gaps, gap between separatrixes • Plasma current, $q(a)$, $q(95\%)$ • Loop voltage ⇒ Fusion power • $\beta_N = \beta_{tor}(aB/I)$ ⇒ Line-averaged electron density ⇒ Impurity and D, T influx (divertor and main plasma) ⇒ Surface temperature (divertor and upper plates) ⇒ Surface temperature (first wall) ⇒ Runaway electrons • Halo currents • Radiated power (main plasma, X-point, and divertor) • Divertor detachment indicator (J_{sat}, n_e, T_e at divertor plate) ⇒ Disruption precursors (locked modes, $m = 2$) • H/L mode indicator • Z_{eff} (line-averaged) • n_T/n_D in plasma core ⇒ ELMs • Gas pressure (divertor and duct) • Gas composition (divertor and duct) • Dust 	<ul style="list-style-type: none"> • Neutron and α-source profile • Helium density profile (core) • Plasma rotation (toroidal and poloidal) • Current density profile (q-profile) • Electron temperature profile (core) • Electron density profile (core and edge) • Ion temperature profile (core) • Radiation power profile (core, X-point, and divertor) • Z_{eff} profile • Helium density (divertor) • Heat deposition profile (divertor) • Edge turbulence • Ionization front position in divertor • Impurity density profiles • Neutral density between plasma and first wall • ne of divertor plasma • T_e of divertor plasma • Alpha particle loss • Low m/n MHD activity • Sawteeth • Net erosion (divertor plate) • Neutron fluence 	<ul style="list-style-type: none"> • Confined α-particles • TAE modes, fishbones • T_e and T_i profile (edge) • n_e, T_e profiles (X-point) • T_i in divertor • Plasma flow (divertor) • $n_T/n_D/n_H$ (edge) • $n_T/n_D/n_H$ (divertor) • T_e fluctuations • n_e fluctuations • Radial electric field and field fluctuations • MHD activity in plasma core

*Consistent with Ref. 11. Measurements with an expected machine protection significance¹⁸⁰ are indicated by an ⇒ and the suggested protection parameter and target values are shown in Table XI.

TABLE XI

List of ITER Machine Protection Measurements Suggested in Ref. 180

Parameter	Limit
Separatrix/wall gaps	>5 cm
First wall surface temperature	≤673 K (hot spots)
Divertor plate surface temperature	≤1073 K (hot spots)
Fusion power	≤1.8 GW (20% above nominal value)
Locked modes	Avoidance
Runaway electron current	≤0.1 I_p
Type I (Giant) ELMs (at full parameters)	Avoidance
Specific impurity emission	To be defined
Line-averaged density (NBI shine-through)	≥0.3 × 10 ²⁰ m ⁻³ for D ^o beams

as the precise role for each measurement will not be known until during the experimental program, and the importance of each measurement will vary by campaign, plasma regime, and details of each experiment. Table XIII assumes that the BPX in question has an initial hydrogen phase for system shakedown. During this phase, manufacturing flaws, control software errors and the like should be revealed and corrected in a relatively straightforward manner. This is followed by a D-T exploration phase, in which regimes of operation and performance limits are identified and selected regimes, some incorporating advanced control loops, are optimized. This is then followed by an exploitation or technology phase, where selected regimes, some incorporating advanced control loops, are further optimized and used extensively to accumulate first wall fluence in order to investigate first wall and nuclear materials issues, such as breeding.

TABLE XII

Measurements Required for Plasma Control (Basic and Advanced) and Measurements Required for Performance Evaluation of ITER for the Most Demanding Case of Steady-State Operation*

Measurements Required for Control	Measurements Required for Evaluation
Plasma shape and position Vertical speed B_{tor}, I_p, V_{loop} Locked modes, $m = 2$ modes, low m/n MHD modes Line-averaged density Runaway electrons Surface temperature of divertor plates and first wall H/L mode indicator ELM occurrence and type Divertor detachment $T_e(r)$ in core, T_i in core P_{rad} from core $P_{fus}, n_{He}(r)$ n_{He} in divertor n_T/n_D in core Divertor ionization front position $v_{tor}(r)$ and $v_{pol}(r)$ β , location of $q = 1.5$ and $q = 2$ surfaces High sensitivity measurements of n_e, T_e Detection and measurement of neoclassical tearing modes Plasma shape and position (for 1000 s) $T_i(r)$ in core $q(r)$, in particular localization and position of q_{min} High resolution measurements of the gradient of T_e and T_i Resistive wall modes	$q(a)$ Halo current Impurity identification and influx $n_e(r)$ in core Line-averaged Z_{eff} Gas pressure and composition (divertor and duct) $q(95\%)$ $n_e(r)$ and $T_e(r)$ at edge $P_{rad}(r)$ Heat deposition profile in divertor Neutron and alpha source profiles Impurity profile $Z_{eff}(r)$ D and T influx Neutral density (near wall) n_e and T_e in divertor Impurity and D-T influxes in divertor with spatial resolution Alpha particle loss Neutron fluence Erosion of divertor tiles

*Adapted from Ref. 11. Closely related measurements that appear twice in the same column exist because the simpler measurement (appearing first) is already in use for control in a less demanding regime.

In Table XIII, availability is defined as the fraction of each expected measurement range for which valid data are available in principle (by design). A regime can have a wide range for the measurement parameter, and it might be impractical to design for the full range. For example, the range of densities spanned by the divertor is very large (about 5 orders of magnitude), and it requires multiple instruments to cover this. Another example is the measurement of edge density profile, where there are limitations on radial coverage: by reflectometry due to the presence of cutoffs and relativistically downshifted absorption and by edge Thomson scattering due to the large variation in plasma shape. For Machine Protection and Basic Control measurements, the availability should span at least the predicted range. In other words, there must be margin for unforeseen plasma behaviour. For Advanced Control, sufficient coverage should be foreseen to explore each regime, with upgrade capability existing to extend the availability for certain regimes to be selected during the exploration phase. In this way, by the technology phase, the measurement availability will have been matched to the by-then known needs for these regimes. For Evaluation measurements, aimed primarily

at physics understanding, only the part of the measurement range that specifically extends physics knowledge of burning plasmas need be planned for, and only for appropriate regimes (for example, density fluctuation measurements have a potentially vast wavenumber and spatial range, but not all needs to be covered). For the technology phase, the operational range of the BPX will likely be restricted so limited availability of Evaluation measurements may be sufficient.

Regarding on-line measurement reliability the classification of the measurement is a good starting point. For the case of machine protection systems, given the scale of investment in a typical BPX (2 to 10 billion € in today's terms) and the correspondingly high cost of core machine component repairs, it is appropriate to ensure that the diagnostic chain is extremely unlikely to fail. For all control measurements failure can be of at least two types: (a) failure to detect a limiting state that requires intervention of the control system and (b) failure that causes the control system to push through a limiting state (for example, failure that causes the control system to move the plasma to the wall, or decrease the gas feed to the divertor plates) at an otherwise quiescent part of the

TABLE XIII

Measurement Availability, Reliability and Redundancy Design Targets for Each Category of Measurement*

Category	Acceptable Measurement Availability by Design	Maximum Failure Rate Target per Measurement per Operational Year (pmpo)	Associated Design Redundancy Factors
Machine protection (1a)	>100% of all expected regimes	$<5 \times 10^{-5}$	2 (method or type) and 2 (location) and 1.2 to 1.5 (component)
Basic control (1a)	100% of all expected regimes	$<5 \times 10^{-3}$	2 (method or type or location) and >1 (component)
Advanced control (1b)	>80% of appropriate regimes in exploration phase 100% for selected measurements in technology phase	$<10^{-1}$ $<5 \times 10^{-3}$	Any 2 (method or type or location)
Evaluation (2)	~50% of appropriate regimes in exploration phase Selected availability in technology phase	$<10^{-1}$	None

*Categories in ITER nomenclature; see text. Fractional redundancy at the component level represents, for example, 120 instead of the needed 100 sightlines to achieve the required level of resolution, giving a redundancy of 1.2.

pulse. The probability of the first type of failure having serious consequences is in principle reduced by the fraction of the plasma time where there is demand for the measurement. However, for a high-performance BPX, the time spent near machine limits should be a relatively high fraction of the total, and it is difficult, therefore, to take credit for this. Assuming then, that the overall probability of failure should be less than 10^{-2} , and distributing this over about 10 machine protection measurements and 20 operational years, leads to a target failure probability of $<5 \times 10^{-5}$ per measurement per operational year (pmpo). This is very difficult to achieve without a significant level of redundancy.

For basic control, this requirement can be relaxed, since it becomes more a question of what is an acceptable operational stoppage rate rather than an issue of machine investment protection. Assuming no more than one pulse is lost per operational year due to a basic control measurement loss (again, about 10 measurements; see, e.g., Table X, first column) suggests a target failure rate of $<5 \times 10^{-2}$ pmpo. This simple picture is complicated by the maintenance requirements of the diagnostic and its elements. The maintenance time for these is measured in weeks or months and a large part of the program will be delayed or lost, unless that part of the measurement chain can be left unused until the next regular maintenance cycle. Typically, this cycle will be more than one operational year away. Software failures revealed in operation can cause almost as long delays. Therefore, a more reasonable specification is 5×10^{-3} pmpo. This gives a $\sim 10\%$ probability over the machine lifetime of a significant delay to the operational program due to this particular measurement/diagnostic.

Regarding advanced control measurement, the situation is slightly different. Typically, only one or two additional measurements at a time are part of advanced control loops. They are by definition “in development” and so pulse losses are expected and must be tolerated by the operational program. Furthermore, failure of these measurements due to hardware or software faults would normally allow switching to another program or regime and any maintenance can either be done in parallel or be postponed to a standard maintenance cycle. Assuming this should not happen more than once a year to avoid loading the maintenance program of the machine leads to a design target failure rate of <0.1 pmpo. During the technology phase, a few Advanced Control measurements may acquire Basic Control roles and their reliability will have to be upgraded if there is no diagnostic redundancy behind the measurement. For certain cases this may be impossible so the ability for increasing robustness by redundancy may have to be designed from the beginning.

For measurements intended for evaluation and physics, similar considerations apply to those used for Advanced Control measurements during the exploration phase. Evaluation and physics measurements are by def-

inition not expected to become part of control loops and so a rather low reliability would still be tolerable.

The level of redundancy for each measurement in order to achieve the aforementioned reliability requirements will therefore have to be decided on a case-by-case basis. Since, in modern tokamaks, control systems are all implemented in the digital domain, what matters is the reliability of the data stream representing this measurement, which may be synthesized from several diagnostics with built-in precedence and fall-back rules. Thus, achieving a certain level of reliability for a measurement is also to some extent a matter of choice on how the data is merged and how the risk of failure is distributed (by choice of reliability target) to the contributing diagnostics. Table XIII also gives some indication of typical redundancies of measurement method (physical principle), type (instrument set used), location (multiple instances of the same method and type), and number (of sensors or sightlines at the same location using the same method and type) that might be suitable. This is best illustrated by the specific case studies in the following section.

V.C. Specific ITER Case Studies

The detailed ITER measurement requirements for these three examples are shown in Table XIV. All examples involve control measurements.

V.C.1. Plasma Shape

Plasma shape measurement in ITER relies primarily on magnetics; the system implementation has changed little since its description in Ref. 85. Primary, backup, and supplementary measurements are described for the plasma shape measurement, to be used for basic control of the plasma wall gaps. Table XV shows the reference arrangement.

In addition to the normal magnetics measurement, for long pulses where integrator outputs may become suspect, alternative estimates for the value of the plasma-wall gaps are expected to be provided by the reflectometer for plasma position¹⁷⁹ and by measurements of the divertor IR thermography footprint¹⁸² and Langmuir probe sets.¹⁸³ Plasma shape for long pulses has been defined as an “advanced control” measurement in the ITER measurement set.

Figure 21 shows, schematically, how failure rates can be assigned to the diagnostics contributing to these measurements. The following scheme is assumed: for each of the primary and secondary (backup) magnetics sets, a triplet of sensors (S11 through S13 and S21 through S23, respectively) is normally summed to derive each poloidal field measurement. Failure of a single sensor can be detected in periods of magnetohydrodynamic (MHD) inactivity (known from the independent HF coil set). An appropriate combination of the two sets can then

TABLE XIV

Selected Measurement Requirements for ITER, from Ref. 11

Measurement	Parameter	Condition	Range or Coverage	Resolution		Accuracy
				Time or Frequency	Spatial or Wave Number	
2. Plasma Position and Shape	Main plasma gaps, Δ_{sep}	$I_p > 2$ MA, full bore	—	10 ms	—	10 mm
		I_p quench	—	10 ms	—	20 mm
	Divertor channel location (r dir.)	Default	—	10 ms	—	10 mm
		I_p quench	—	10 ms	—	20 mm
	dZ/dt of current centroid	Default	0 to 5 m/s	1 ms	—	0.05 m/s (noise) + TBD% (absolute)
23. Electron Temperature Profile	Core T_e	$r/a < 0.9$	0.5 to 40 keV	10 ms	a/30	10%
	Edge T_e	$r/a > 0.9$	0.05 to 10 keV	10 ms	5 mm	10%
16. Divertor Operational Parameters	Maximum surface temperature		200 to 2500°C	2 ms	—	10%
	Erosion rate		1 to 10×10^{-6} m/s	2 s	10 mm	30%
	Net erosion		0 to 3 mm	Per pulse	10 mm	12×10^{-6} m
	Gas pressure		1×10^{-4} to 20 Pa	50 ms	Several points	20% during pulse
	Gas composition	$A = 1$ to 100 $\Delta A = 0.5$	TBD	1 s	Several points	20% during pulse
	Position of the ionization front		0 to TBD m	1 ms	100 mm	—

TABLE XV

Substitution and Replacement Strategy for the Plasma Current, Vertical Speed and Shape Measurements Following Loss of a Single Sensor from the Primary Set

Measurement	I_p, zI_p	Shape			Performance
Main Subsystem(s)	Inner Vessel Tangential Field Coils	Inner Vessel Tangential Field Coils	In Vessel Saddles and Normal Field Coils	Divertor Coils	
1st backup	----- Substitute from secondary set -----				None or little loss
2nd backup	Substitute from the HF set with outer vessel set supplement	Substitute from the HF set with outer vessel set supplement	—	—	
			Substitute from MHD saddles and/or outer vessel sensors	—	Some loss
After that	----- Accept reduced inputs (10 to 50%) -----				Further loss
Finally	Replace inner vessel coils		Replace HF coil with normal field coil	Repair or replace instrumented cassette	Restore

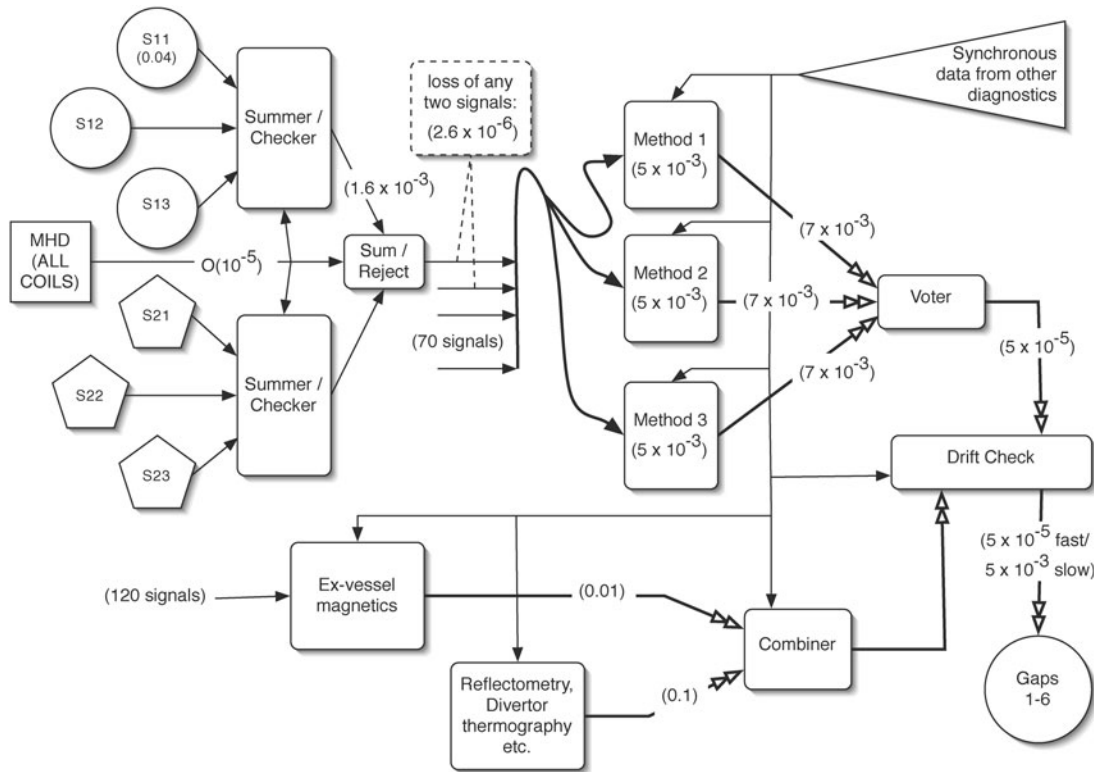


Fig. 21. Example of a simple failure rate assignment model to individual sub-systems for shape measurement, which is a machine protection and basic control measurement for ITER. Failure rates in brackets () are equivalent per operational year and are not repeated where identical for similar subcomponents. Double arrow paths represent sets of 6 gap measurements used to control the plasma shape.

be selected online and all the signals (about 70) can be used to generate the required gap information in three different ways. The ITER set has been designed so that the gap estimates are resistant to loss of any one signal (by engineering sufficient local poloidal redundancy), but if two key signals are lost a gap may be corrupted. A sufficient condition for this not to happen is that the probability of loss of any two signals is below a certain value. A further sanity check (“vote”) can be used to decide which gap set is passed on to the control system and, at this stage, checks against drift-resistant systems, such as the set of ex-vessel magnetics, and other diagnostics can be used to provide corrections for the advanced control of long pulses. Using this scheme, a failure rate of individual sensors of 0.04 per year (2.5×10^{-5} per pulse), amounting to about 5 sensors failing per operational year, seems acceptable from the point of view of online reliability of what is a machine protection system. It is marginal from the point of view of long-term performance: The chances of a sensor triplet failing amount to 12% per year; that both triplets (primary and secondary) do so $\sim 1.5\%$ per year and sensitivity studies using the Function Parametrisation approach suggest that the effective redundancy in the ITER set is $\sim 30\%$ (Ref. 184).

This gives a time to system failure of 20 operational years, the same as the ITER lifetime (although this is still a “soft” failure as it is still possible to run the machine with increased gaps). This suggests that a better target for the sensors themselves is $<1\%$ per operational year.

Systematic effects can also distort this picture. It is relatively easy to provide two types of construction for pickup coils. It is somewhat more difficult for flux loops but, for example, different manufacturers and composition of MI cable can be chosen for each of the two sets. It is harder still to devise two distinct designs for the in-vessel wiring. At the same time, it is easiest to replace the pickup coils, less easy to replace the saddle loops, and practically impossible to replace the wiring. For this reason considerable effort still needs to be spent in designing and qualifying wiring loom designs for the in-vessel magnetics.

V.C.2. Core Electron Temperature

Electron temperature on ITER is an advanced control measurement that is, however, rather likely to acquire a basic control role in the later phase of ITER operation. In particular, for certain advanced scenarios,

the gradient of T_e , or its value at selected regions, could be used as a feedback control parameter. Two diagnostics are planned to supply this information: Electron Cyclotron Emission (ECE) and a pair of Thomson Scattering systems, one each for the core and edge regions, respectively.¹¹ It is instructive to examine whether the combination of these systems is likely to meet the reliability targets for basic control measurements.

The ECE system has been described in Refs. 185 and 186 and its performance analyzed by Bartlett and Bind-slev¹⁸⁷ and more recently by Austin.¹⁸⁸ It can easily meet the ITER T_e measurement requirements with respect to time resolution and accuracy but will not match the spatial resolution, both in hot gradient region of Internal Transport Barriers (ITBs) and near the edge, due to the effects of relativistic broadening and burn-through. The core LIDAR system has been described in Ref. 189. It can meet the measurement requirements for time resolution or accuracy, but achieving both in steady-state (a requirement for control) will demand a high repetition (100 Hz), short pulse (300 ps), and very intense (2 J) laser, which is at the limits of presently envisaged technology.¹⁹⁰ Thus, the system to be implemented may have to be slightly compromised in this regard, for example, using an interlaced set of lasers with (10 ms, 0.6 J) and (100 ms, 2 J) repetition rate and energy, respectively. The edge Thomson scattering system planned for ITER is a conventional system using imaging optics.¹⁹¹ It can achieve the edge spatial resolution required in the upper flux expansion region at the same time as the time resolution. It uses two laser drivers for improved reliability.

Of the instruments used for this measurement, only the ECE heterodynes are expected to be operational 100% of the time, a basic requirement for stability. The remaining instruments have internal mechanical, chemical, and/or thermally stressed systems that will probably be placed on stand-by between pulses to improve service life. For this reason, the failure probability requirement for a control measurement with redundancy ($<5 \times 10^{-2}$ pmpo) has been translated to a requirement of $<3 \times 10^{-5}$ per measurement per pulse.

The combination of two methods of measurement based on different physical principles is expected to provide a first level of redundancy. Furthermore, within the ECE system

1. there are two separate sightlines giving redundancy of location
2. there are separate Michelson and Heterodyne instruments for each mode that can both be used at the required timescale of 10 ms giving further redundancy of measurement type
3. the LIDAR system has a main and a backup laser giving some numerical redundancy at the component level
4. the edge Thomson system can be designed with two feeder lasers also giving some numerical redundancy at the component level.

This situation is shown diagrammatically in Fig. 22 (for the core measurement). In Fig. 22, tolerable failure rates per pulse are also shown. At the component level,

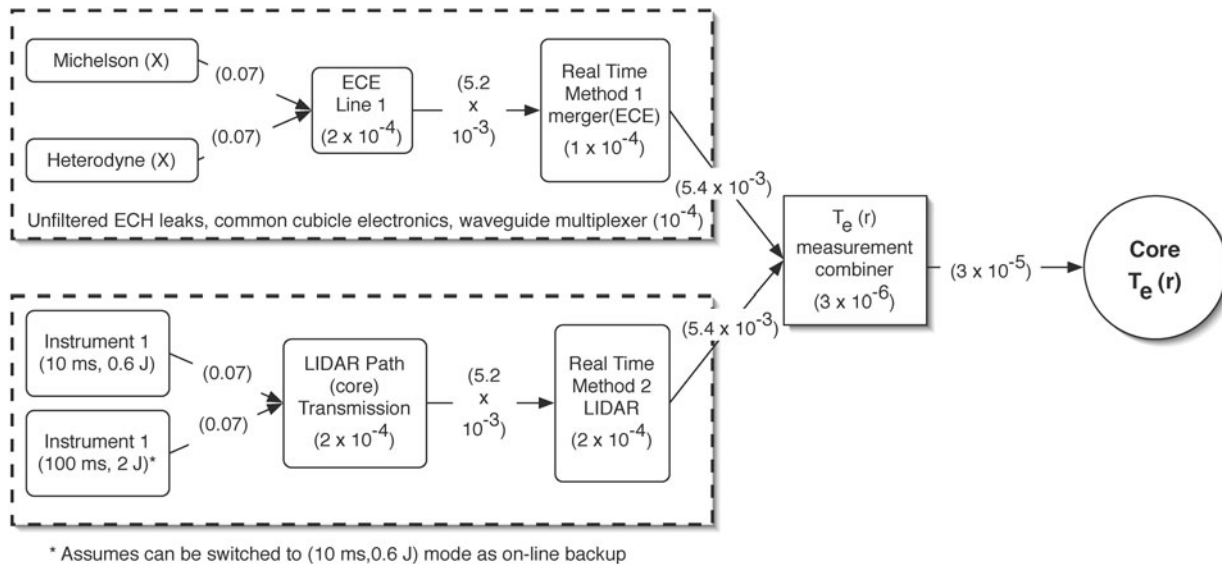


Fig. 22. Example of a simple failure rate assignment model to individual diagnostics and elements for the core electron temperature measurement as an active control measurement. Failure rates in brackets () are per pulse. A similar figure could be composed for edge temperature by substituting the edge Thomson scattering system for LIDAR.

the failure rate requirement seems modest, but neglects the maintenance downtime for the component. Thus, a failure probability of 0.07/pulse is tolerable in a laser only if this is a self-correcting occasional “glitch” or if the maintenance downtime is a pulse. If the maintenance time of the lasers and Michelsons is a year, then their tolerable failure rate will be less than 0.25 per operational year or 2×10^{-4} per pulse. This level could be achieved in a spinning Michelson¹⁹² but is unlikely in a laser.

Figure 22 also highlights the importance of common-mode failures. For example, the waveguide switch system used in the ECE system can in principle invalidate all ECE data streams and should be designed for a failure rate well below 10^{-4} per pulse. For the LIDAR system, the first mirror is a weak point. It undermines the redundancy achieved at great cost by providing independent laser systems and, to a certain extent, transmission lines. In fact, all common elements of the transmission line potentially reduce the reliability, but the first mirror is the weakest link, as it has to operate in the most extreme environment (in the port plug) and, because of optical design and constraints cannot be made arbitrarily large. This mirror is subject to deposition (see Sec. IV) but is also subject to severe cyclic thermal stress due to laser pulsing. The mechanism of its degradation under load is very similar to a fatigue deformation,¹⁹³ as it is heated with every laser pulse for well over 10^8 cycles. Laser damage threshold experiments (to 2×10^5 shots¹⁹⁴) are shown in Fig. 23. These results are shown as solid points together with approximation (dots) up to a normalized laser-induced damage threshold ratio, LIDTR = F_N/F_1 , of 0.1 (Refs. 195 and 196). Here F_1 is the damage threshold for a single laser shot and F_N the value after N laser shots. It is seen that, of three mirror materials tested, only a monocrystalline Mo mirror has the necessary extrapolated lifetime. Even for this mirror, the power density

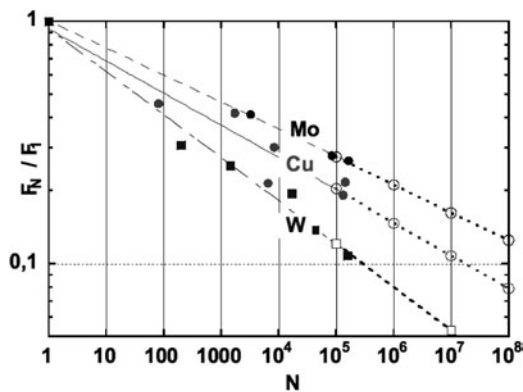


Fig. 23. Laser induced damage threshold as a function of pulse number, for monocrystalline Mo and W and polycrystalline copper. Solid points are results of measurements, open points and dotted lines—extrapolated.

must be reduced by enlarging the beam. This in turn places a limitation on the mirror diameter, which must be at least 12 cm. There is no real statistical information in these data. However, their scatter suggests that the standard deviation in the fatigue lifetime (N) for a given energy is large (about a factor of 2) so that, to achieve a nominal failure rate of 10^{-3} pa, or 10^{-2} over the life of ITER, at least a factor of 10 margin would be required in the planned N (3 standard deviations away from the nominal life). This requires an impractically large mirror, even if a nonideal component (W does not have the best reflectivity for this application) were acceptable. A way to bypass this problem is to modify the design to place the laser first mirror outside the port plug and make it a planned maintenance component. This modification is included in the latest proposal.¹⁹⁰

V.C.3. Divertor Ionization Front Position

The direct measurement of the location of the ionization front in the divertor plasma, and advanced control measurement, is thought to be one possible way to control the operation of the divertor in a BPX. Other ways include the measurement of divertor plate temperature using infrared,¹⁹⁷ and the ionization current in Langmuir probes. The main actuators are the fuel and impurity gas feeds, with the fuel feed largely constrained by the core fuelling requirements.

For the ionization front itself, methods that have been proposed include the spectroscopic measurement of T_e using the divertor impurity monitor,¹⁵⁷ which would be able to detect the sharp drop of T_e marking the ionization front, and divertor interferometry, originally proposed as part of a reflectometer system¹⁷⁹ and, more recently, proposed to be by a multichannel FIR interferometer.¹⁹⁸ Bolometry¹⁷⁸ is also a potential measurement. All methods are expected not to be 100% reliable in practice; however, they do represent true redundancy of method as the conditions for measurement failure are likely to be quite different. The measurements are largely complementary: the impurity monitor provides in some sense the most direct measurement, whereas the interferometer would infer the position of the front from the line integral density pattern near the target, and the bolometer will look for a change in the pattern of emission down the divertor leg. The impurity monitor is expected to have a time resolution of 10 ms (adequate); faster resolution is expected of the interferometer and the bolometer.

For this measurement to meet the advanced control reliability targets, assuming a reasonable ionization front position estimate could be made for either instrument, would require a failure rate of $<50\%$ per operational year for each instrument. Should this measurement evolve into a routine basic control measurement in a later phase of ITER, this would require an increase in the robustness of the measurement to the level required of a basic control measurement (a few pulses lost per year, or $<17\%$ per operational year for each of these three diagnostics).

These targets may be hard to meet with the interferometer, which is sensitive to fringe jumps. They may also be difficult to achieve with the divertor impurity monitor, which, like all spectroscopic instruments, is potentially subject to background effects to which the interferometer system is largely immune. The bolometer is influenced by neutral particle bombardment and may require sophisticated real-time processing in this service. Worse, transient events are likely to confuse all three measurements at the same time. From the hardware failure point of view, the reliability of the interferometer is expected to be well below the 17% level per operational year, that of the bolometer moderate comparable to it [a camera failure per 5 operational years seems possible in the divertor (after systematic faults have been eliminated by improving the bolometers at divertor maintenance intervals)] and that of the impurity monitor cannot be established in advance, as it depends on the deposition rates and the success or otherwise of mitigation measures. It is likely, therefore, that reliable divertor control for the purposes of accumulating neutron fluence will require the full set of divertor diagnostics to be used and the development of techniques to cope with the loss of diagnostic information without termination of the pulse.

VI. THE FUTURE

VI.A. Development of Diagnostics for Future Power Plants

BPXs are an intermediate technological step between the present-day large experimental physics machines and a prototype power reactor. Such power reactors will face similar radiation flux problems, but the fluence problems will be far more severe. It is evident that in the next generations of reactor after BPX, for example, ARIES-ST [3.1 GW(thermal), (Ref. 199)], DEMO [\sim 2GW(thermal), (Refs. 200 and 201)], ARIES-CS [\sim 2.4 GW(thermal), (Ref. 202)], and PROTO [\sim 1.5 GW(electric), (Ref. 203)] measurement will resemble the fission reactor more in terms of operational pattern and maintenance requirements.

The goal of DEMO, for example, will be to produce continuously more than 2 GW of fusion power compared with 500 MW for 500 s for BPX, and with plant availability at more than 75% the scale of a modern electric power plant. The main DEMO design conditions are a surface heat flux of 0.5 MW/m² with peaking factor of x2, a neutron wall load of 3.5 MW/m² (peaking factor x1.5) and a neutron fluence of about 10 MW·yr/m². Although the confinement scheme used for DEMO is unsure, the technologies developed for, and tested on BPXs, such as remote maintenance, tritium breeding high temperature blankets, high heat flux components, and diagnostics, will provide essential design input. In particular, the operational scenario for DEMO would have to be developed on a burning plasma tokamak, such as

ITER. A subset of the ITER measurement set will be essential in the control of DEMO, and the target measurement requirements for this will be developed during the latter part of the ITER program. This subset may incorporate advanced control features and will have enhanced reliability targets.

The front-end, in-vessel diagnostic equipment required to service these measurements in DEMO will have to be well tested and proven. It is likely that there will need to be equipment for

1. electrical signal transmission components (cables, connectors, feedthroughs)
2. magnetic diagnostic components (coils, loops, Hall probes)
3. first mirrors and retroreflectors (mirrors, mounts, and shutters)
4. electrical sensors (bolometers cameras, X-ray detectors, pressure gauges, residual gas analyzers, thermocouples)
5. in-vessel neutron flux monitors
6. light, neutron, and X-ray apertures and collimators
7. waveguides, antennas, calibration sources
8. optical and neutron windows.

Small electrical sensors and possibly microwave systems employing small waveguides will dominate the diagnostics near the plasma. Optical access will be possible but it is likely that mirrors and other optical components will have to be recessed further from the plasma to provide for less intrusive maintenance. At suitable locations, optical fibers will become more important because of their nonintrusive nature, easy replacement, and excellent multiplexing capabilities.

Because of the desire to fast-track to DEMO, much of the R&D of diagnostic techniques and hardware needed must be performed in BPXs. These must be conceived and designed now and provision made for simple implementation. The BPXs in their final operating regimes will be some of the test beds for DEMO diagnostics and diagnostic equipment along with other devices such as the International Fusion Material Irradiation Facility^{204,205} (IFMIF) and similar material testing facilities.

VI.B. Readiness for a BPX

The years of preparation for ITER diagnostics, starting with the conceptual design activity (CDA) and continuing to the present activities, have provided a solid base for the detailed design of a large number of diagnostic systems. Indeed, the ITER diagnostic set is planned to be as comprehensive as any modern tokamak within the technological limitations imposed by burning plasma environment, and the ITER-specific challenge of high first wall fluence arising from the technological testing part of its programmatic objectives. As a result, the

remaining key design uncertainties facing a BPX diagnostic designer are few:

1. *Magnetic diagnostics:* The combination of nuclear heating and fluence-modified thermoelectric effects means that a sensor guaranteed to perform as required for the full ITER life is proving difficult to design and is the subject of ongoing R&D. At the same time, mitigating measures (secondary sensors and backup gap measurements) can be included (as on ITER) to ensure that the shape measurement requirements can be met in most cases. The development of a steady state in-vessel sensor that can be cross-calibrated to inductive measurements is highly desirable for ITER and beyond.

2. *Optical and Spectroscopic systems:* After many years of effort, it is still impossible to predict with certainty the lifetime of a first mirror in ITER. Whilst continuous progress is being made, this state of affairs is likely to remain for the foreseeable future. For this reason, mitigating measures must be put in place, including easy first mirror replacement, protection, and cleaning. These are space and resource-intensive and in addition require their own up front R&D program. Another area of active research involves radiation-hard refractive materials. While the present ITER designs have found acceptable solutions based on presently available fibers and lens materials, all can benefit from further radiation hardening of fibers and lenses that can simplify the front-end design of these systems. Finally, there are emerging radiation-resistant detector technologies²⁰⁶ that can potentially have useful lifetimes in BPX diagnostic modules and will allow multi-sightline diagnostics in the X-ray region, and BPX designers should be ready to benefit from these.

In progressing to DEMO and beyond, it is likely that some of the solutions adopted for ITER will be found wanting. In particular, diagnostics requiring ceramic to metal bonds in high fluence regions [such as magnetics in most present implementations, but also bolometry, Langmuir probes, and in-vessel soft X-ray (SXR) detectors] will need to be implemented in readily maintainable forms and exchanged at regular intervals if they are to be placed at locations providing similar measurement performance as on today's devices and ITER. The application of refractive components and solid-state or composite detector modules will also become significantly harder without an exchangeable module approach. The knowledge gained in the ITER design activity shows that exchangeable modules with a fast turnaround time are difficult to develop without affecting the basic machine design and maintenance concepts. Therefore, these considerations will have to be included early in the prototype reactor design process, and the list of indispensable measurements for a prototype reactor will have to be defined at a similarly early stage.

ACKNOWLEDGMENTS

This report was prepared as an account of work by or for the ITER Organization. The members of the organization are the People's Republic of China, the European Atomic Energy Community, the Republic of India, Japan, the Republic of Korea, the Russian Federation, and the United States of America. The views and opinions expressed herein do not necessarily reflect those of the members or any agency thereof. Dissemination of the information in this paper is governed by the applicable terms of the ITER Joint Implementation Agreement.

REFERENCES

1. A. T. RAMSEY, *Rev. Sci. Instrum.*, **66**, 1, 871 (1995).
2. A. MAAS et al., "Diagnostic Experience During Deuterium-Tritium Experiments in JET, Techniques and Measurements," *Fusion Eng. Des.*, **47**, 247 (1999).
3. D. VAN HOUTTE et al., "Recent Fully Non-Inductive Operation Results in Tore Supra with 6 Min, 1 GJ Plasma Discharges," *Nucl. Fusion*, **44**, L11 (2004).
4. Y. NAKAMURA et al., "Plasma Performance and Impurity Behaviour in Long Pulse Discharges on LHD," *Nucl. Fusion*, **43**, 219 (2003).
5. J. B. LISTER et al., "Technical Issues Associated with the Control of Steady State Tokamaks," *Nucl. Fusion*, **40**, 1167 (2000).
6. H.-J. HARTFUSS, R. KOENIG, and A. WERNER, "Diagnostics for Steady State Plasmas," *Plasma Phys. Control. Fusion*, **48**, R83 (2006).
7. A. COSTLEY, "Requirements and Issues in Diagnostics for Next Step Burning Plasma Experiments," *Advanced Diagnostics for Magnetic and Inertial Fusion*, p. 1, P. E. STOTT et al., Eds., Kluwer Academic/Plenum Press, New York (2002).
8. S. ROLLET and P. BATISTONI, *Rev. Sci. Instrum.*, **63**, 4551 (1993).
9. K. M. YOUNG, "Challenges for Plasma Diagnostics in a Next Step Device (FIRE)," *Proc. 19th Symp. Fusion Engineering*, p. 192, Atlantic City, New Jersey, January 22–25, 2002, Institute of Electrical and Electronics Engineers (2002).
10. "ITER Diagnostics," ITER CDA Documentation Series No. 33, International Atomic Energy Agency (1989).
11. A. J. H. DONNÉ et al., "Progress in the ITER Physics Basis: Chapter 7: Diagnostics," *Nucl. Fusion*, **47**, S337 (2007).
12. "ITER Technical Basis," ITER EDA Documentation Series No. 24, International Atomic Energy Agency (2001).
13. R. HIWATARI, Y. ASAOKA, K. OKANO, T. YOSHIDA, and K. TOMABECHI, "Generation of Net Electric Power with a Tokamak Reactor Under Foreseeable Physical and Engineering Conditions," *Nucl. Fusion*, **44**, 106 (2004).
14. R. V. BUDNY, "Fusion Alpha Parameters in Tokamaks with High DT Fusion Rates," *Nucl. Fusion*, **42**, 1383 (2002).
15. R. PAMPIN, P. J. KARDITSAS, A. SHIMIZU, T. ANDO, and M. AKIBA, *Fusion Eng. Des.*, **81**, 1231 (2006).
16. A. MÖSLANG et al., "Suitability and Feasibility of the International Fusion Materials Irradiation Facility (IFMIF) for Fusion Materials Studies," *Nucl. Fusion*, **40**, 619 (2000).

17. L. C. JOHNSON et al., "Fusion Product Measurements in DT Plasmas in ITER," *Diagnostics for Experimental Thermonuclear Fusion Reactors*, p. 369, P. E. STOTT et al., Eds., Plenum Press, New York (1996).
18. L. DE KOCK et al., "The Implementation of the Diagnostic Systems on ITER," *Plasma Physics Reports*, **24**, 97 (1998).
19. C. I. WALKER et al., "Nuclear Aspects of Diagnostics for RTO/RC ITER," *Fusion Eng. Des.*, **51–52**, 377 (1998).
20. A. E. COSTLEY et al., "Requirements for ITER Diagnostics," *Diagnostics for Experimental Fusion Reactors*, p. 23, P. E. STOTT et al., Eds., Plenum Press, New York (1996).
21. A. E. COSTLEY et al., "Overview of the ITER Diagnostic System," *Diagnostics for Experimental Thermonuclear Fusion Reactors 2*, p. 41, P. E. STOTT et al., Eds., Plenum Press, New York (1998).
22. C. I. WALKER et al., "Diagnostic Access for ITER," *Diagnostics for Experimental Thermonuclear Fusion Reactors*, p. 57, P. E. STOTT et al., Eds., Plenum Press, New York (1996).
23. C. I. WALKER, A. E. COSTLEY, K. ITAMI, T. KONDOH, T. SUGIE, and G. VAYAKIS, "ITER Diagnostics: Integration and Engineering Aspects," *Rev. Sci. Instrum.*, **75**, 4243 (2004).
24. G. KALININ et al., "Assessment and Selection of Materials for ITER In-Vessel Components," *J. Nucl. Mater.*, **283–287**, 10 (2000).
25. C. GORDON et al., "An Overview of Results in the ITER Generic Site Safety Report (GSSR)," *Proc. 19th Fusion Energy Conf.*, Lyon, France, October 14–19, 2002, IAEA-CN-94, CT/P-17 (2002).
26. C. GORDON, H.-W. BARTELS, M. ISELI, H. OKADA, J. RAEDER, and N. TAYLOR, "Safety Analysis for ITER Licensing," *Fusion Eng. Des.*, **75–79**, 1247 (2005).
27. G. JANESCHITZ et al., "Integration of Diagnostics into the ITER Machine," *Proc. 17th IAEA Fusion Energy Conf.*, Yokohama, Japan, October 19–24, 1998, IAEA-CN-69, ITERP1/15 (1998).
28. C. I. WALKER et al., "Integration of In-Vessel Diagnostic Sensors in ITER," *Fusion Eng. Des.*, **56–57**, 883 (2001).
29. E. MARTIN et al., "Remote Maintenance of the ITER Equatorial Ports," *Proc. 20th Symp. Fusion Technology (SOFT-20)*, Marseille, France, September 7–11, 1998, p. 1119, Commissariat à l'Énergie Atomique (1998).
30. S. YAMAMOTO et al., "Impact of Irradiation Effects on Design Solutions for ITER Diagnostics," *J. Nucl. Mater.*, **283–287**, 60 (2000).
31. P. NIELSEN et al., "LIDAR Thomson Scattering for the ITER Core Plasma" in *Diagnostics for Experimental Fusion Reactors 2*, p. 217, P. E. STOTT et al., Eds., Plenum Press, New York (1998).
32. G. I. SHATALOV, A. BORISOV, S. SHELUDJAKOV, and A. SERIKOV, "Neutronics for ITER Diagnostic Systems and Ports," *Fusion Eng. Des.*, **42**, 221 (1998).
33. G. SHATALOV, Private Communication (2000).
34. A. BORISOV, C. I. WALKER, G. SHATALOV, and S. SHELUDIAKO, "Neutronic Analysis of Diagnostic Systems in Ports of ITER," *22nd Symp. Fusion Technology Book of Abstracts*, p. 228, S. TÄHTINEN et al., Eds., VTT Symposium 220, VTT, Finland (2002).
35. A. E. COSTLEY, D. J. CAMPBELL, S. KASAI, K. E. YOUNG, and V. ZAVERIAEV, "ITER R&D: Auxiliary Systems: Plasma Diagnostics," *Fusion Eng. Des.*, **55**, 331 (2001).
36. R. T. SANTORO, V. KHRIPUNOV, H. IIDA, and R. R. PARKER, "Radionuclide Production in the ITER Water Coolant," *17th IEEE/NPSS Symp. Fusion Engineering*, Vol. 1, p. 137, Institute of Electrical and Electronics Engineers (1997).
37. S. SATO, H. IIDA, M. YAMAUCHI, and T. NISHITANI, "Shielding Design of the ITER NBI Duct for Nuclear and Bremsstrahlung Radiation," *Radiat. Prot. Dosim.*, **116**, 28 (2005).
38. L. H. ROVNER and G. R. HOPKINS, "Ceramic Materials for Fusion," *Nucl. Technol.*, **29**, 274 (1976).
39. E. R. HODGSON, "General Radiation Problems for Insulating Materials in Future Fusion Devices," *J. Nucl. Mater.*, **258–263**, 226 (1998).
40. E. R. HODGSON, "Radiation Problems and Testing of ITER Diagnostic Components," *Diagnostics for Experimental Thermonuclear Fusion Reactors 2*, p. 261, P. STOTT et al., Eds., Plenum Press, New York (1998).
41. S. YAMAMOTO et al., "Radiation Problems and Testing of ITER Diagnostic Components," *Diagnostics for Experimental Fusion Reactors 2*, p. 269, P. E. STOTT et al., Eds., Plenum Press, New York (1998).
42. T. SHIKAMA, K. YASUDA, S. YAMAMOTO, C. KINOSHITA, S. J. ZINKLE, and E. R. HODGSON, *J. Nucl. Mater.*, **271–272**, 560 (1999).
43. E. R. HODGSON, "Challenges for Insulating Materials in Fusion Applications," *Nucl. Instrum. Methods Phys. Res., Sect. B: Beam Interactions with Materials and Atoms*, **191**, 744 (2002).
44. A. IBARRA and E. R. HODGSON, "The ITER Project: The Role of Insulators," *Nucl. Instrum. Methods Phys. Res. Sect. B: Beam Interactions with Materials and Atoms*, **218**, 29 (2004).
45. M. DECRETON, T. SHIKAMA, and E. R. HODGSON, "Performance of Functional Materials and Components in a Fusion Reactor: The Issue of Radiation Effects in Ceramics and Glass Materials for Diagnostics," *J. Nucl. Mater.*, **329–333**, 125 (2004).
46. "Irradiation Effects on Plasma Diagnostic Components (II)," Report JAERI-Research 2002-007, T. NISHITANI, Ed., Japan Atomic Energy Research Institute (2002).
47. "12th IEA Workshop on Radiation Effects in Ceramic Insulators," Report EUR-CIEMAT 94, E. R. HODGSON, Ed., Ciemat, Madrid (2002).
48. T. SHIKAMA et al., *Nucl. Fusion*, **43**, 517 (2003).
49. "TW1/2-TPD-IRR CER Final Report on Irradiation Effects in Ceramic for Heating and Current Drive and Diagnostic Systems," report EUR-CIEMAT 95, E. R. HODGSON, Ed., Ciemat, Madrid (2003).
50. A. V. BONDARENKO et al., "A Study of Radiation Resistance of Silica Optical Fibers under Conditions of Reactor Irradiation," *Instrum. Exp. Techn.*, **49**, 130 (2006).
51. "13th IEA Workshop on Radiation Effects in Ceramic Insulators," Report JAERI-Review 2004-004, T. NISHITANI, Ed., Japan Atomic Energy Research Institute (2004).
52. "14th IEA Workshop on Radiation Effects in Ceramic Insulators," report EUR-CIEMAT 96, E. R. HODGSON, Ed., Ciemat, Madrid (2004).
53. A. GUSAROV et al., "In Situ In-Reactor Testing of Fusion Materials and Components," *Fusion Eng. Des.*, **75–79**, 819 (2005).
54. "15th IEA Workshop on Radiation Effects in Ceramic Insulators, Dec 2005," report EUR-CIEMAT 98, E. R. HODGSON, Ed., Ciemat, Madrid (2006).
55. A. ROSE, *Phys. Rev.*, **97**, 322 (1955).
56. R. C. HUGHES, "Generation, Transport, and Trapping of Excess Charge Carriers in Czochralski-Grown Sapphire," *Phys. Rev. B*, **19**, 5318 (1979).

57. R. W. KLAFFKY, B. H. ROSE, A. N. GOLAND, and G. J. DIENES, "Radiation-Induced Conductivity of Al_2O_3 : Experiment and Theory," *Phys. Rev. B*, **21**, 3610 (1980).
58. E. R. HODGSON and S. CLEMENT, "The Effect of Iron on the Radiation Induced Conductivity in Gamma- and Electron-Irradiated MgO" *Radiat. Eff. Defects Solids*, **97**, 251 (1986).
59. G. P. PELLIS, *Radiat. Effects*, **97**, 39 (1986).
60. A. MOROÑO and E. R. HODGSON, "An Initial Model for the RIED Effect," *J. Nucl. Mater.*, **283–287**, 880 (2000).
61. T. SHIKAMA and S. J. ZINKLE, *J. Nucl. Mater.*, **258–263**, 1861 (1998).
62. K. YASUDA, K. TANAKA, M. SHIMADA, T. YAMAMOTO, S. MATSUMURA, and C. KINOSHITA, *J. Nucl. Mater.*, **329–333**, 1451 (2004).
63. G. P. PELLIS and E. R. HODGSON, *J. Nucl. Mater.*, **226**, 286 (1995).
64. W. KESTERNICH, "Radiation-Induced Electrical Degradation: An Effect of Surface Conductance and Microcracking," *J. Nucl. Mater.*, **253**, 167 (1998).
65. A. MOROÑO and E. R. HODGSON, "Surface and Volume Electrical Degradation in Wesgo AL995," *J. Nucl. Mater.*, **233–237**, 1299 (1996).
66. A. MOROÑO and E. R. HODGSON, "Role of Environment on the Surface Degradation of Wesgo AL995," *J. Nucl. Mater.*, **258–263**, 1798 (1998).
67. H. OOMS et al., *24th Symp. Fusion Technology (SOFT)*, Warsaw, Poland, September 11–15, 2006, *Fusion Eng. Des.*, **82**, 253 (2007).
68. G. HAAS and H. S. BOSCH, "In Vessel Pressure Measurement in Nuclear Fusion Experiments with Asdex Gauges," *Vacuum*, **51**, 39 (1998).
69. "European Fusion Technology Programme 1998–2001 T492 Final Report on Irradiation Effects in Ceramic for Heating and Current Drive and Diagnostic Systems," report EUR-CIEMAT 93, p. 12, E. R. HODGSON, Ed., Ciemat, Madrid (2001).
70. R. VAN NIEUWENHOVE, "Study of Radiation Effects on a Pressure Gauge," Report SCK•CEN R-3714, Mol, Belgium (2003).
71. R. REICHLER et al., "Bolometer for ITER," *Diagnostics for Experimental Thermonuclear Fusion Reactors*, p. 559, P. E. STOTT et al., Eds., Plenum Press, New York (1996).
72. K. F. MAST, J. C. VALLET, C. ANDELFINGER, P. BETZLER, H. KRAUS, and G. SCHRAMM, "A Low Noise Highly Integrated Bolometer Array for Absolute Measurement of VUV and Soft X Radiation," *Rev. Sci. Instrum.*, **62**, 744 (1991).
73. R. REICHLER et al., "Radiation Hardness Test of Mica Bolometers for ITER in JMTR," *28th EPS Conf. Controlled Fusion and Plasma Physics*, Funchal, Portugal, June 18–22, 2001, Europhysics Conference Abstracts 25A, p. 1293 (2001).
74. M. GONZÁLEZ and E. R. HODGSON "Radiation Resistant Alternative Substrates for ITER Bolometers," *Fusion Eng. Des.*, **66–68**, 881 (2003).
75. M. GONZALEZ and E. R. HODGSON "Radiation Resistant Bolometers Using Platinum on Al_2O_3 and AlN," *Fusion Eng. Des.*, **74**, 875 (2005).
76. M. GONZALEZ and E. R. HODGSON "Electrical and Mechanical Behaviour of Improved Platinum on Ceramic Bolometers," *Proc. 24th Symp. Fusion Technology (SOFT)*, Warsaw, Poland, September 11–15, 2006, *Fusion Eng. Des.*, **82**, 1277 (2007).
77. A. GUSAROV, S. HUYSMANS, L. VERMEEREN, E. R. HODGSON, and M. DECRÉTON, "In Situ In-Reactor Testing of Potential Bolometer Materials for ITER Plasma Diagnostics," *Fusion Eng. Des.*, **82**, 1179 (2007).
78. R. GIANELLA, Private Communication (2005).
79. M. DI MAIO, R. REICHLER, and R. GIANELLA "Design of a Ferroelectric Bolometer," *Proc. 17th IEEE/NPSS Symp. Fusion Engineering*, Vol. 2, San Diego, California, October 6–10, 1997, p. 775, Institute of Electrical and Electronics Engineers (1997).
80. R. BITTNER et al., "Dielectric Properties of Irradiated Ferroelectric and Antiferroelectric Thin Films," *Integrated Ferroelectrics*, **47**, 143 (2002).
81. D. V. KULIKOV et al., "The Effect of Neutron Irradiation on the Curie-Weiss Temperature of an Antiferroelectric Lead Zirconate Film," *Tech. Phys. Lett.*, **28**, 628 (2002).
82. R. BITTNER et al., "Radiation-Induced Defects in Antiferroelectric Thin Films," *Fusion Eng. Des.*, **66–68**, 833 (2003).
83. A. STERNBERG et al., "Antiferroelectric PbZrO_3 Thin Films: Structure, Properties and Irradiation Effects," *J. Eur. Ceram. Soc.*, **24**, 1653 (2004).
84. T. SHIKAMA et al., *Nucl. Instr. Meth. in Phys. Res.*, **B122**, 650 (1997).
85. G. VAYAKIS et al., *Rev. Sci. Instrum.*, **74**, 2409 (2003).
86. C. ALLAN and G. F. LYNCH, *IEEE Trans. Nucl. Sci.*, **NS-27** 1, 764 (1980); see also U.S. Patent 4,284,893 (1981).
87. T. SHIKAMA et al., *Fusion Eng. Des.*, **51–52**, 171 (2000).
88. S. E. BENDER, V. M. CHERNOV, P. V. DEMENKOV, O. A. PLAKSIN, and V. A. STEPANOV, "Investigation of RIEMF Nature in Magnetic Sensors for ITER," *Fusion Eng. Des.*, **56–57**, 911 (2001).
89. S. E. BENDER, V. M. CHERNOV, P. V. DEMENKOV, O. A. PLAKSIN, and V. A. STEPANOV, "Electrophysical Processes in MI-Cables During Pulsed Irradiation at BARS-6 Fission Reactor," *Plasma Devices and Operations*, **11**, 185 (2003).
90. S. E. BENDER, P. V. DEMENKOV, O. A. PLAKSIN, V. A. STEPANOV, and V. M. CHERNOV "Effect of the Dose Rate and Temperature on Radiation-Induced Charge Separation in Cables with Mineral Insulation under Pulsed Reactor Irradiation," *Instrum. Exp. Tech.*, **47**, 163 (2004).
91. L. VERMEEREN, "Experimental Study of Radiation-Induced Currents in Copper and Stainless Steel Core Mineral-Insulated Cables in the BR2 Research Reactor," *Fusion Eng. Des.*, **74**, 885 (2005).
92. L. VERMEEREN and R. VAN NIEUWENHOVE, *Rev. Sci. Instrum.*, **74**, 4667 (2003).
93. R. VAN NIEUWENHOVE and L. VERMEEREN, *Rev. Sci. Instrum.*, **74**, 4675 (2003).
94. T. NISHITANI et al., *J. Nucl. Mater.*, **329–333**, 1461 (2004).
95. G. VAYAKIS et al., *Rev. Sci. Instrum.*, **75**, 4324 (2004).
96. R. VILA and E. R. HODGSON, *J. Nucl. Mater.*, **329–333**, 1524 (2004).
97. R. VILA and E. R. HODGSON, Private Communication (2005).
98. R. VILA and E. R. HODGSON, Private Communication; see also R. VILA, "Update on RIEMF/TIEMF," *Proc. 15th IEA Workshop on Radiation Effects in Ceramic Insulators*, Santa Barbara, California, December 2005, Report EUR-CIEMAT 98 (2006), p. 67 (2006).
99. L. VERMEEREN and M. WÉBER, "Induced Voltages and Currents in Copper and Stainless Steel Core Mineral Insulated Cables Due to Radiation and Thermal Gradients," *Fusion Eng. Design*, **82**, 1185 (2007).

100. R. VILA and E. R. HODGSON, "Thermally Induced EMF in Unirradiated MI Cables," *J. Nucl. Mater.*, **367–370**, 1044 (2007) .
101. R. VILA and E. R. HODGSON, "TIEMF in Unirradiated Cu Cored MI Cables: Microstructure," *Fusion Eng. Des.*, **82**, 1271 (2007).
102. G. CHITARIN, L. GRANDO, N. POMARO, S. PERUZZO, and C. TACCON, "Design Developments for the ITER In-Vessel Equilibrium Pick-Up Coils and Halo Current Sensors," *Proc. 24th Symp. Fusion Technology, Fusion Eng. Des.*, **82**, 1341 (2007).
103. H. TAKAHASHI et al., "Magnetic Probe Construction Using Thick-Film Technology," *Rev. Sci. Instrum.*, **72**, 3249 (2001) .
104. A. ENCHEVA, G. VAYAKIS, R. CHAVAN, A. KARPUSHOV, and J-M MORET, "Design Optimisation of the ITER Divertor Magnetic Probes Using FEM Analyses," *Fusion Eng. Des.* (to be published).
105. A. MOROÑO and E. R. HODGSON, "Radioluminescence Problems for Diagnostic Windows," *J. Nucl. Mater.*, **224**, 216 (1995).
106. D. ORLINSKI et al., *J. Nucl. Mater.*, **212–215**, 1059 (1994).
107. M. GARCIA-MATOS, A. MOROÑO, and E. R. HODGSON, "KU1 Quartz Glass for Remote Handling and LIDAR Diagnostic Optical Transmission Systems," *J. Nucl. Mater.*, **283–287**, 890 (2000).
108. A. MOROÑO and E. R. HODGSON, "KU1 and KS-4V Quartz Glass Lenses for Remote Handling and Diagnostic Optical Transmission Systems," *J. Nucl. Mater.*, **329–333**, 1438 (2004).
109. T. NISHITANI, T. SUGIE, N. MORISHITA, and N. YOKOO, *Fusion Eng. Des.*, **74**, 871 (2005).
110. T. SUGIE, T. NISHITANI, S. KASAI, J. KANEKO, and S. YAMAMOTO, *J. Nucl. Mat.*, **307–311**, 1264 (2002).
111. K. YU. VUKOLOV and B. A. LEVIN, *Fusion Eng. Des.*, **66–68**, 861 (2003).
112. A. T. RAMSEY and K. W. HILL "Nuclear Radiation Effects in Fused SiO₂ Lightguides," *Rev. Sci. Instrum.*, **63**, 4735 (1992).
113. A. O. VOLCHEK, V. M. LISITSYN, A. I. GUSAROV, V. YU. YAKOVLEV, and V. I. ARBUZOV, "Transient Optical Transmission Changes Induced by Pulsed Electron Radiation in Commercial Crown Silicate Glasses," *Nucl. Instrum. Methods in Phys. Res., Sect. B: Beam Interactions with Materials and Atoms*, **211**, 100 (2003).
114. P. MARTIN, A. MOROÑO, and E. R. HODGSON, "Surface Degradation Effects on Laser Damage in KU1 Quartz Glass Windows for LIDAR Applications," *J. Nucl. Mater.*, **307–311**, 1260 (2002).
115. P. MARTIN, A. MOROÑO, and E. R. HODGSON, "Laser Induced Damage Enhancement Due to Stainless Steel Deposition on KS-4V and KU1 Quartz Glasses," *J. Nucl. Mater.*, **329–333**, 1442 (2004).
116. A. V. GORBUNOV, N. V. KLASSEN, D. V. ORLINSKI, and K. YU VUKOLOV, "Laser Damage of KU-1 Quartz Glass Coated with Hydrocarbon Films," *Fusion Eng. Des.*, **74**, 815 (2005).
117. S. M. GONZALEZ, A. MOROÑO, and E. R. HODGSON "Optical and Electrical Degradation of H+ Implanted KS-4V Quartz Glass," *Fusion Eng. Des.*, **74**, 831 (2005).
118. F. SAT, T. IIDA, Y. OYAMA, F. MAEKAWA, and Y. IKEDA, *J. Nucl. Mater.*, **258–263**, 1897 (1998).
119. T. YOSHIDA, T. II, T. TANABE, H. YOSHIDA, and K. YAMAGUCHI, *J. Nucl. Mater.*, **307–311**, 1268 (2002).
120. A. MOROÑO and E. R. HODGSON, "Radiation Induced Optical Absorption and Radioluminescence in Electron Irradiated SiO₂," *J. Nucl. Mater.*, **258–263**, 1889 (1998).
121. B. BRICHARD et al., "Radiation-Hardening Techniques of Dedicated Optical Fibres Used in Plasma Diagnostic Systems in ITER," *J. Nucl. Mater.*, **329–333**, 1456 (2004).
122. B. BRICHARD, "Experiment SMIRNOV V Absorption and Luminescence Spectroscopy," Report SCK•CEN R-4082 (2005).
123. A. F. KOSOLAPOV, S. L. SEMJONOV, and A. L. TOMASHUK, "Improvement of Radiation Resistance of Multimode Silica-Core Holey Fibers," *Proc. SPIE*, **6193**, 61931E (2006).
124. S. NAGATA, K. TOH, B. TSUCHIYA, N. OHTSU, and T. SHIKAMA, *Proc. 50th Annual Mtg. International Society for Optical Engineering*, San Diego, California, Proc. **5199**, 132 (2004).
125. K. OKAMOTO et al., *J. Nucl. Mater.*, **329–333**, 1503 (2004).
126. O. A. PLAKSIN, N. KISHIMOTO, and T. SHIKAMA *J. Nucl. Mater.*, **329–333**, 1490 (2004).
127. D. SPOREA, A. SPOREA, and B. CONSTANTINESCU, *Fusion Eng. Des.*, **74**, 763 (2005).
128. K. TOH et al., *J. Nucl. Mater.*, **329–333**, 1495 (2004).
129. A. T. RAMSEY et al., *Rev. Sci. Instrum.*, **68**, 632 (1997).
130. D. L. GRISCOM, *J. Appl. Phys.*, **77**, 5008 (1995).
131. T. HERNANDEZ, A. MOROÑO, and E. R. HODGSON, "Radiation Enhanced Degradation of Aluminium Mirrors for Remote Handling and Diagnostics Applications: Effect of Humidity," *Fusion Eng. Des.*, **69**, 177 (2003).
132. T. HERNANDEZ, A. MOROÑO, and E. R. HODGSON, "Radiation Enhanced Degradation of SiO Overcoated Aluminium Mirrors," *Fusion Eng. Des.*, **74**, 793 (2005).
133. T. HERNANDEZ, A. MOROÑO, and E. R. HODGSON, "Mirrors for Diagnostic and Remote Handling Applications in ITER: Problems with Specifications for Commercial Mirrors," *Proc. 24th Symp. Fusion Technology (SOFT)*, Warsaw, Poland, September 11–15, 2006, *Fusion Eng. Des.*, **82**, 1258 (2007).
134. W. DIENST, "Investigations on Ceramic Materials for Fusion Technology," *J. Nucl. Mater.*, **174**, 102 (1990).
135. W. DIENST, "Reduction of the Mechanical Strength of Al₂O₃, AlN and SiC Under Neutron Irradiation," *J. Nucl. Mater.*, **191–194**, 555 (1992).
136. W. DIENST, "Mechanical Properties of Neutron-Irradiated Ceramic Materials," *J. Nucl. Mater.*, **211**, 186 (1994).
137. G. P. PELLIS and R. M. BOOTHBY, *J. Nucl. Mater.*, **256**, 25 (1998).
138. G. P. PELLIS, "European Technology Fusion Programme, T246 Final report," Report EUR-CIEMAT 92, E. R. HODGSON, Ed. (1998).
139. R. HEIDINGER, "Mechanical Strength of Neutron-Irradiated Window Materials," *J. Nucl. Mater.*, **307–311**, 2, 1254 (2002).
140. A. NAGASHIMA et al., *Diagnostics for Experimental Thermo-nuclear Fusion Reactors 2*, p. 257, P. STOTT et al., Eds., Plenum Press, New York (1998).
141. M. MISSIRLIAN, J. SCHLOSSER, M. LIPA, R. MITTEAU, PH. CHAPPAUIS, and C. PORTAFAIX, "Methodology for the Design of Diagnostic Windows for Tore Supra," *Fusion Eng. Des.*, **66–68**, 911 (2003).
142. B. SCHULZ., *J. Nucl. Mater.*, **155–157**, 348 (1988).
143. M. ROHDE and B. SCHULZ, *J. Nucl. Mater.*, **173**, 289 (1990).
144. R. HEIDINGER et al., "Design and Analysis of Windows and Structural Components for the ITER ECRH Upper Port Plug," *Proc. 13th Joint Workshop on ECE and ECRH (EC-13)*, Nizhny Novgorod, Russia, May 17–20, 2004 (2004); available online at <http://www.ec13.iapras.ru/>
145. "15th IEA Workshop on Radiation Effects in Ceramic Insulators, Dec 2005," Report EUR-CIEMAT 98, E. R. HODGSON, Ed. (2006).

146. S. B. GILLIAM et al., "Retention and Surface Blistering of Helium Irradiated Tungsten as a First Wall Material," *J. Nucl. Mater.*, **347**, 289 (2005).
147. N. YOSHIDA, H. IWAKIRI, K. TOGUNAGA, and T. BABA, "Impact of Low Energy Irradiation on Plasma Facing Metals," *J. Nucl. Mater.*, **337–339**, 946 (2005).
148. N. OHNO, S. KAJITA, DAI NISHIJIMA, and S. TAKAMURA "Surface Modification at Tungsten and Tungsten Coated Graphite Due to Low Energy and High Fluence Plasma and Laser Pulse Irradiation," *J. Nucl. Mater.*, **363–365**, 1153 (2007).
149. A. EBIHARA, M. TOKITANI, K. TOKUNAGA, T. FUJIWARA, A. SAGARA, and N. YOSHIDA, "Irradiation Effects of Low Energy Helium Ions on Optical Reflectivity of Metallic Mirror," *J. Nucl. Mater.*, **363–365**, 1195 (2007).
150. R. BEHRISH, G. FEDERICI, A. KUKUSHKIN, and D. REITER, "Material Erosion at the Vessel Walls of Future Fusion Devices," *J. Nucl. Mater.*, **313–316**, 388 (2003).
151. A. KUKUSHKIN, Private Communication (2006).
152. G. FEDERICI et al., "Plasma-Material Interactions in Current Tokamaks and Their Implications for Next Step Fusion Reactors," *Nucl. Fusion*, **41**, 1967 (2001).
153. V. VOITSENYA et al., "Diagnostic First Mirrors for Burning Plasma Experiments (Invited)," *Rev. Sci. Instrum.*, **72**, 475 (2001).
154. A. F. BARDAMID et al., "Ion Energy Distribution Effects on Degradation of Optical Properties of Ion-Bombarded Copper Mirrors," *Surface and Coatings Technology*, **103–104**, 365 (1998).
155. M. BALDEN et al., "Surface Roughening and Grain Orientation Dependence of the Erosion of Polycrystalline Stainless Steel by Hydrogen Irradiation," *J. Nucl. Mater.*, **329–333**, 1515 (2004).
156. K. YU. VUKOLOV, Private Communication (2003); see also A. A. MEDVEDEV, E. V. ALEXANDROV, A. V. GORSHKOV, and K. YU. VUKOLOV, *Proc. 10th Int. Conf. and School on Plasma Physics and Controlled Fusion*, Alushta, Crimea, Ukraine, September 13–18, 2004, p. 224 (2004).
157. T. SUGIE et al., *J. Plasma Fusion Res.*, **79**, 1051 (2003).
158. E. E. MUKHIN and G. T. RAZDOBARIN, *Proc. 30th EPS Conf. Controlled Fusion and Plasma Physics, Europhysics Conference Abstracts*, St. Petersburg, Russia, July 7–11, 2003, **27A**, O-1.5A (2003).
159. S. TUGARINOV et al., *Rev. Sci. Instrum.*, **74**, 3, 2075 (2003).
160. A. MALAQUIAS et al., "Active Beam Spectroscopy Diagnostics for ITER: Present Status (Invited)," *Rev. Sci. Instrum.*, **75**, 3393 (2004).
161. V. S. VOITSENYA et al., "Simulation of Environment Effects on Retroreflectors in ITER," *Rev. Sci. Instrum.*, **76**, 083502 (2005).
162. V. S. VOITSENYA et al., *Proc. 12th Int. Congress on Plasma Physics*, Nice, France, October 25–29, 2004, available online at [http://hal.ccsd.cnrs.fr/ICPP2004/en/\(2004\)](http://hal.ccsd.cnrs.fr/ICPP2004/en/(2004)).
163. H. YOSHIDA, O. NAITO, T. HATAE, and A. NAGASHIMA, "Solution for a Window Coating Problem Developed in the JT-60U Thomson Scattering System," Report JAERI-Research 96-062, Japan Atomic Energy Research Institute (1996).
164. V. S. VOITSENYA et al., *Rev. Sci. Instrum.*, **70**, 790 (1999).
165. G. DE TEMMERMAN, R. A. PITTS, V. S. VOITSENYA, L. MAROT, G. VERES, M. MAURER, and P. OELHAFEN, "First Mirror Tests for ITER: Influence of Material Choice on the Erosion/Deposition Mechanisms Affecting Optical Reflectivity," *J. Nucl. Mater.*, **363–365**, 259 (2007).
166. V. S. VOITSENYA, *Rev. Sci. Instrum.*, **70**, 787 (1999).
167. W. BOHMEYER, G. FUSSMAN, C. IBOTT, A. MARKIN, and H.-D. REITER, "Formation of Hydrocarbon Films in the Plasma Generator PSI-2," *30th EPS Conf. Controlled Fusion and Plasma Physics*, St. Petersburg, Russia, July 7–11, 2003, *Europhysics Conference Abstracts* **27A**, European Physical Society, P-3.184 (2003).
168. A. LITNOVSKI et al., "Diagnostic Mirrors for ITER: A Material Choice and an Impact of Erosion and Deposition on Their Performance," *J. Nucl. Mater.*, **363–365**, 1395 (2007).
169. M. M. KOCHERGIN et al., "Research on Mirror Cleaning in Inductively and Capacitively Driven Radio-Frequency Discharges," *Plasma Devices and Operations*, **14**, 171 (2006).
170. K. VUKOLOV, A. GORSHKOV, and S. ZVONKOV, "Cleaning of Metal Mirrors from Contaminations by the Radiation of Eximer Laser. Problems for Atomic Science and Technology," *Thermonuclear Fusion*, **1**, 61 (2001) (in Russian).
171. K. YU. VUKOLOV, M. I. GUSEVA, S. A. EVSTIGNEEV, A. A. MEDVEDEV, and S. N. ZVONKOV, *Plasma Devices and Operations*, **12**, 193 (2004).
172. D. NAUJOKS and W. ECKSTEIN, *J. Nucl. Mater.*, **230**, 93 (1996).
173. K. OHYA et al., *J. Nucl. Mater.*, **337–339**, 882 (2005).
174. T. KONDOH, Y. KOWANO, A. E. COSTLEY, A. MALAQUIAS, T. SUGIE, and C. WALKER, "Toroidal Interferometer/Polarimeter Density Measurement System for Long Pulse Operation on ITER," *30th EPS Conf. Controlled Fusion and Plasma Physics*, St. Petersburg, Russia, July 7–11, 2003, *Europhysics Conference Abstracts* **27A**, European Physical Society, P-4.64 (2003).
175. V. ROHDE et al., *J. Nucl. Mater.*, **337–339**, 847 (2005).
176. A. E. COSTLEY, "Laser-Based Diagnostics for ITER and Beyond," *Proc. 12th Int. Symp. Laser Aided Plasma Diagnostics*, Snowbird, Utah, September 26–29, 2005 (2005).
177. T. NISHITANI et al., *Fusion Eng. Des.*, **51–52**, 153 (2000).
178. L. C. INGESSON et al., *Fusion Sci. Technol.*, **53**, 528 (2008).
179. G. VAYAKIS et al., "Status and Prospects for mm-Wave Reflectometry in ITER," *Nucl. Fusion*, **46**, S836 (2006).
180. ITER PHYSICS EXPERT GROUP ON DIAGNOSTICS and ITER PHYSICS BASIS EDITORS, "Chapter 7: Measurement of Plasma Parameters," *Nucl. Fusion*, **39**, 2541 (1999).
181. J. B. LISTER, J. W. FARTHING, M. GREENWALD, and I. YONEKAWA, "The ITER CODAC Conceptual Design," *Fusion Eng. Des.*, **82**, 1167 (2007).
182. R. REICHLER et al., "Concept for Spectrally Resolved ITER Divertor Thermography with Fibres," *32nd EPS Conf. Plasma Physics, Europhysics Conference Abstracts*, **29**, P4.083 (2005).
183. L. DE KOCK et al., "Langmuir Probes and Optical Diagnostics for the ITER Divertor," *Diagnostics for Experimental Thermonuclear Reactors*, p. 591, P. STOTT et al., Eds., Plenum Press, New York (1996).
184. A. MORABITO, Private Communication (2005).
185. G. VAYAKIS et al., "The ITER ECE Diagnostic Front End Design," *Diagnostics for Experimental Fusion Reactors 2*, P. E. STOTT et al., Eds., Plenum, New York (1998).
186. G. VAYAKIS, D. V. BARTLETT, A. E. COSTLEY, and the ITER JCT and HOME TEAMS, "ECE Diagnostics for RTO/RC ITER," *Fusion Eng. Des.*, **53**, 221 (2001).
187. D. V. BARTLETT and H. BINDSLEV, "Physics Aspects of ECE Te Measurements in ITER," *Diagnostics for Experimental Fusion Reactors 2*, p. 171, P. E. STOTT et al., Eds., Plenum Press, New York (1998).
188. M. AUSTIN, Private Communication (2007).

189. P. NIELSEN et al., "LIDAR Thomson Scattering for the ITER Core Plasma," *Diagnostics for Experimental Thermonuclear Fusion Reactors 2*, p. 217, P. E. STOTT et al., Eds., Plenum Press, New York (1998).
190. M. J. WALSH et al., "Design Challenges and Analysis of the ITER Core LIDAR Thomson Scattering System," *Rev. Sci. Instrum.*, **77**, 10E525 (2006).
191. T. HATAE, O. NAITO, M. NAKATSUKA, and H. YOSHIDA, "Applications of Phase Conjugate Mirror to Thomson Scattering Diagnostics (Invited)," *Rev. Sci. Instrum.*, **77**, 10E508 (2006).
192. E. DE LA LUNA et al., "Recent Developments of ECE Diagnostics at JET," *Proc. 13th Joint Workshop on ECE and ECRH (EC-13)*, Nizhny Novgorod, Russia, May 17–20, 2004 (2004); available online at <http://www.ec13.iapras.ru/>
193. V. S. VOITSENYA et al., *Rev. Sci. Instrum.*, **70**, 2016 (1999).
194. A. GORSHKOV, I. BEL'BAS, V. SANNIKOV, and K. VUKOLOV, "Frequency Laser Damage of Mo Mirrors," *22nd Symp. Fusion Technology Book of Abstracts*, p. 238, S. TÄHTINEN et al., Eds., VTT Symposium 220, VTT, Finland (2002).
195. V. S. VOITSENYA and D. V. ORLINSKI, *Bulletin on Atomic Energy*, **5**, 53 (2006) (in Russian).
196. V. S. VOITSENYA, "Problems of In-Vessel Mirrors in ITER and Their Possible Solution," *AIP Conference Proceedings*, **812**, 211 (2006).
197. G. VAYAKIS et al., "Plasma Diagnostics in ITER Control," *1998 International Congress on Plasma Physics combined with the 25th European Physical Society Conference on Controlled Fusion and Plasma Physics, Europhysics Conference Abstracts*, **22C**, P3.095 (1998).
198. D. L. BROWER, Private Communication (2007).
199. F. NAJMABADI, "Spherical Torus Concept as Power Plants—The ARIES-ST Study," *Fusion Eng. Des.*, **65**, 143 (2003).
200. K. TOBITA et al., *Fusion Eng. Des.*, **81**, 1151 (2006).
201. P. SARDAIN et al., *Fusion Eng. Des.*, **81**, 2673 (2006).
202. F. NAJMABADI, A. R. RAFFRAY, and the ARIES TEAM, "Recent Progress in the ARIES Compact Stellarator Study," *Fusion Eng. Des.*, **81**, 2679 (2006).
203. D. KING et al., "Conclusions of the Fusion Fast Track Experts Meeting Held on 27 November 2001 on the Initiative of Mr. De Donnea, President of the Research Council," report available from http://ec.europa.eu/research/energy/pdf/kingreport_en.pdf.
204. "IFMIF CDA Team IFMIF Conceptual Design Activity, Final Report," ENEA Frascati Report RT/ERG/FUS/96/11, M. MARTONE, Ed. (1996).
205. T. KONDO, "IFMIF, Its Facility Concept and Technology," *J. Nucl. Mater.* **258–263**, *1*, 47 (1998).
206. E. F. EIKENBERRY et al., "PILATUS: A Two-Dimensional X-Ray Detector for Macromolecular Crystallography," *Nucl. Instrum. Methods Phys. Res. Sect. A: Accelerators, Spectrometers, Detectors and Associated Equipment*, **501**, *1*, 260 (2003).